Iminophosphine ligands and their metal binding properties

A thesis presented in partial fulfilment of the requirements for the degree of

Master of Science

In

Chemistry

At Massey University, Palmerston North

New Zealand

Kurt Allen McBeth

2003

Abstract

This work focuses on the complexes of two iminophosphine ligands, *N*-(2-diphenylphosphinobenzylidine)-aniline (NP) and *N*-(2-diphenylphosphinobenzylidine)-4'-(benzo-15-crown-5) (O_5NP), and their complexes with Cu(I), Ag(I), Au(I), Cr(0), Mo(0) and W(0). The cation binding properties of the complexes of O_5NP have been investigated.

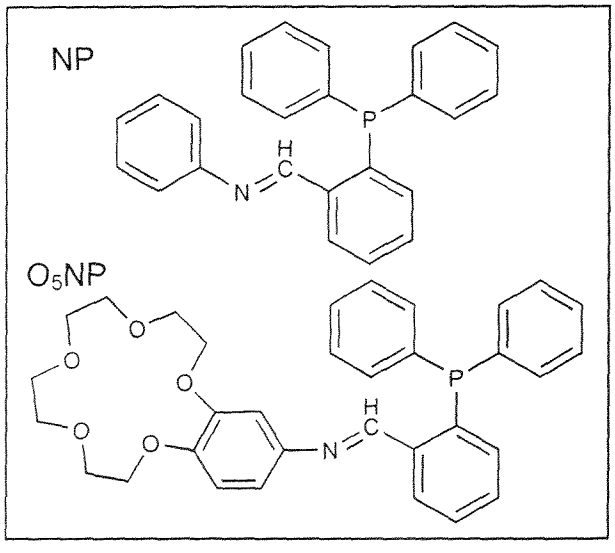

Chapter One describes the aims of this work and also provides a brief introduction to ligands containing phosphorus and nitrogen donor atoms as well as crown ethers and their inclusion in transition metal complexes. The analytical technique of electrospray mass spectroscopy (ESMS) is introduced and its use in the study of cation binding to crown ethers and cryptands discussed.

Chapter Two looks at the Cu(I), Ag(I) and Au(I) complexes of NP and O_5NP, such as $[M(L)_2][PF_6]$ (M = Cu, Ag, Au; L = NP, O_5NP), $[M(NP)X]_2$, $[M(O_5NP)Cl]_2$ (M = Cu, Ag), Au(NP)X and Au(O_5NP)Cl (X = Cl, Br, I). Reported in this chapter are the X-ray structural analyses of O_5NP, $[Cu(NP)_2][PF_6]$, $[Ag(NP)_2][PF_6]$, $[Au(NP)_2][PF_6]$, $[Cu(NP)Br]_2$, Au(NP)Cl and Au(NP)Br. Far and Near IR, ^{1}H and ^{31}P NMR and ESMS were used to investigate the nature of the complexes. The $[M(L)_2][PF_6]$ complexes displayed a clear trend in which the number of coordinated imines decreased as the soft nature of the metal centre increased. Both the Far IR and crystal structure analyses showed the Cu(I) and Ag(I) halo complexes to be dimeric with bridging halides and the

Au(I) halo complexes to be monomeric with terminal halides. The ^{31}P NMR signal was found to be dependent on the mass of the metal centre.

In Chapter Three the Cr(0), Mo(0) and W(0) carbonyl complexes of NP and O_5NP are discussed. To characterise the complexes, IR, ESMS and ^{1}H, ^{31}P and ^{13}C NMR techniques were employed. X-ray structural analyses of $Mo(CO)_4(NP)$ and $Mo(CO)_4(O_5NP)$ were also used. It was found that the metal centres had an octahedral geometry with the ligands being bidentate via the P and N atoms and having a *cis* conformation. Upon coordination, the ^{1}H NMR signal of the imine proton moves to lower frequencies, whereas the ^{31}P NMR signal moves to higher frequencies. It was also demonstrated that the presence of the crown ether has no significant effect on the structure of the metal centre.

Cation binding to the complexes of O_5NP, the free ligand, and starting material, 4'-aminobenzo-15-crown-5 (O_5NH_2), is discussed in Chapter Four. Electrospray mass spectroscopy (ESMS) was used as a qualitative measure of the relative cation binding strengths. The X-ray structural analyses of the inclusion complexes $W(CO)_4(O_5NP)Na(PF_6)$ and $[Cu(O_5NP)_2]K[PF_6]_2$ were determined, and provided information on the coordination of alkali cations by these complexes. $W(CO)_4(O_5NP)$ binds Na^+ within the cavity of the benzo-15-crown-5 moiety which experiences significant change to its conformation. $[Cu(O_5NP)_2][PF_6]$ binds K^+ in a sandwich formation suggesting that rotation of the ligands occurs about the Cu(I) centre. The starting material, O_5NH_2, and free ligand, O_5NP, were selective towards K^+, forming a 1:1 species. The complexes $M(CO)_4(O_5NP)$ (M = Cr, Mo, W) and $[M(O_5NP)_2][PF_6]$ (M = Cu, Ag, Au) were selective towards Na^+ and K^+ respectively with a 1:1 formation. The halide complexes, $[Cu(O_5NP)Cl]_2$, $[Ag(O_5NP)Cl]_2$ and $Au(O_5NP)Cl$, displayed different selectivities from each other. Both $[Cu(O_5NP)Cl]_2$ and $[Ag(O_5NP)Cl]_2$ dissociated in solution to give the monomers which selectively bound Li^+ and K^+ respectively in a 1:1 species. The $Au(O_5NP)Cl$ complex was selective towards Na^+.

Acknowledgements

Associate Professor Eric Ainscough and Professor Andrew Brodie are the first to be thanked. They have been a constant help and I deeply respect them both. Eric always has a reassuring comment and interesting pieces of information to entertain with. Andrew has been a constant source of motivation for me while being an accessible and knowledgeable source of advice.

Dr. Andreas Derwahl is greatly deserving of thanks both for the huge amount of effort that he put into the crystal structures within this work and for the help that he gave me in every day survival.

Graham Freeman for basically looking after me these past six or so years. He has given good advice when it was needed, brilliant technical assistance and is a good friend. Graham has been a major influence to my studies and is the reason why I am not currently in a marriage of convenience.

Associate Professor C. Rickard, University of Auckland for collection of X-ray structure data sets. Professor Geoff Jameson for his expert assistance with the X-ray structure analyses. Professor G. Bowmaker, University of Auckland for recording of Far IR spectra David Lun for his assistance with the ESMS device. Dr. Pat Edwards for assistance with the NMR spectra and Dr. Steven Kennedy for past work.

Thanks goes to Delwyn Cooke, Gavin Collis, Rachel Williamson, Clair Nelson, Catherine Hardacre, Celia Webby, Amy Bellantyne, Giovanna "G" Moretto, Adrian Jull, Krishanthi Jayasundera, Julie Locke, Carol Taylor (for the coffee), Penny Abercrombie and Barbara Gunn, Engineering Services and Bob Parsons.

I gratefully acknowledge the financial assistance of the David Levine Trust and the IFS Graduate Research Fund.

THANK YOU TO YOU ALL

Kurt McBeth

Thursday, 21 August 2003.

Table of Contents.

Chapter 3

List of Figures

List of Tables

List of Schemes

Abbreviations.

NP	*N*-(2-diphenylphosphinobenzylidine)-aniline
O_5NP	*N*-(2-diphenylphosphinobenzylidine)-4'-(benzo-15-crown-5)
2PCHO	2-(diphenylphosphino)benzaldehyde.
$ArNH_2$	Aniline.
O_5NH_2	4'-aminobenzo-15-crown-5.
Ph_2Ppy	2-(diphenylphosphino)pyridine
NBD	2,5-norbornadiene.
Pip	Piperidine.
Ph	Phenyl
Bz	Benzo group
Cy	Cyclohexyl
Me	Methyl
L	Ligand (chemical), Litre (measurement)
IR	Infrared
NMR	Nuclear magnetic resonance
ESMS	Electrospray mass spectrometry
FAB+	Fast atom bombardment, positive mode
δ	Chemical shift in ppm.
ppm	Parts per million
Hz	Hertz.
J^{χ}_{XY}	Coupling constant over χ bonds between atoms X and Y.
s	Singlet (spectral)
d	Doublet (spectral)
t	Triplet (spectral)
sep	Septuplet (spectral)
m	Multiplet (spectral)
ν(X–Y)	Stretching frequency of X–Y bond.
m/z	Mass per charge.
ORTEP	The computer program used to produce illustrations of X-ray crystallography structural analyses.
MLCT	Metal to ligand charge transfer

LLCT	Ligand to ligand charge transfer
logK	Formation constants
E_f	Redox potential
ΔE	Change in redox potential
$CDCl_3$	Deuterated chloroform
CD_3CN	Deuterated acetonitrile
TMS	Tetramethylsilane
RT	Room temperature
FW	Formula weight
μ	Gyromagnetic constant
U(eq)	Displacement parameters
g	Grams
mg	Milligrams
mmol	Millimoles
ml	Millilitres
h	Hours
$molL^{-1}$	Moles per litre

Chapter 1

Introduction

1.1 Phosphorus and Nitrogen Donor Ligands

There is interest in ligands that offer both hard and soft donor atoms for coordination to metals.[1-7] Heterofunctionalised P∩N ligands are used extensively in catalytic systems due to the variety of coordination modes that they are able to adopt. In this way P∩N ligands are more versatile than either N∩N or P∩P ligands. Their coordination modes include P monodentate, N monodentate, chelating and bridging (Scheme 1.1), where the coordination of the ligand depends on factors such as the P∩N bite angle, the rigidity of the chelate ring and the hardness or softness of the metal or metals involved. A small bite angle will give a labile chelate ring and favour bridging or monodentate coordination with a soft metal centre bonding to the phosphorus and a hard metal centre bonding to the nitrogen atoms. A medium bite angle will provide a non-labile chelate ring.

Scheme 1.1. Possible coordination modes.

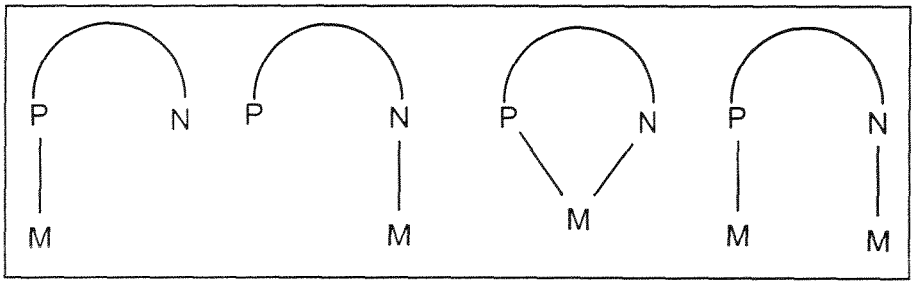

P∩N ligands have another advantage over P∩P or N∩N ligands. In certain conditions they present a vacant site, a process known as hemilability. This partial lability means that one of the donor groups can dislocate from the metal centre leaving a vacant site for the coordination of substituents.[1,2] The ability to present an open coordination site combined with the ability to adopt multiple coordination modes is essential in many catalytic systems.[3] Since it is mainly the middle or late transition metals that are used in these systems the soft phosphorus atom remains attached while the harder nitrogen atom dissociates from the metal centre.

There are three main types of bidentate P∩N ligands: Aminophosphines, iminophosphines and heteroaromatic phosphines. All of these have a soft P atom but the aminophosphines has a hard N and the iminophosphines and heteroaromatic

phosphines have a semi-hard nitrogen with potential π-acceptor character (Scheme 1.2).[4,5]

Scheme 1.2. The three main types of P∩N ligands, (a) aminophosphine, (b) iminophosphine and (c) heteroaromatic phosphine.

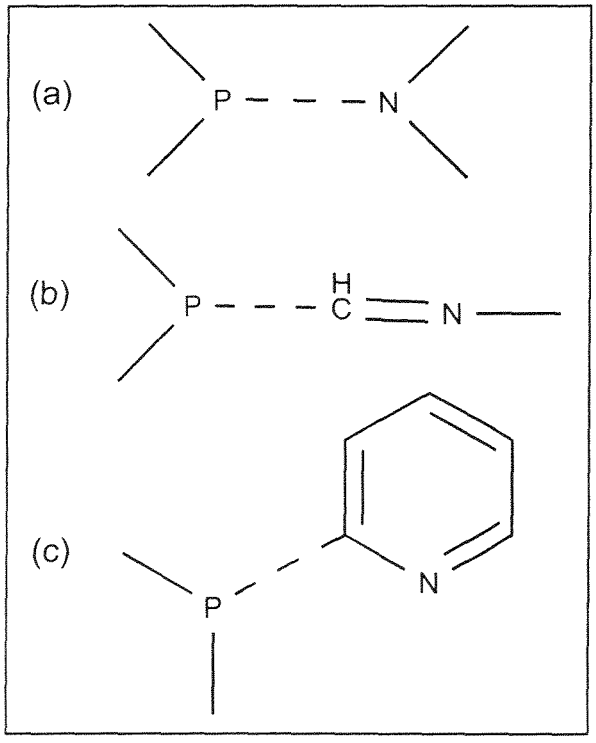

The heteroaromatic phosphine ligand 2-(diphenylphosphino)pyridine (Figure 1.1) is a P∩N ligand with a small rigid bite angle which results in it acting as a bridging ligand that can stabilize complexes with two different metal centres. It also stabilizes metal–metal bonds. Thus allowing the study of complexes that were not previously available, such as $[Ru(CO)_2Cl_2(\mu\text{-}Ph_2Ppy)_2PdCl]$, and is an example of the innovations that a P∩N ligand system can lead to.[6]

Figure 1.1. 2-(diphenylphosphino)pyridine.

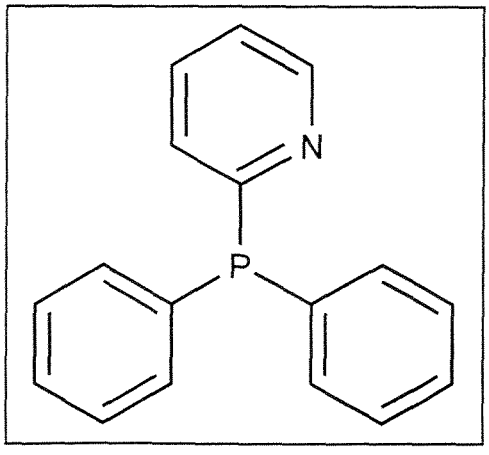

Aminophosphine systems have received much attention. The aminophosphine complexes $[M(adpp)_2][PF_6]$, where M = Cu, Ag, Au and adpp = (2-aminophenyl)diphenylphosphine (Figure 1.2a) were synthesised and shown to have cytotoxic activities. The nature of the metal had little effect on the cytotoxic activity. Increasing the number of ligands on the metal increased the activity, suggesting the aminophosphine ligand adpp is responsible for the cytotoxicity.[7] Another use of aminophosphine ligands is catalytic oxidation of alkanes and alkenes. It was found that a ruthenium complex of *N,N'*-bis[2-(diphenylphosphanyl)benzyl]-1*R*,2*R*-cyclohexanediamine (Figure 1.2b) was able to catalyse the reaction of molecular oxygen with both styrene and octane to give a variety of products.[8] Diaminodiphosphines have also been used in solvent extraction, for example the compound *N,N'*-bis[2-(diphenylphosphino)phenyl]propane-1,3-diamine (Figure 1.2c) has been studied as a transporter of transition metals across a liquid-liquid interface. It was found that the tetradentate ligand was able to complex to Cu^{2+}, in the presence of chloride, and selectively transport the Cu^{2+} across the interface.[9]

Figure 1.2. Aminophosphines.

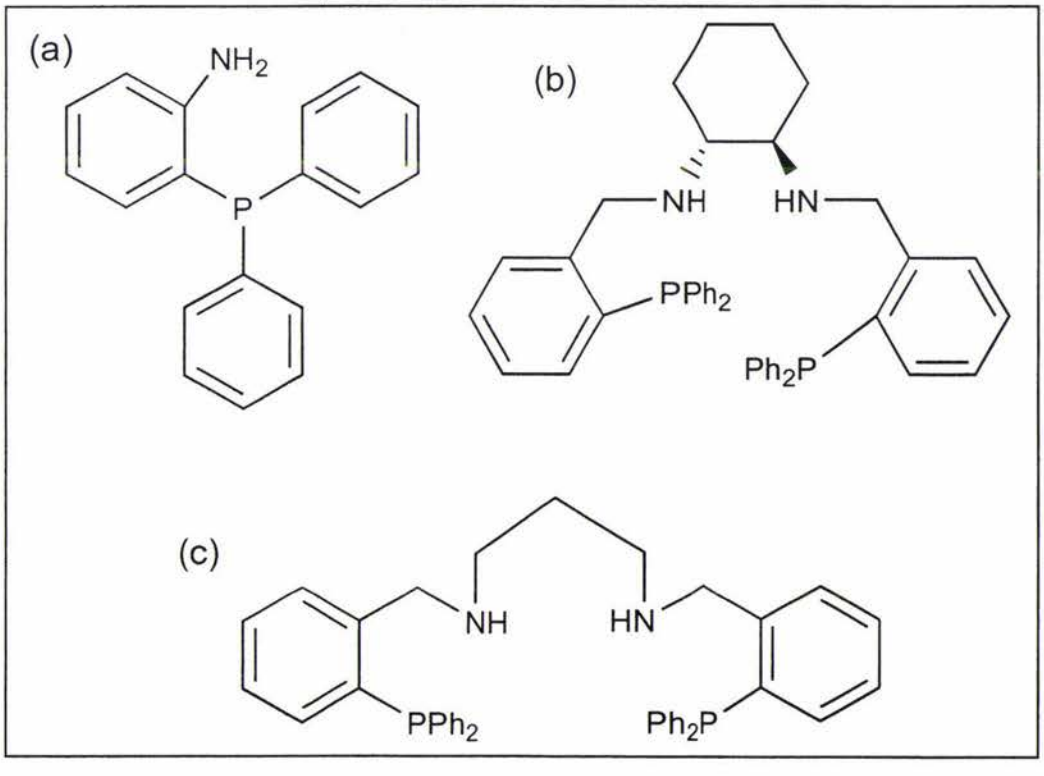

Catalytic properties of iminophosphines (Figure 1.3) have allowed the selective oligomerisation of ethene by controlling steric hindrance at the donor groups. This oligomerisation was aided by the unusual stability of the complex at high temperatures and in polar solvents.[10] Other palladium iminophosphine complexes have been used to catalyse the insertion of benzene into an alkynyl-tin bond[11] thus providing a variety of useful synthetic *ortho*-substituted precursors.

Figure 1.3. Pd(I) iminophosphine catalyst.

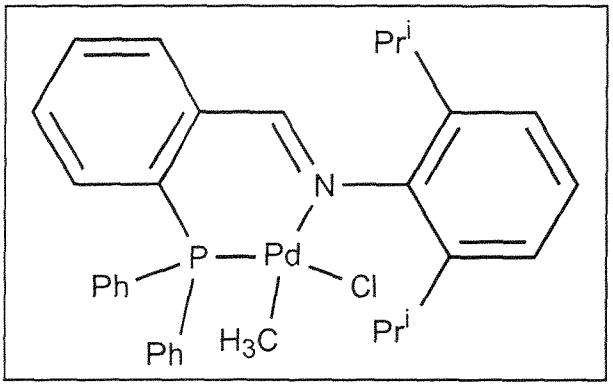

Iminophosphine ligands have the ability to stabilize less common oxidation states and coordination modes of metal ions. The imino groups are known to stabilize low oxidation states due to their π-acceptor ability, for example the zero valent palladium complex (Figure 1.4).[12]

Figure 1.4. *N*-(2-diphenylphosphino)benzylidene) (2-(2-pyridyl)ethyl)amine palladium(0).

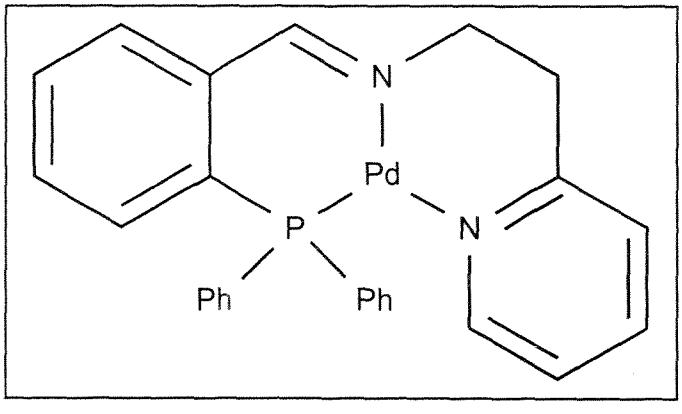

The hemilability of some P∩N ligands has been used to stabilise changes in oxidation states of a metal centre.[12,13] Such activity, along with the ability to achieve multiple coordination modes has allowed P∩N ligands to be used in catalytic process such as allylic alkylation,[12,8] cross coupling reactions[12] and co-polymerisation reactions.[1] If the P∩N ligand has a stereocentre, such as the Pd complex of the iminophosphine in Figure 1.5, there is the possibility of it catalysing enantioselective reactions.

Figure 1.5. (*R*)-((2-(diphenylphosphino)phenyl)methylene) (1-(2,4,6-trimethylphenyl)ethyl)amine.

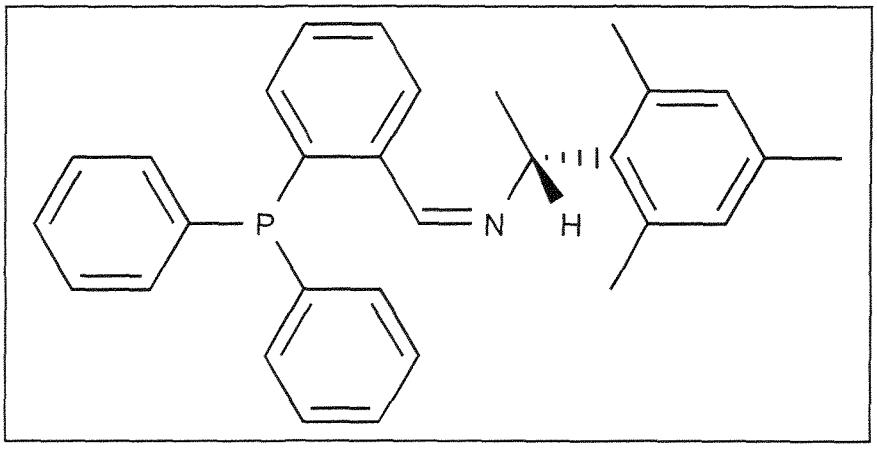

Many of the P∩N complexes used for catalysis have only been prepared *in situ* and hence have not been fully characterised. Therefore much investigative work concerning their fundamental properties remains to be done.

1.2 A Brief History of Crown Ethers

"Beyond molecular chemistry based on the covalent bond there lies the field of supramolecular chemistry, whose goal it is to gain control over the intermolecular bond ... it is a sort of molecular sociology!".[14]

Crown ethers (Scheme 1.3) were discovered by Pederson[15] and are a well-known piece of machinery in the world of supramolecular chemistry. Crown ethers use a ring of evenly placed ether groups to bind cations via a dipole-ion bond.

Scheme 1.3. Examples of crown ethers.

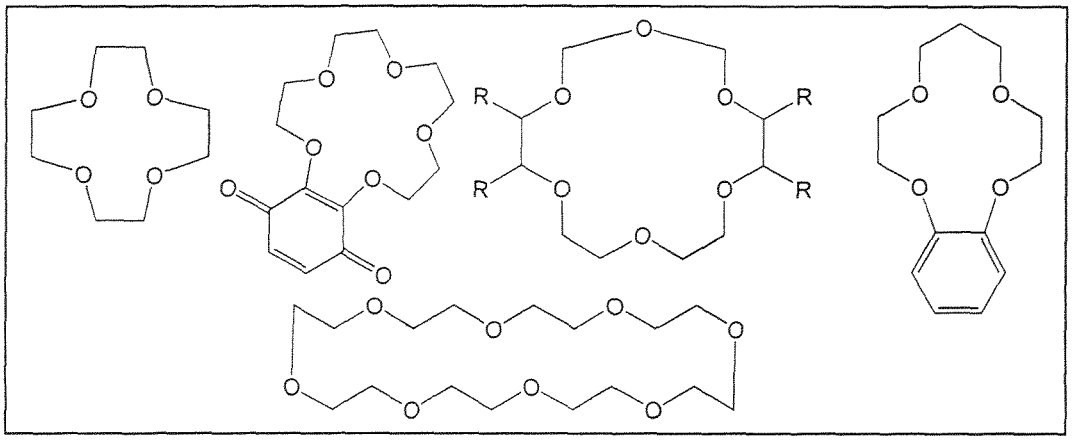

They are able to selectively bind cations depending on the size of the cation versus the cavity size (Scheme 1.4). This selectivity has opened up the field of supramolecular chemistry and has lead to a proliferation of research into crown ethers and similar compounds.

Scheme 1.4. Selective binding.

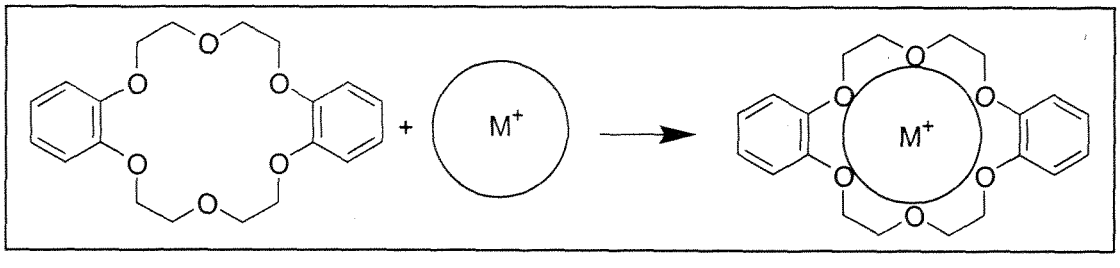

The selectivity of crown ethers is generally well known and understood.[16-19] A crown ether will form the most stable complexes with the cation that best fits its cavity size (Table 1.1). Alkali metal ions that do not fit within the cavity have smaller formation constants (Table 1.2). For example benzo-15-crown-5 forms the strongest complex with the Na^+ cation because Na^+ has the best fit within the cavity. Generally enthalpies of complexation tend to show the same trends as the observed formation constants. Solvation effects and changes in ligand conformation with complexation will also influence the selectivity.

With larger cations, sandwich complexes can form between two crown ethers and a single cation (Figure 1.6).[20-24] Very large cations can produce species where the cation binds to the crown with anions bridging between these bound cations (Figure 1.7).[25]

Table 1.1. Crown cavity and ionic diameters (Å).[20,26]

Crown type	Hole diameter	Ion	Ionic diameter
14-crown-4	1.2-1.5	Li^+	1.36
15-crown-5	1.7-2.2	Na^+	1.94
18-crown-6	2.6-3.2	K^+	2.66
21-crown-7	3.4-4.3	Rb^+	2.94
		Cs^+	3.34

Table 1.2. Formation constants of benzo-15-crown-5 with alkali cations.

	Li^+	Na^+	K^+	Rb^+	Cs^+
Conductance in Propylene Carbonate, perchlorate salts, T=25°C [27]	3.77	4.35	2.78	2.38	2.03
Calorimety in 70% MeOH, T=25°C [17]	-	1.99	1.5[a]	1.8[b]	1.7
Polarography, MeCN, 0.05 M Bu_4NClO_4, T=22°C [17]	-	4.55	3.40	2.90	3.10

a) $\log K_2 = 2.65$; b) $\log K_2 = 1.97$.

Figure 1.6. Idealised 2:1 and 3:2 sandwich complexes.[20]

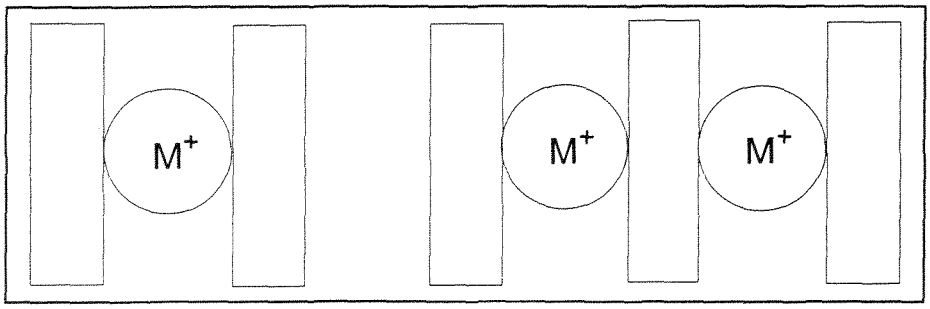

Figure 1.7. Benzo-18-crown-6 with CsNCS.[25]

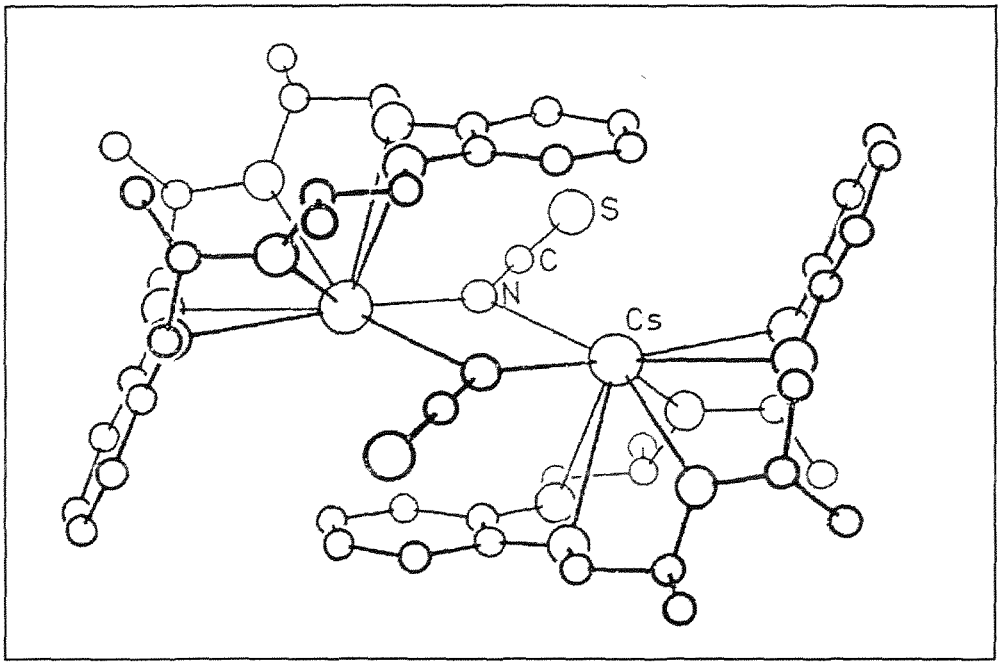

1.3 Crown Ethers and Transition Metals

There are only a few reports of compounds where a crown ether is part of a ligand. In such a case the crown is covalently attached to a functional group that is itself bound to a metal centre, in this situation the cavity of the crown remains vacant (Scheme 1.5).

Scheme 1.5. A metal complex with a crown ether moiety.

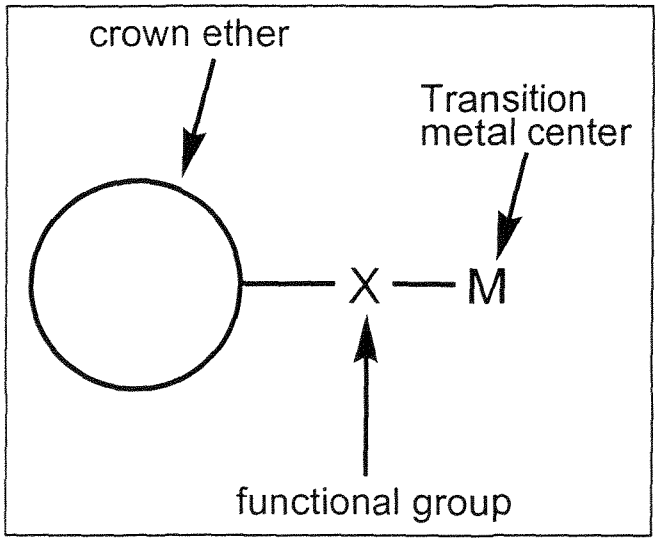

Molecular recognition is an important theme in supramolecular chemistry. If a molecular device has a receptor (host) such as a crown ether and is able to bind a substrate (guest) such as an alkali cation, then a sensor is obtained if a signalling unit (X—M) can record this uptake. This unit may sense a change in the redox potential or the colour of the complex.

For example work by Yam *et al.* focused on the investigation of UV-vis absorption bands, due to metal to ligand charge transfer (MLCT) or ligand to ligand charge transfer (LLCT), of these systems (Scheme 1.5) and the effect that cation concentration has on the absorption bands. It was shown that various metal complexes (Figure 1.8) experience a blue shift in their electronic absorption upon cation binding.[28-34] This shift is absent when the crown-free analogues are in the presence of the cations. Yam *et al.* also used electronic absorption spectra to determine the formation constants (logK) of cation binding to the complexes of the above metal centres using a non-linear least squares fit model of the absorbance versus the concentration of ion added.[31-33] Further evidence has been provided by

Electrospray mass spectrometry (ESMS) that the complexes containing bound cations are present in the gas phase.[28,30-32,34-37]

Figure 1.8. A Cu(I) complex that has a blue shift in its MLCT upon cation uptake.

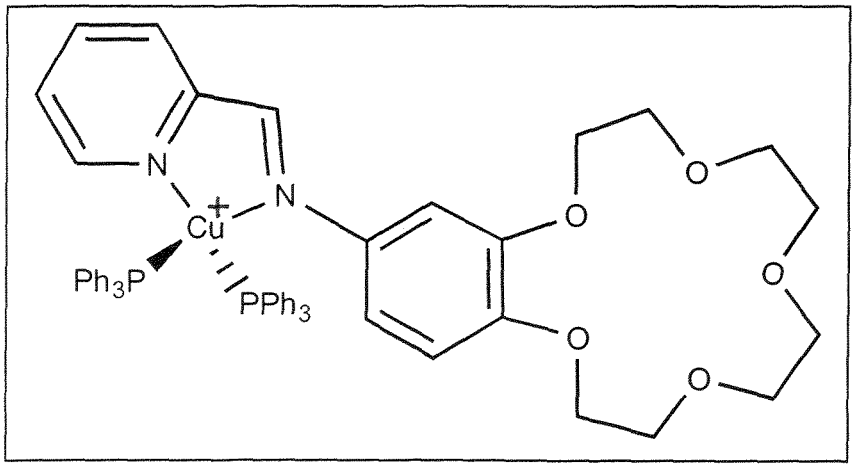

In another example, a crown ether bound to a phosphine can coordinate to a transition metal via the P atom leaving the crown vacant and able to bind alkali cations (Scheme 1.6). Studies have shown that $Ni(CO)_3L$ (L = benzo-3,4-(15-crown-5)-diphenylphosphine) (Scheme 1.6) experiences changes to the IR ν(CO) frequencies upon cation binding although these changes are small.[38] It has also been found that addition of cations causes significant changes to the redox potential of the Ni atom, which are dependent on the cation added and the polarity of the solvent used. ^{31}P NMR spectroscopy was found to be an ineffective method of monitoring cation uptake.[39]

Scheme 1.6. A $Ni(CO)_3L$ complex binding Na^+ ions.

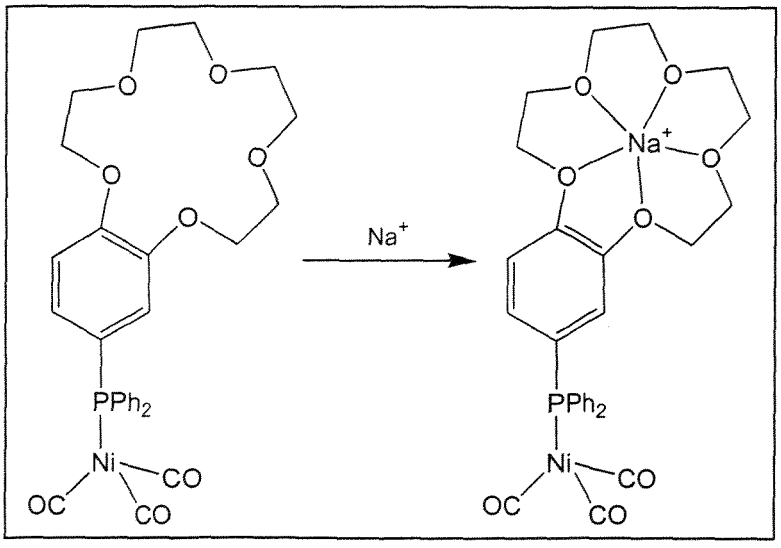

Another sensing system focused on the reduction of Co(III) to Co(II). The cobalt is complexed with a tetraamine macrocycle that is attached to benzo crown ethers of varying size (Figure 1.9). An anodic shift occurs upon addition of Li^+, Na^+ or K^+, thus demonstrating significant communication between the receptor and signalling unit.[40]

Figure 1.9. A Co(II) complex of a tetraamine with a 12-crown-4 pendant ligand.

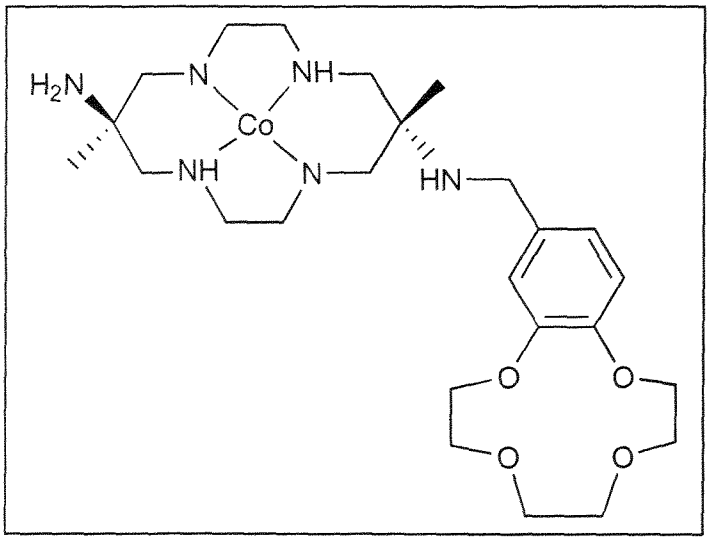

Beer has done much work on crown ethers that contain redox active ferrocene centres (compounds A and B in Figure 1.10) as signalling devices for cation binding. Investigations using cyclic voltammetry show that significant communication is only achieved between the ferrocene and crown ether units if the linker is conjugated. If the linker is saturated the ferrocene is insensitive to the cations binding to the crown.[41] It was also found that the polarizing power, i.e. charge density, of the cation is responsible for the magnitude of change in redox potential. This can be seen in Table 1.3 where Mg^{2+} has a change in redox potential (ΔE) twice that of Na^+ and more than twice that of K^+ for both compounds A and B. The ionic diameter of Mg^{2+} is 1.44 Å,[42] which is smaller than Na^+ or K^+ (Table 1.1).[41]

The number of crown ethers per compound also affects the shift in redox potential. Upon the addition of Na^+, K^+ or Mg^{2+}, compound B (Figure 1.10) experiences a shift in redox potential roughly twice that experienced by compound A (Figure 1.10). This difference is attributed to the presence of two crown ethers in compound B compared to one in compound A.[41]

Table 1.3. Electrochemical data (mV)[a].[41]

	A	B
E_f[b]	+400	+340
$\Delta E(Na^+)$	30	55
$\Delta E(K^+)$	20	35
$\Delta E(Mg^{2+})$	60	110
$\Delta E(Na^+/K^+)$		35
$\Delta E(Na^+/K^+/Mg^{2+})$		40

a) See Figure 1.10 for compounds; b) E_f of parent ferrocene compound.

When equimolar mixtures of Na^+/K^+ and $Na^+/K^+/Mg^{2+}$ were added to the crown ether B for competition experiments (Table 1.3) the ΔE values were the same as those for K^+. This suggested the *bis*-crown ether, compound B, acts as a selective sensor for K^+ in a cation mixture.

Figure 1.10. Ferrocene compounds with one (A) and two (B) benzo-15-crown-5 moieties.

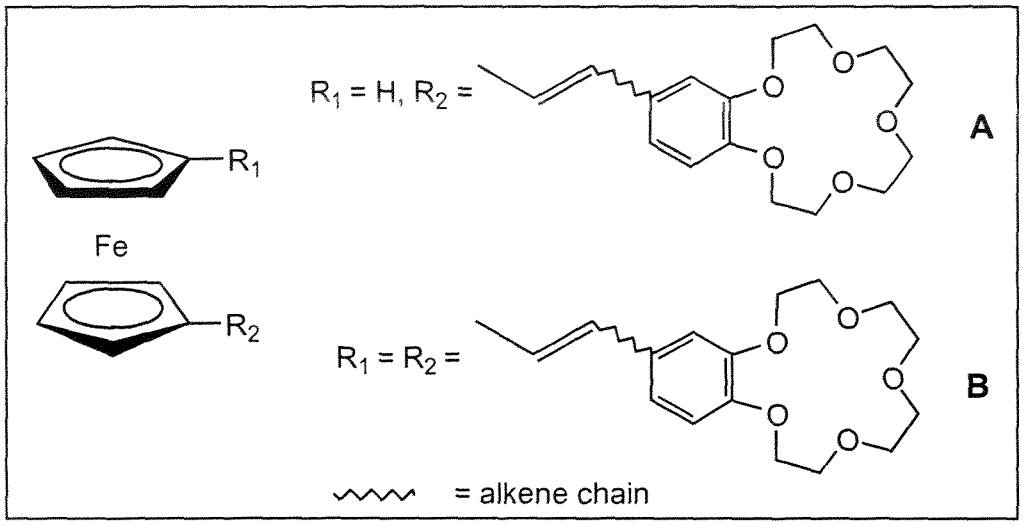

1.4 Electrospray Mass Spectrometry

1.4.1 Principles of ESMS

Mass spectrometry is a well-known, efficient and effective instrumental analytical procedure that requires very small amounts of sample. In the mid 1980s the technique of electrospray mass spectrometry (ESMS) was developed providing an ionisation method with mild conditions allowing the parent ion of a fragile species to be observed. A large range of ESMS applications in inorganic and organometallic chemistry now exist.[43]

The ESMS method involves dissolving the sample in an appropriate solvent to produce the sample ions. Neutral compounds can be charged by protonation at a basic site, usually done by the use of a protic solvent such as MeCN/H_2O or MeOH to give species of the type $[M+H]^+$. Aprotic solvents may be used by using alkali metals or silver ions as the ionisation source instead of protons. Loss of a halide also provides an ionic species, such as $[M-X]^+$. Ionic species such as $[M-X+solvent]^+$ are also possible, for example the complex *cis*-$[PtCl_2(PPh_3)_2]$ displays a $[M-Cl+pyridine]^+$ cation in pyridine.[44] This is also seen for complexes of Hg(II) , Ni(II) , Au(III) and other complexes of Pt(II) .[44] ESMS is ideally suited to ionic species as the charge is already present. Cations are analysed in the positive ion mode, while anions can be analysed in the negative ion mode.[43] Neutral compounds can be analysed by addition of negative species to give a $[M+anion]^-$ species.

The sample is passed into the ESMS device as shown in Figure 1.11 and the solution is then injected from a capillary kept at a high voltage (3000-4000 V) into a chamber at 1 atm. This voltage produces the spray and forces the ions into the gas phase (Figure 1.12). The chamber that the sample solution enters has a drying gas, usually N_2, which removes the excess solvent reducing the size of the drops hence increasing the charge density. There are two theories as to how the ions enter the gas phase. The first states that due to electrostatic repulsion intact gas-phase ions are desorbed from the surface of the droplets. This occurs as the droplets reach a certain radius ($r \leq 10$ nm). The second theory suggests that the charged droplets undergo a series of columbic explosions once the charge density reaches a critical level. This decreases

the droplet size until a final columbic explosion places the individual sample ions in the gas phase.[44] Before being transferred to the mass analyser the sample is passed through skimmers at increasing vacuum to minimize collisions. The sample then enters an ion separation device such as a quadrupole before being analysed (Figure 1.11).[43,44]

Because cations are formed in solution before the sample enters the spectrometer the results are representative of the conditions in solution. This, and the soft nature of the ionisation process of ESMS, allows the study of supramolecular chemistry. Increasingly, ESMS is being employed as a powerful analytical method for assessing cation binding behaviour.

Figure 1.11. Features of an electrospray mass spectrometer.[43]

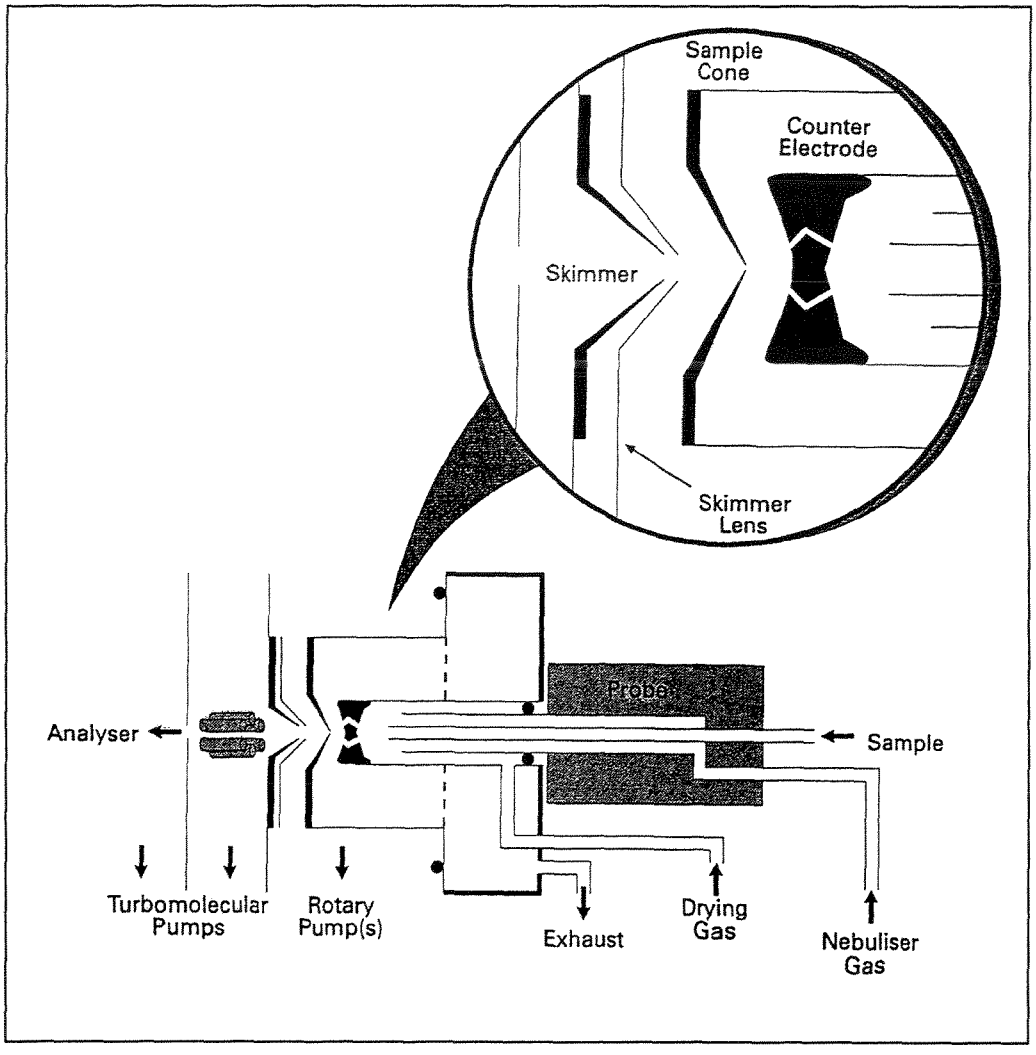

Figure 1.12. The spray produced by a high potential difference.[43]

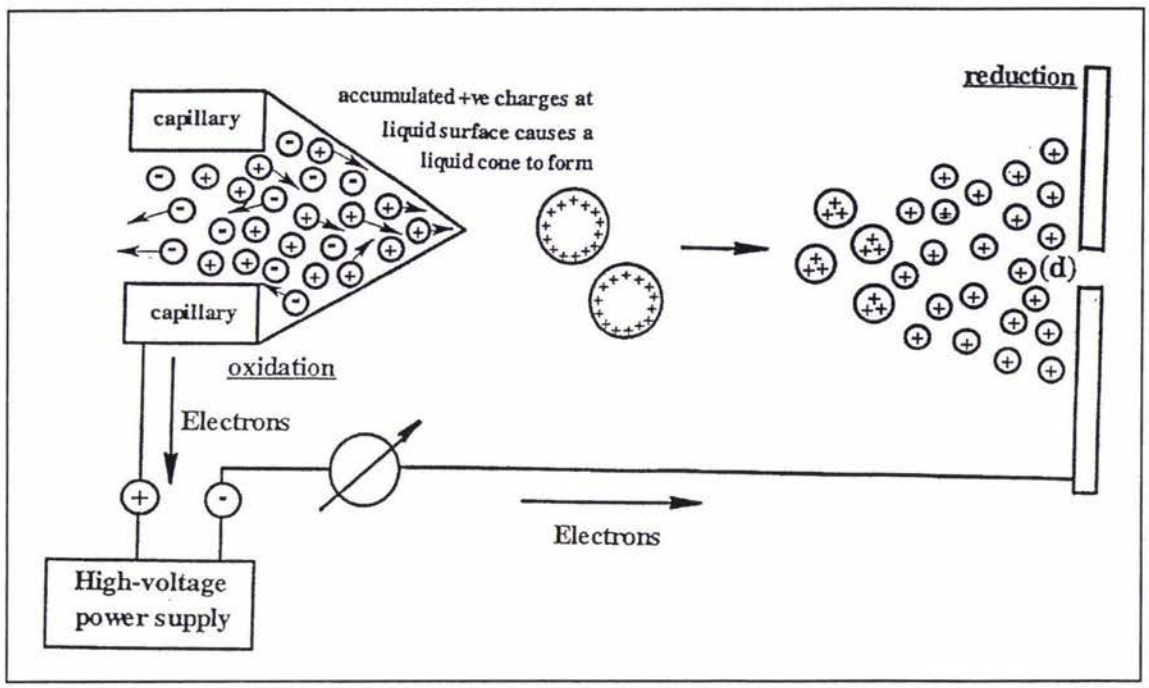

1.4.2 Host-Guest Selectivity and ESMS

The evaluation of binding selectivity of crown ethers and cryptands has traditionally been measured by photometric, NMR, electrochemical or UV-visible methods. ESMS has been shown to offer an alternative method to estimate relative binding selectivities along with structural information including non-covalent interactions. There are also reports that ESMS reflects the host-guest equilibrium that exists in solution,[45] which has been validated for both crown ethers and cryptands.[46]

Good correlation between the ESMS data obtained by measuring relative intensities (giving relative stability determinations) of host-guest complexes and the expected binding selectivities have been observed in experiments where mass spectra were obtained for solutions containing equimolar and excess concentrations of both individual and mixtures of alkali cations.[37,46,47] This has lead to the use of relative peak intensities to give qualitative assessment of cation uptake and selectivity . The results suggest that ESMS is of great benefit for assisting the determination of the composition of host guest species formed in systems of these types and is a useful tool for rapidly establishing the relative metal selectivity of appropriate new ligand systems.[37,45-47]

Since there are several factors that affect the process of the sample cations entering the gas phase, controversy exists on how ESMS spectra quantitatively reflect the nature of stability constants.[37,48] Johnstone *et al.* expressed the relationship between solution and spectra as:

$$C_{complex} = t \times I$$

C is the concentration, I is the peak intensity and t is a proportionality constant[49]

Using this equation Young *et al.* developed a method for the determination of stability constants using one host-guest complex as an internal reference to normalise the relative ESMS efficiency of a second complex.[50]

$$\frac{K_a}{K_b} = S^x \frac{I_{[\text{crown ether} + a]}}{I_{[\text{crown ether} + b]}}$$

K_a and K_b are stability constants for ions a and b bound to crown ethers. S^x is the relative cationization efficiency. I is the mass spectra intensities.

From the above equation, if K_b is known from the literature then K_a may be found. A graphical procedure is used to determine S^x where the values are generally not equal to one. Serious discrepancies in the K values will occur if S^x is not accurately determined. A requirement of this formula is that the unknown complex has a binding constant similar to that of the internal reference complex. Hence the ion intensities are directly proportional to the stability constants of species in solution.

Using the equation of Young *et al.*, Allain *et al.* studied the extraction of alkali cations by calyx-4-crowns. By comparing the relative peak intensities of the Cs^+/Na^+ inclusion complexes it was qualitatively found that Cs^+ had a higher stability in the gas phase. Using the known logK of Na^+ ions in CH_3CN, the logK of Cs^+ ions was estimated.[48]

Recently another method for investigating stability constants using ESMS data has been reported. A calculation curve for the concentration of the reference host guest complex versus its peak intensity is used based on the ESMS of a series of solutions prepared at well-defined concentrations. Then a second host is added to a solution of the reference host guest system thus establishing a competitive equilibrium. Since both the binding constant and concentration are known for the reference host-guest complex, the binding constant and concentration of the second host guest complex may be determined by observing the intensity of the reference species.[51]

The above studies indicate that peak intensity is proportional to stability. ESMS shows good correlation between spectral results and known solution behaviour and thus it can be used to determine relative stabilities of host-guest complexes. ESMS provides an efficient, effective and qualitative method of stability assessment which does not require large amounts of compound.

1.5 The Present study

The ligands that are the focus of this study are *N*-(2-diphenylphosphinobenzylidine)-aniline (NP) and *N*-(2-diphenylphosphinobenzylidine)-4'-(benzo-15-crown-5) (O_5NP) (Figure 1.13). O_5NP contains a benzo-15-crown-5 moiety, which remains vacant upon coordination of the ligand to a transition metal ion.

Figure 1.13. The ligands NP and O_5NP.

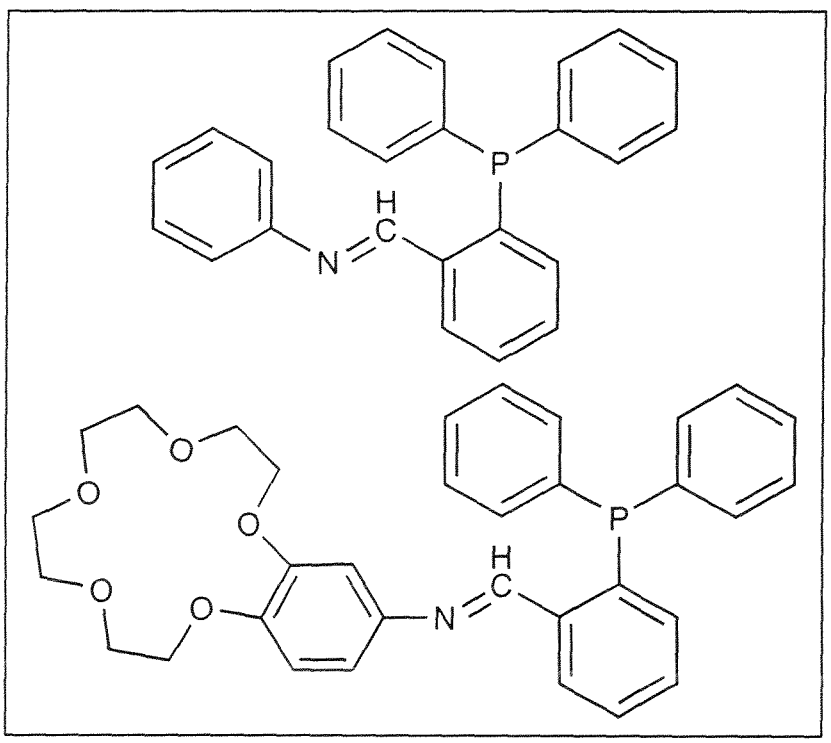

This study aims to investigate:

- The synthesis and characterization of the iminophosphine ligands NP and O_5NP.
- The coordination of both ligands to zerovalent Cr, Mo, W and monovalent Cu, Ag and Au.
- The stoichiometry, coordination number, and geometry of the metal centre.
- The structures of the complexes of the ligands NP and O_5NP.
- The ability of the complexes of O_5NP to bind alkali cations.
- The use of electrospray mass spectroscopy to study the selectivity of the O_5NP complexes.

1.6 References

1. G. Sanchez, J. Vives, J. Serrano, J. Perez and G. Lopez, *Inorg. Chim. Acta.*, 328, (2002), 74-80.
2. G. Sanchez, J. Serrano, M. Moral, J. Perez, E. Molins and G. Lopez, *Polyhedron.*, 18, (1999), 3057-3064.
3. H. Song, Z. Zhang and T. Mak, *Polyhedron.*, 21, (2002), 1043-1050.
4. L. Crociani, G. Bandoli. A. Dolmella, M. Basato and B. Corain, *Eur. J. Inorg. Chem.*, (1998), 1811-1820.
5. P. Wehman, H. van Donge, A. Hagos, P. Kamer and P. van Leeuwen, *J. Organomet. Chem.*, 535, (1997), 183-193.
6. Z. Zhang and H. Cheng, *Coord. Chem. Rev.*, 147, (1996), 1-39.
7. P. Papathanasiou, G. Salem, P. Waring and A. Willis, *J. Chem. Soc., Dalton Trans.*, (1997), 3435-3443.
8. W. Wong, X. Chen, W. Pan, J. Guo and W. Wong, *Eur. J. Inorg. Chem.*, (2002), 231-237.
9. Y. Chen, D. Schiffrin, P. Guerriero and P. Vigato, *Inorg. Chem.*, 33, (1994), 765-769.
10. E. van der Beuken, W. Smeets, A. Spek and B. Feringa, *Chem. Commun.*, (1998), 223-224.
11. H. Yoshida, Y. Honda, E. Shirakawa and T. Hiyama, *Chem. Commun.*, (2001), 1880-1881.
12. R. Rulke, V. Kaasjager, P. Wehman, C. Elsevier, P. van Leeuwen and K. Vrieze, *Organometallics.*, 15, (1996), 3022-3031.
13. F. Tisato, G. Pilloni, F. Refosco, G. Bandoli, C. Corvaja and B. Corain, *Inorg. Chim. Acta.*, 275-276, (1998), 401-409.
14. J. Lehn, *Supramolecular chemistry.* 1995. VCH Verlagsgesellschaft, Weinheim.
15. C. Pedersen, *J. Am. Chem. Soc.*, 89, (1967), 7017-7036.
16. V. Yam, Y. Pui, K. Lo and K. Cheung, *J. Chem. Soc., Dalton Trans.*, (1998), 3615-3621.
17. R. Izatt, J. Bradshaw, S. Nielsen, J. Lamb and J. Christensen, *Chem. Rev.*, 85, (1985), 271-339.
18. G. Gokel, *Crown Ethers and Cryptands.* 1991. The Royal Society of Chemistry, Cambridge.

19. R. Izatt, K. Pawlak and J. Bradshaw, *Chem. Rev.*, 91, (1991), 1721-2085.
20. C. Pedersen, *J. Am. Chen. Soc.*, 92, (1970), 386-391.
21. P. Mallinson and M. Truter, *J. Chem. Soc., Perkin Trans. 2.*, (1972), 1818-1823.
22. J. Owen, *J. Chem. Soc., Dalton Trans.*, (1980), 1066-1067.
23. E. Weber and M. Czugler, *Inorg. Chim. Acta.*, 61, (1982), 33-38.
24. P. Beer, M. Drew, R. Knubley and M. Ogden, *J. Chem. Soc., Dalton Trans.*, (1995), 3117-3123.
25. A. Layton, P. Mallinson, D. Parsons and M. Truter, *J. Chem. Soc., Chem. Comm.*, (1973), 694-695.
26. C. Pedersen and H. Frensdorff, *Angew. Chem., Int. Ed. Engl.*, 11, (1972), 16-25.
27. Y. Takeda, *Bull. Chem. Soc. Jpn.*, 55, (1982), 2040-2041.
28. V. Yam, K. Wong, V. Lee, K. Lo and K. Cheung, *Organometallics.*, 14, (1995), 4034-4036.
29. V. Yam, K. Lo and K. Cheung, *Inorg. Chem.*, 34, (1995), 4013-4014.
30. V. Yam, V. Lee, F. Ke and K. Siu, *Inorg. Chem.*, 36, (1997), 2124-2129.
31. V. Yam, R. Tang, K. Wong, C. Ko and K. Cheung, *Inorg. Chem.*, 40, (2001), 571-574.
32. V. Yam, R. Tang, K. Wong, X. Lu, K. Cheung and N. Zhu, *Chem. Eur. J.*, 8, (2002), 4066-4076.
33. V. Yam, R. Tang, K. Wong and K. Cheung, *Organometallics.*, 20, (2001), 4476-4482.
34. V. Yam, Y. Pui, K. Cheung and N. Zhu, *New J. Chem.*, 26, (2002), 536-542.
35. V. Yam, C. Lam and K. Cheung, *Inorg. Chim. Acta.*, 316, (2001), 19-24.
36. V. Yam, C. Li and C. Chan, *Angew. Chem., Int. Ed. Engl.*, 37, (1998), 2857-2859.
37. A. Tsuda, H. Moriwaki and T. Oshima, *J. Chem. Soc., Perkin Trans. 2.*, (1999), 1235-1240.
38. L. Barg, R. Byrn, M. Carr, D. Nolan, B. Storhoff and J. Huffman, *Organometallics.*, 17, (1998), 1340-1346.
39. C. Nataro, H. Baseski, C. Thomas, B. Wiza and K. Rourke, *Polyhedron.*, 20, (2001), 1023-1028.
40. P. Bernhardt and E. Hayes, *Inorg. Chem.*, 41, (2002), 2892-2902.
41. P. Beer, *Endeavour.*, 16, (1992), 182-189.
42. P. Atkins, *Physical Chemistry.* 1998. Oxford University Press, Oxford.

43. W. Henderson, B. Nicholson and L. McCaffrey, *Polyhedron.*, 17, (1998), 4291-4313.

44. C. Decker. *Electrospray friendly ligands for the mass spectral analysis of transition metal complexes.* DPhil Thesis, 2002, University of Waikato.

45. D. Young, H. Hung and L. Liu, *J. Mass Spec.*, 32, (1997), 432-437.

46. S. Blair, J. Brodbelt, A. Marchand, K. Kumar and H. Chong, *Anal. Chem.*, 72, (2000), 2433-2445.

47. S. Ralph, P. Iannitti, R. Kanitz and M. Sheil, *Eur. Mass Spectrom.*, 2, (1996), 173-179.

48. F. Allain, H. Virelizier, C. Moulin, C. Jankowski, J. Dozol and J. Tabet, *Spectroscopy.*, 14, (2000), 127-139.

49. R. Johnstone, I. Lewis and M. Rose, *Tetrahedron.*, 39, (1983), 1597-1603.

50. D. Young, H. Hung and L. Liu, *Rapid Commun. Mass Spectrom.*, 11, (1997), 769-773.

51. E. Kempen and J. Brobdelt, *Anal. Chem.*, 72, (2000), 5411-5416.

Chapter 2

The Iminophosphine Complexes of Cu(I), Ag(I) and Au(I)

2.1 Introduction

This chapter deals with the synthesis and characterisation of Cu(I), Ag(I) and Au(I) complexes of two iminophosphine ligands *N*-(2-diphenylphosphinobenzylidine)aniline (NP) and *N*-(2-diphenylphosphinobenzylidine)-4'-(benzo-15-crown-5) (O_5NP), the later possessing a crown ether moiety. Unlike the corresponding bidentate N∩N or P∩P ligands fewer studies have been performed on the mixed N∩P systems, but differences in behaviour may be expected due to this system having both semi-hard and soft donor atoms.

The coordination characteristics of the ligand were obtained by X-ray structural analyses of $[M(NP)_2][PF_6]$ (M = Cu(I), Ag(I), Au(I)), $[Cu(NP)Br]_2$ and Au(NP)X (X = Cl, Br). Far and Near IR, ESMS and NMR spectra provided further structural information.

2.2 Experimental

2.2.1 Instrumentation

^{1}H and ^{31}P NMR spectra were obtained in 5mm grade 527-PP sample tubes on a Bruker Avance 400 MHz spectrometer. The NMR solvent for the ligands and the copper, silver and gold complexes was $CDCl_3$ supplied by Merck. The internal standard for ^{1}H was TMS. The external standard for ^{31}P was 85% H_3PO_4. ^{1}H NMR spectra were collected at a frequency of 400 MHz and ^{31}P NMR spectra at 162 MHz.

Infrared (IR) spectra were obtained on a FT-IR Perkin-Elmer Paragon 1000 spectrometer as nujol mulls between NaCl disks. Far IR was performed at Chemistry Department, Auckland University on a Bio-Rad Win-IR.

X-ray data was collected at the Chemistry Department, Auckland University. X-ray structures were solved by Dr. Andreas Derwahl.

Elemental analyses for carbon, hydrogen and nitrogen were performed by the Campbell Microanalytical Laboratory, University of Otago, Dunedin.

Electrospray mass spectra were obtained using a Micromass ZMD ESMS quadrupole spectrometer with CH_3CN as the solvent and mobile phase.

2.2.2 Materials

All solvents were AR grade, except where otherwise stated, and supplied by commercial suppliers. All were used without further purification except for toluene, which was dried over sodium, and MeOH, dried over molecular sieves. The starting materials were provided by commercial suppliers: 2-(diphenylphosphino)benzaldehyde (2PCHO) and aniline ($ArNH_2$) from Aldrich, 4'-aminobenzo-15-crown-5 (O_5NH_2) was provided by Fluka. Starting complexes $[M(CH_3CN)_4][PF_6]$ (M = Cu, Ag), CuX, AgX and $[NBu_4][AuX_2]$ (X = Cl, Br, I) were provided by Graeme Freeman, Massey University.

2.2.3 The Ligands

2.2.3.1 *N*-(2-diphenylphosphinobenzylidine)aniline (NP)

2-(diphenylphosphino)benzaldehyde (2PCHO) (2.549 g, 8.78 mmol) and aniline ($ArNH_2$) (1.712 g, 18.38 mmol) in MeOH (60 ml) with 3 Å molecular sieves (~3 g) were refluxed under N_2 for 3 hours with constant stirring. Upon cooling the solid was separated and the filtrate collected. The white solid was then washed with $CHCl_3$ giving a yellow solution, which was taken to dryness giving a yellow oil. The oil was recrystallised from toluene and hexane and dried *in vacuo* giving the product as bright yellow crystals. ESMS: $[MH]^+$ - 366 (26%). Analysis: found: C, 82.05; H, 5.81; N, 3.89%. Calculated for $C_{25}H_{20}NP$: C, 82.17; H, 5.52; N, 3.83%. M.p. 115-117°C (lit 106-108°C[1]). Yield 1.57 g, 4.30 mmol, 49%.

2.2.3.2 *N*-(2-diphenylphosphinobenzylidine)-4'-(benzo-15-crown-5) (O_5NP)

2PCHO (0.504 g, 1.74 mmol), 4'-aminobenzo-15-crown-5 (O_5NH_2) (0.49 g, 1.73 mmol), *p*-toluene sulfonic acid (27 mg) and 3 Å molecular sieves (~3 g) were refluxed in toluene (30 ml) with constant stirring under N_2 for 7 hours. While hot, the molecular sieves were removed and the solution was reduced in volume to give the crude product as a yellow oil. The oil was dissolved in boiling hexane and was decanted, leaving solid

impurities. The hexane was removed *in vacuo* giving the product as a bright yellow oil which was kept at 4°C for 2 days and then converted to a solid by trituration in ice-cold hexane. The solid was dried *in vacuo* giving the product as a yellow powder. A second crop was obtained from the washings. ESMS: $[MH]^+$ - 556 (87%). Analysis: found: C, 71.23; H, 6.43; N, 2.50%. Calculated for $C_{33}H_{34}NO_5P$: C, 71.34; H, 6.17; N, 2.52%. M.p. 117-119°C. Yield: 0.789 g, 1.42 mmol, 85%.

2.2.4 The complexes of copper

2.2.4.1 Preparation of $[Cu(NP)_2][PF_6]$

NP (0.276 g, 0.76 mmol) with $[Cu(CH_3CN)_4][PF_6]$ (0.143 g, 0.38 mmol) was mixed in CH_2Cl_2:EtOH (1:1, 30 ml). The solution became red immediately. The reaction was refluxed under N_2 with stirring for 7 minutes. The reaction was then stirred for 1 hour at RT. The volume was reduced and the crude product isolated on addition of hexane. The product was obtained by slow recrystallization from hot CH_2Cl_2/Et_2O and dried *in vacuo* giving an orange powder. ESMS: $[M\text{-}PF_6]^+$ - 794 (73%). Analysis: found: C, 60.43; H, 3.88; N, 2.88%. Calculated for: $CuC_{50}H_{40}N_2P_3F_6.¾CH_2Cl_2$: C, 60.77; H, 4.17; N, 2.79%. Yield: 0.266 g, 0.28 mmol, 73%.

2.2.4.2 Preparation of $[Cu(NP)Cl]_2$

NP (0.164 g, 0.45 mmol) and CuCl (0.040 g, 0.40 mmol) were mixed in $CHCl_3$ (10 ml) giving an orange solution. Upon stirring under reflux for 10 minutes all the CuCl dissolved, giving a dark red solution. The volume was reduced and the solution placed in an ice bath. Cold hexane was added giving a dark red oil. The hexane:$CHCl_3$ layer was decanted off and Et_2O added causing the oil to solidify. The product was dried *in vacuo* giving a dark red powder. ESMS: $[Cu_2(NP)_2Cl]^+$ - 893 (<1%). Analysis: found: C, 64.26; H, 4.07; N, 3.08%. Calculated for: $Cu_2C_{50}H_{40}N_2P_2Cl_2$: C, 64.66; H, 4.34; N, 3.02%. Yield: 0.115 g, 0.12 mmol, 60%.

2.2.4.3 Preparation of $[Cu(NP)Br]_2$

NP (0.149 g, 0.41 mmol) and CuBr (0.056 g, 0.39 mmol) were mixed in $CHCl_3$ (5 ml) giving an orange solution that became dark red. When no more reaction was evident the solid impurities were filtered off and the volume reduced. Et_2O was added giving dark red microcrystals. These were recrystallised from $CHCl_3/Et_2O$ and dried *in vacuo* giving the product as dark red crystals. ESMS: $[Cu_2(NP)_2Br]^+$ - 937 (<1%). Analysis: found: C, 57.45; H, 3.68; N, 2.60%. Calculated for: $Cu_2C_{50}H_{40}N_2P_2Br_2.¼CHCl_3$: C, 57.61; H, 3.87; N, 2.67%. Yield: 0.129 g, 0.13 mmol, 67%.

2.2.4.4 Preparation of $[Cu(NP)I]_2$

NP (0.151 g, 0.41 mmol) and CuI (0.078 g, 0.41 mmol) were mixed in $CHCl_3$ (5 ml) giving a yellow solution. The reaction was stirred for 3 hours producing a pale orange suspension that was isolated and washed with Et_2O giving the product as orange flakes which were dried *in vacuo*. ESMS: $[Cu_2(NP)_2I]^+$ - 984 (<1%). Analysis: found: C, 51.55; H, 3.12; N, 2.65%. Calculated for: $Cu_2C_{50}H_{40}N_2P_2I_2.½CHCl_3$: C, 51.78; H, 3.48; N, 2.39%. Yield: 0.211 g, 0.19 mmol, 93%.

2.2.4.5 Preparation of $[Cu(O_5NP)_2][PF_6]$

O_5NP (0.206 g, 0.371 mmol) and $[Cu(CH_3CN)_4][PF_6]$ (0.070 g, 0.19 mmol) in CH_2Cl_2 (30 ml) gave a red solution. The volume was reduced and Et_2O added. The product was isolated and dried *in vacuo* giving an orange-brown powder. ESMS: $[Cu(O_5NP)_2]^+$ - 1174 (39%). Analysis: found: C, 58.54; H, 4.79; N, 2.19%. Calculated for: $CuC_{66}H_{68}N_2O_{10}P_3F_6.½CH_2Cl_2$: C, 58.64; H, 5.11; N, 2.06%. Yield: 0.205 g, 0.16 mmol, 86%.

2.2.4.6 Preparation of $[Cu(O_5NP)Cl]_2$

O_5NP (0.204 g, 0.37 mmol) and CuCl (0.036 g, 0.36 mmol) in $CHCl_3$ (7 ml) gave a red solution. The reaction was refluxed under N_2 with stirring for 10 minutes then stirred at RT for 1 hour giving a dark red colour. The volume was reduced and Et_2O added. The

product was isolated and dried *in vacuo* giving a dark red powder. ESMS: $[Cu_2(O_5NP)_2Cl]^+$ - 1273 (<1%). Analysis: found: C, 58.52; H, 4.94; N, 2.48%. Calculated for: $Cu_2C_{66}H_{68}N_2O_{10}P_2Cl_2.½CHCl_3$: C, 58.35; H, 5.04; N, 2.05%. Yield: 0.162 g, 0.12 mmol, 68%.

2.2.5 The complexes of silver

2.2.5.1 Preparation of $[Ag(NP)_2][PF_6]$

NP (0.219 g, 0.60 mmol) and $[Ag(CH_3CN)_4][PF_6]$ (0.134 g, 0.32 mmol) were refluxed in CH_2Cl_2:EtOH (1:1, 30 ml) under N_2 with stirring for 10 minutes then stirred at RT for 1.5 hours giving a cloudy lime green solution. Solid impurities were removed and the filtrate reduced in volume. A small amount of Et_2O was added and the solution placed overnight in the fridge. The product was isolated, washed with Et_2O and dried *in vacuo* giving yellow/green crystals. ESMS: $[Ag(NP)_2]^+$ - 839.5 (39%). Analysis: found: C, 59.65; H, 4.08; N, 2.88%. Calculated for: $AgC_{50}H_{40}N_2P_3F_6.{}^1/_3CH_2Cl_2$: C, 59.74; H, 4.05; N, 2.77%. Yield: 0.241 g, 0.25 mmol, 76%.

2.2.5.2 Preparation of $[Ag(NP)Cl]_2$

NP (0.151 g, 0.41 mmol) and AgCl (0.059 g, 0.41 mmol) in CH_3CN (10 ml) was refluxed for 24 hours with stirring, under N_2. Solid impurities were removed and the volume reduced. Hexane was added giving the crude product as an oil. Trituration of the oil in Et_2O gave the product as a pale yellow powder. The product was dried *in vacuo.* ESMS: $[Ag_2(NP)_2Cl]^+$ - 981 (1%). Analysis: found: C, 58.29; H, 3.72; N, 2.69%. Calculated for: $Ag_2C_{50}H_{40}N_2P_2Cl_2$: C, 59.02; H, 3.96; N, 2.75%. Yield: 0.111 g, 0.08 mmol, 39%.

2.2.5.3 Preparation of $[Ag(NP)Br]_2$

NP (0.101 g, 0.28 mmol) and AgBr (0.052 g, 0.27 mmol) in CH_3CN (5 ml) were refluxed under N_2 with stirring for 3 hours. Another 24 hours of stirring gave a yellow suspension. The suspension was isolated and dried *in vacuo* giving the product as a pale yellow powder. ESMS: $[Ag_2(NP)_2Br]^+$ - 1027 (2%). Analysis: found: C, 54.07; H, 3.39;

N, 2.52%. Calculated for: $Ag_2C_{50}H_{40}N_2P_2Br_2$: C, 54.28; H, 3.64; N, 2.53%. Yield: 0.072 g, 0.05 mmol, 37%.

2.2.5.4 Preparation of $[Ag(NP)I]_2$

NP (0.107 g, 0.29 mmol) and AgI (0.066 g, 0.28 mmol) in CH_3CN (5 ml) were refluxed under N_2 with stirring for 24 hours. A bright yellow precipitate formed. The volume was reduced and hexane added. The product was isolated and dried *in vacuo* giving bright yellow microcrystals. Analysis: found: C, 49.12; H, 2.94; N, 2.40%. Calculated for: $Ag_2C_{50}H_{40}N_2P_2I_2$: C, 50.03; H, 3.36; N, 2.33%. Yield: 0.132 g, 0.08 mmol, 57%.

2.2.5.5 Preparation of $[Ag(O_5NP)_2][PF_6]$

O_5NP (0.157 g, 0.28 mmol) and $[Ag(CH_3CN)_4][PF_6]$ (0.058 g, 0.14 mmol) in CH_2Cl_2 (30 ml) were refluxed under N_2 with stirring for 45 minutes and then stirred at RT for 3 hours. The volume was reduced and Et_2O was added. The product was isolated and dried *in vacuo* giving a pale yellow powder. ESMS: $[Ag(O_5NP)_2]^+$ - 1219 (6%). Analysis: found: C, 57.57; H, 5.13; N, 1.87. Calculated for: $AgC_{66}H_{68}N_2O_{10}P_3F_6.¼CH_2Cl_2$: C, 57.44; H, 4.98; N, 2.02%. Yield: 0.149 g, 0.18 mmol, 78%.

2.2.5.6 Preparation of $[Ag(O_5NP)Cl]_2$

O_5NP (0.204 g, 0.37 mmol) and AgCl (0.054 g, 0.38 mmol) in CH_3CN (5 ml) were refluxed under N_2 with stirring for 24 hours. The volume was reduced resulting in precipitation of the product. It was isolated and dried *in vacuo* giving a bright yellow powder. ESMS: $[Ag_2(O_5NP)_2Cl]^+$ - 1273 (<1%). Analysis: found: C, 56.59; H, 4.77; N, 2.22%. Calculated for: $Ag_2C_{66}H_{68}N_2O_{10}P_2Cl_2$: C, 56.71; H, 4.90; N, 2.00%. Yield: 0.196 g, 0.12 mmol, 65%.

2.2.6 *The complexes of gold*

2.2.6.1 Preparation of $[Au(NP)_2][PF_6]$

NP (0.155 g, 0.42 mmol) and $[NBu_4][AuCl_2]$ (0.107 g, 0.21 mmol) in CH_2Cl_2 (5 ml) were heated under N_2 with stirring until boiling occurred. The solution was then stirred for 1 hour without heating. The CH_2Cl_2 solution was washed with H_2O (3×20 ml) and then dried over $MgSO_4$. $[Ag(CH_3CN)_4][PF_6]$ (0.158 g, 0.37 mmol) was added and the AgCl that formed was removed by filtration. The filtrate was washed with H_2O (20 ml) and then dried over $MgSO_4$. The product recrystallised from CH_2Cl_2/Et_2O and dried *in vacuo* to give pale yellow crystals. ESMS: $[Au(NP)_2]^+$ - 937.19 (100%). Analysis: found: C, 52.87; H, 3.49; N, 2.35%. Calculated for: $AuC_{50}H_{40}N_2P_3F_6$: C, 52.91; H, 3.66; N, 2.42%. Yield: 0.131 g, 0.12 mmol, 57%.

2.2.6.2 Preparation of Au(NP)Cl

NP (0.102 g, 0.28 mmol) with $[NBu_4][AuCl_2]$ (0.140 g, 0.27 mmol) in $CHCl_3$ (4 ml) was refluxed under N_2 with stirring for 2 hours. The volume was reduced and hexane added. The product was isolated and dried *in vacuo* giving a yellow powder. ESMS $[Au(NP)]^+$ - 562.1 (1%). Analysis: found: C, 46.81; H, 2.69; N, 2.23%. Calculated for: $AuC_{25}H_{20}NPCl.½CHCl_3$: C, 46.58; H, 3.14; N, 2.13%. Yield: 0.150 g, 0.25 mmol, 93%.

2.2.6.3 Preparation of Au(NP)Br

NP (0.106 g, 0.29 mmol) and $[NBu_4][AuBr_2]$ (0.167 g, 0.28 mmol) in $CHCl_3$ (4 ml) were refluxed for 1.5 hours under N_2 with stirring. The volume was reduced and hexane added. After 2 hours the product was isolated, washed with hexane and dried *in vacuo* giving yellow crystals. ESMS $[Au(NP)]^+$ - 562.1 (<1%). Analysis: found: C, 43.87; H, 2.60; N, 2.08%. Calculated for: $AuC_{25}H_{20}NPBr.½CHCl_3$: C, 43.63; H, 2.94; N, 2.00%. Yield: 0.159 g, 0.25 mmol, 89%.

2.2.6.4 Preparation of Au(NP)I

NP (0.106 g, 0.29 mmol) and $[NBu_4][AuI_2]$ (0.182 g, 0.26 mmol) in $CHCl_3$ (4 ml) were refluxed under N_2 with stirring for 1 hour. The volume was reduced and hexane added. After 2 hours the product was isolated, washed with hexane and dried *in vacuo* giving red crystals. ESMS $[Au(NP)]^+$ - 562.1 (<1%). Analysis: found: C, 40.24; H, 2.45; N, 1.95%. Calculated for: $AuC_{25}H_{20}NPI.½CHCl_3$: C, 40.89; H, 2.76; N, 1.87%. Yield: 0.112 g, 0.16 mmol, 62%.

2.2.6.5 Preparation of $[Au(O_5NP)_2][PF_6]$

O_5NP (0.207 g, 0.37 mmol) and $[NBu_4][AuCl_2]$ (0.097 g, 0.19 mmol) in CH_2Cl_2 (7 ml) were heated under N_2 with stirring until boiling occurred. The heat was removed and the reaction stirred for 1 hour. $[Ag(CH_3CN)_4][PF_6]$ (0.086 g, 0.21 mmol) was added and the reaction stirred for 0.5 hour. Further $[Ag(CH_3CN)_4][PF_6]$ (0.080 g, 0.19 mmol) was added and the solution stirred for 1 hour. AgCl was removed by filtration through kieselguhr. The CH_2Cl_2 filtrate was washed with H_2O (3×20 ml) and then dried over $MgSO_4$. The volume was reduced and Et_2O added thus precipitating the product, which was isolated and dried *in vacuo* giving a bright yellow powder. ESMS: $[Au(O_5NP)_2]^+$ - 1307.31 (33%). Analysis: found: C, 54.52; H, 4.77; N, 1.87%. Calculated for: $AuC_{66}H_{68}N_2O_{10}P_3F_6$: C, 54.55; H, 4.72; N, 1.93%. Yield: 0.183 g, 0.13 mmol, 70%.

2.2.6.6 Preparation of $Au(O_5NP)Cl$

O_5NP (0.206 g, 0.56 mmol) and $[NBu_4][AuCl_2]$ (0.185 g, 0.36 mmol) in CH_2Cl_2 (7.5 ml) were refluxed under N_2 with stirring for 45 minutes. The volume was reduced and Et_2O added to give a precipitate. The product was isolated, dissolved in CH_2Cl_2 (10 ml) and washed with H_2O (4×20 ml). The addition of Et_2O affected precipitation and the product was isolated and dried *in vacuo*. ESMS $[Au(O_5NP)]^+$ - 752.17 (34%). Analysis: found: C, 50.20; H, 4.37; N, 1.60%. Calculated for: $AuC_{33}H_{34}NO_5P_2F_6$: C, 50.30; H, 4.35; N, 1.78%. Yield: 0.173 g, 0.22 mmol, 79%.

2.3 Results and Discussion

2.3.1 Synthesis

2.3.1.1 Synthesis of the Ligands

The ligands NP and O_5NP were both produced by a Schiff base reaction between an aldehyde and a primary amine (Scheme 2.1).

Scheme 2.1. A Schiff base condensation reaction.

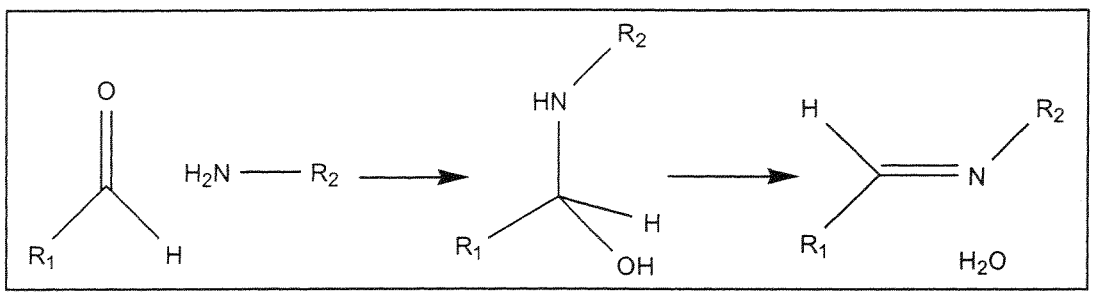

Initially the ligand NP was produced by a method based on a procedure of Wehman *et al.*[1] that required 18 hours of refluxing in toluene. It was later found that a method by Chen *et al.*,[2] which used methanol, produced a higher purity product and required only three hours of reflux.

A procedure similar to that of Wehman *et al.*[1] was used to synthesise the O_5NP ligand. To maximize the yield the crude reaction product was extracted into hot hexane.

2.3.1.2 Synthesis of the Complexes

The copper and silver complexes $[M(L)_2][PF_6]$ (M = Cu, Ag; L = NP, O_5NP) were produced by the displacement of acetonitrile by NP or O_5NP from the appropriate $[M(CH_3CN)_4][PF_6]$ salt. The reactions proceeded immediately upon mixing of the reactants with heating being applied for a short time. In all cases diethylether was used to effect precipitation.

For the gold complexes $[Au(L)_2][PF_6]$ the acetonitrile precursor was unavailable. Instead $[NBu_4][AuCl_2]$ was reacted with the appropriate ligand in a 1:2 ratio in CH_2Cl_2 to produce $Au(L)_2Cl$. The side product $[NBu_4]Cl$ was removed by washing the CH_2Cl_2 solution with H_2O. Reaction of $Au(L)_2Cl$ with $[Ag(CH_3CN)_4][PF_6]$ effected the

precipitation of AgCl and production of $[Au(L)_2][PF_6]$. Adequate yields were obtained by this method.

The halo complexes $[M(L)X]_2$ (M = Cu, Ag) and AuLX (L = NP, O_5NP; X = Cl, Br, I) were produced by reaction of the free ligand with the appropriate metal halide salt. The reactants were refluxed and/or stirred in either $CHCl_3$, for copper and gold halides, or CH_3CN, for the silver halides. In most cases the yield was above 50%.

2.3.2 Crystal structures

2.3.2.1 The Structure of O_5NP

The structure of *N*-(2-diphenylphosphinobenzylidine)-4'-(benzo-15-crown-5), (O_5NP) was determined by X-ray crystallography (Figure 2.1). The crystals were grown from a n-heptane extract over several weeks. For structure refinement and crystal data see Table 2.1, selected bond lengths and angles Table 2.2 and Table 2.3 for selected torsion angles.

The imine bond (N=C) has an *E* conformation, with the largest groups *trans* to each other across the double bond to minimize steric interactions. It has a length of 1.264(4) Å which is in the range found for similar ligands (1.442-1.230 Å[2-10]) but shorter than a formal imine bond of 1.32 Å.[11] The N—C(1) bond length of 1.413(4) Å and the C—C(112) bond length of 1.456(5) Å are as expected for single bonds. The bond angles about the imine bond, C-N-C(1) 117.1(3)° and N-C-C(112) 123.7(3)° fall into the acceptable range.

The benzo-15-crown-5 moiety has average CH_2—O and Bz—O bond lengths of 1.419 Å and 1.357 Å respectively. Both these values compare well with similar benzo-15-crown-5 compounds that have CH_2—O bond lengths of 1.356-1.472 Å and Bz—O bond lengths of 1.332-1.389 Å. The C-O-C angles of O_5NP have an average of 113.1° that also compares well with the literature range of 106.3-120.8°.[12-17] However the C(13)-O(4A)-C(12) angle (153.3(17)°) is large due to disorder within the crystal

Since the aromatic carbon C(111) has rigid bond angles and is attached to the phosphorus atom, the position of C(111) gives a good indication of the position and orientation of P. The torsion angle N-C-C(112)-C(111) 176.7(3)° shows that C(111) is on the opposite side from the nitrogen atom, relative to the C-C(112) bond, and hence so is the phosphorus atom. This is evident from Figure 2.1. The orientation of the nitrogen and phosphorus atoms may result from a need to minimize the interaction between the lone electron pairs. The C-N-C(1)-C(2) torsion angle of 138.5(3)° shows that the aromatic ring and the attached crown are twisted away from planarity with the imine bond while the C(1)-N-C-C(112) torsion angle of 178.2(3)° shows the imine bond to be planar in the chain.

Figure 2.1. ORTEP diagram of O_5NP. Thermal ellipsoids are at 50% probability.

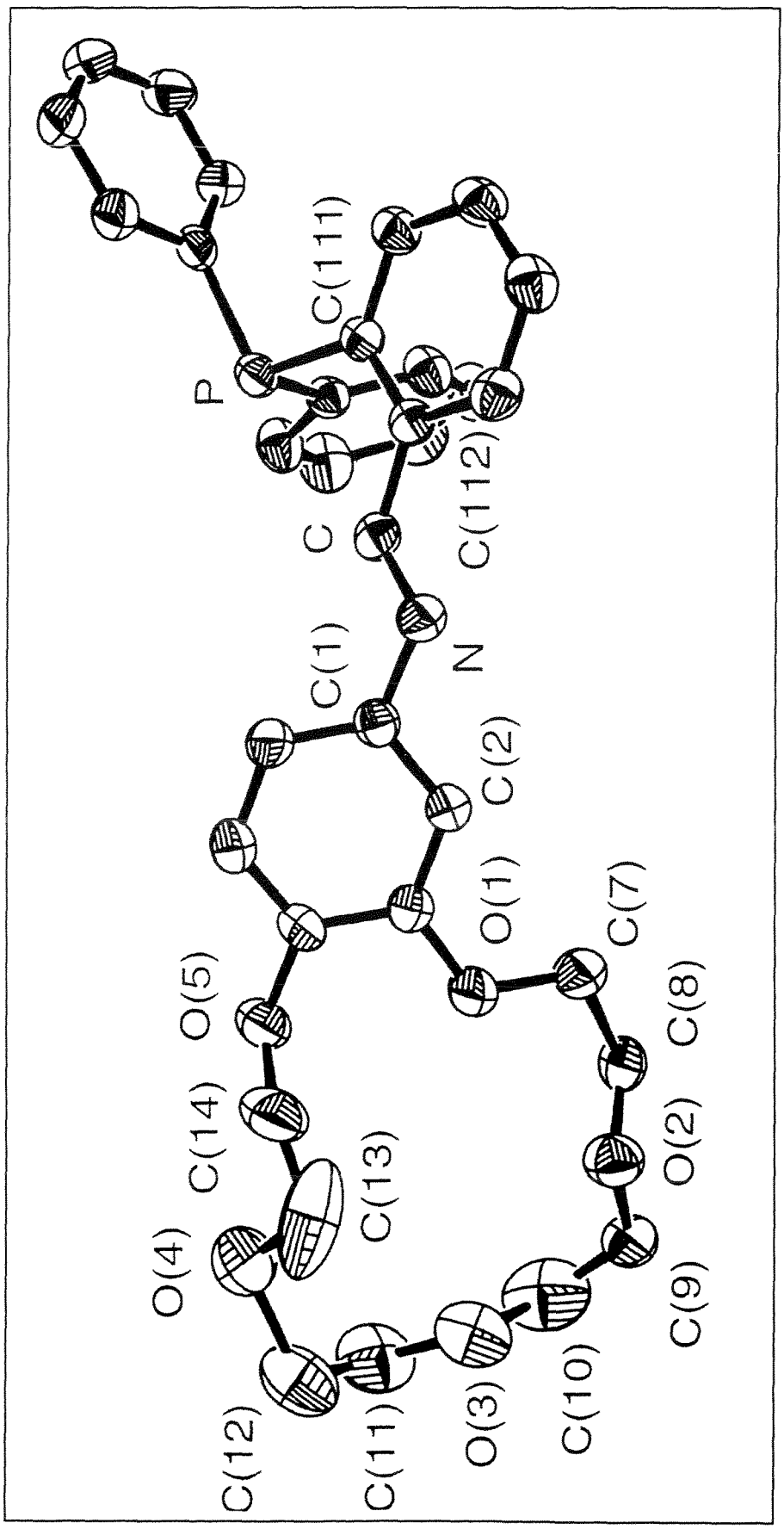

Table 2.1. Crystal data and structure refinement for O_5NP.

Identification code	amb3	
Empirical formula	$C_{33}H_{40}NO_5P$	
Formula weight	561.63	
Temperature	293(2) K	
Wavelength	0.71073 A	
Crystal system, space group	Triclinic, P-1	
Unit cell dimensions	a = 10.084(4) Å	α = 94.75(2)°
	b = 10.784(4) Å	β = 102.88(5)°
	c = 13.878(6) Å	γ = 94.62(3)°
Volume	1458.5(10) $Å^3$	
Z, Calculated density	2, 1.279 Mg/m^3	
Absorption coefficient	0.137 mm^{-1}	
F(000)	600	
Crystal size	0.16 x 0.12 x 0.10 mm	
Theta range for data collection	1.51 to 19.98°	
Limiting indices	$0 \le h \le 9$, $-10 \le k \le 10$, $-13 \le l \le 13$	
Reflections collected / unique	2930 / 2722 [R(int) = 0.0146]	
Completeness to theta = 0.50	0.0 %	
Absorption correction	Empirical via \y scans	
Max. and min. transmission	0.9865 and 0.9785	
Refinement method	Full-matrix least-squares on F^2	
Data / restraints / parameters	2722 / 0 / 406	
Goodness-of-fit on F^2	1.034	
Final R indices [I>2sigma(I)]	R1 = 0.0465, wR2 = 0.1334	
R indices (all data)	R1 = 0.0556, wR2 = 0.1432	
Largest diff. peak and hole	0.212 and -0.203 $e.A^{-3}$	

Table 2.2. Selected bond lengths (Å) and angles (°) for O_5NP.

N-C	1.264(4)	N-C(1)	1.413(4)
P-C(131)	1.832(3)	C-C(112)	1.456(5)
P-C(111)	1.857(3)	P-C(121)	1.807(4)
C(4)-O(5)	1.370(4)	C(7)-O(1)	1.380(5)
C(8)-O(2)	1.340(10)	C(9)-O(2)	1.412(9)
C(10)-O(3)	1.409(8)	C(11)-O(3)	1.402(6)
C(12)-O(4)	1.699(16)	C(13)-O(4)	1.321(19)
C(14)-O(5)	1.386(6)	C(3)-O(1)	1.343(4)
C(121)-P-C(131)	102.16(15)	N-C-C(112)	123.7(3)
C(131)-P-C(111)	102.31(14)	C-N-C(1)	117.1(3)
C(121)-P-C(111)	102.66(15)	C(3)-O(1)-C(7)	120.1(3)
C(8)-O(2)-C(9)	111.5(8)	C(11)-O(3)-C(10)	114.1(6)
C(13)-O(4A)-C(12)	153.3(17)	C(4)-O(5)-C(14)	115.3(3)

Table 2.3. Selected torsion angles (°) for O_5NP.

C(1)-N-C-C(112)	178.2(3)
N-C-C(112)-C(111)	176.7(3)
C-N-C(1)-C(2)	138.5(3)

2.3.2.2 The Structure of $[Cu(NP)_2][PF_6]$

The copper has a tetrahedral coordination with both NP ligands acting in a bidentate manner through the phosphorus and imine nitrogen atoms (Figure 2.2). Structure refinement and crystal data are in Table 2.4, selected bond lengths and angles in Table 2.5 and selected torsion angles in Table 2.6. Crystals were obtained from slow recrystallization of the complex from CH_2Cl_2 layered with Et_2O. The Cu(1)-P(2) 2.2174(11) Å and Cu(1)-P(1) 2.2205(11) Å bond lengths are in agreement with similar compounds.[18,19] The Cu-P bond lengths are similar, however, the Cu-N bond lengths, Cu(1)-N(1) 2.145(3) Å and Cu(1)-N(2B) 2.063(8) Å are significantly different. The chelate angles N(1)-Cu(1)-P(1) 84.32(10)° and N(2B)-Cu(1)-P(2) 92.1(2)° are smaller than the normal tetrahedral angle of 109.5° due to the chelate ring. The angle between the two nitrogen atoms N(2B)-Cu(1)-N(1) 86.6(3)° is also small. Subsequently some of the other angles about the Cu(1) are large, such as P(2)-Cu(1)-P(1) 133.01(4)°, the steric hindrance of the phenyl groups may also influence this angle. Due to the unique nature of this complex and its coordination it is difficult to find appropriate comparisons for this complex. However a series of Cu(I) imine complexes have Cu—N lengths of 2.118(9), 2.106(5) and 2.095(7) Å[18,20] which compare well with this compound.

The imine bonds have lengths of C(19)-N(1) 1.276(5) Å and C(44B)-N(2B) 1.311(15) Å which fall within the expected range (1.442(3)-1.230(1) Å[2-10]) for coordinated imines. The angles around the imine bonds are as expected with the angles about the N atom being smaller than those about the C atom in both cases.

The torsion angles of C(18)-C(19)-N(1)-C(20) -179.5(4)° and C(43B)-C(44B)-N(2B)-C(45B) -176.0(12)° show the aromatic rings are *trans* across the double bond, giving an *E* conformation, for both ligands. The P atom is on the same side as the N atom relative to the C(13)-C(18)-C(19) moiety shown by C(13)-C(18)-C(19)-N(1) 14.5(7)° and C(38B)-C(43B)-C(44B)-N(2B) 0(2)°.

Figure 2.2. ORTEP diagram of $[Cu(NP)_2][PF_6]$. Thermal ellipsoids are at 50% probability. The PF_6^- ion and solvent have been admitted for clarity.

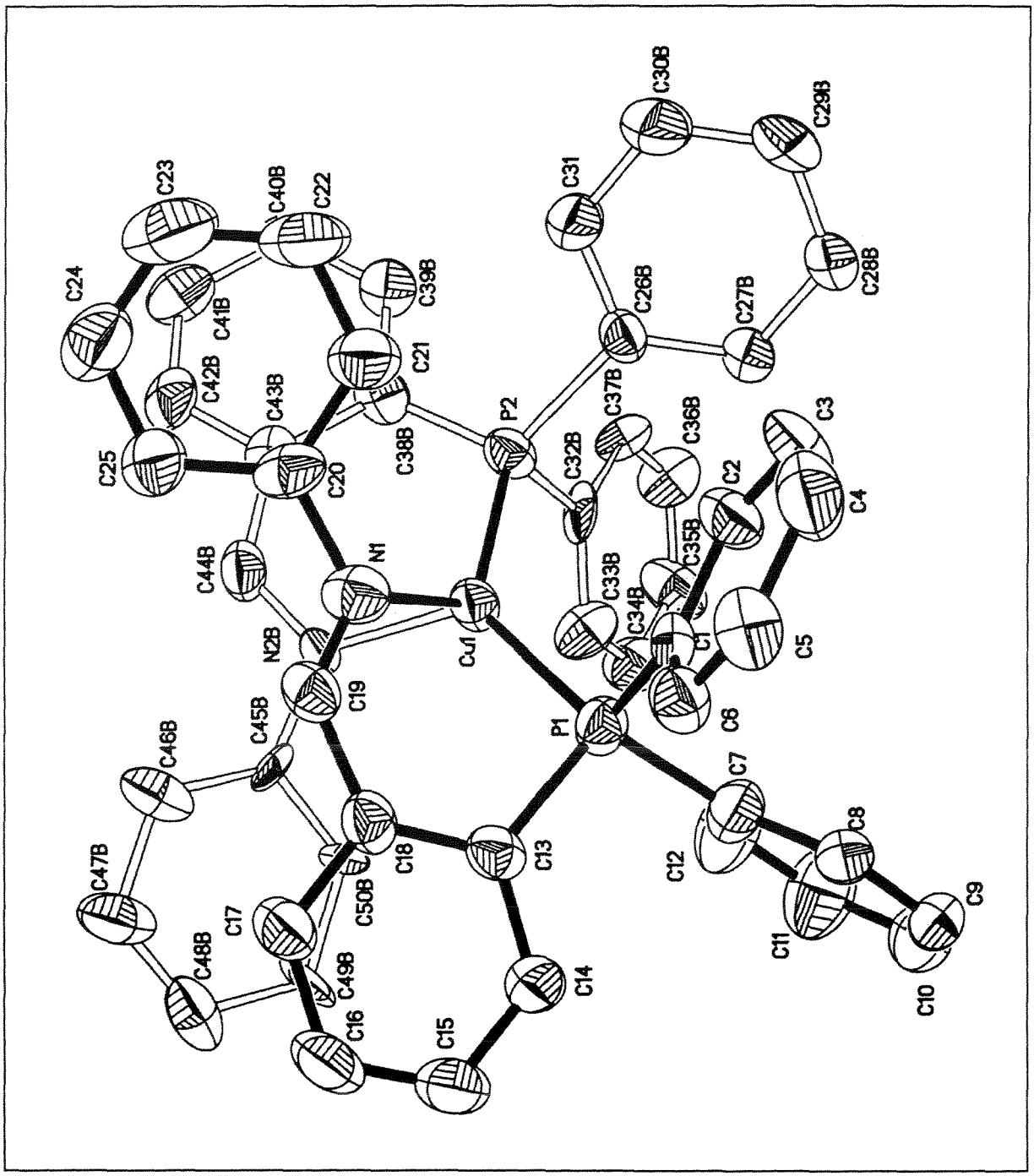

Table 2.4. Crystal data and structure refinement for $[Cu(NP)_2][PF_6]$.

Identification code	squeezed	
Empirical formula	$C_{50}H_{40}CuN_2P_2$	
Formula weight	794.32	
Temperature	150(2) K	
Wavelength	0.71073 Å	
Crystal system	Monoclinic	
Space group	P2(1)/c	
Unit cell dimensions	a = 14.0805(2) Å	α= 90°
	b = 19.9011(3) Å	β= 107.17(10)°
	c = 17.5943(2) Å	γ = 90°
Volume	4710.50(11) Å^3	
Z	4	
Density (calculated)	1.120 Mg/m^3	
Absorption coefficient	0.564 mm^{-1}	
F(000)	1652	
Crystal size	0.38 x 0.24 x 0.16 mm^3	
Theta range for data collection	1.51 to 25.16°	
Index ranges	$-16 \le h \le 16, 0 \le k \le 23, 0 \le l \le 21$	
Reflections collected	8345	
Independent reflections	8345 [R(int) = 0.0000]	
Completeness to theta = 25.16°	98.9 %	
Absorption correction	None	
Max. and min. transmission	0.9152 and 0.8143	
Refinement method	Full-matrix least-squares on F^2	
Data / restraints / parameters	8345 / 992 / 687	
Goodness-of-fit on F^2	1.086	
Final R indices [I>2sigma(I)]	R1 = 0.0616, wR2 = 0.1597	
R indices (all data)	R1 = 0.0891, wR2 = 0.1717	
Largest diff. peak and hole	1.167 and -0.936 e.Å^{-3}	

Table 2.5. Selected bond lengths (Å) and angles (°) for $[Cu(NP)_2][PF_6]$.

Cu(1)-N(1)	2.145(3)	N(1)-Cu(1)-P(1)	84.32(10)
Cu(1)-P(1)	2.2205(11)	N(1)-Cu(1)-P(2)	124.76(10)
P(1)-C(1)	1.821(4)	P(2)-Cu(1)-P(1)	133.01(4)
P(1)-C(7)	1.833(4)	N(1)-C(19)-C(18)	124.9(4)
P(1)-C(13)	1.834(4)	C(19)-N(1)-C(20)	119.2(4)
C(18)-C(19)	1.447(6)	C(1)-P(1)-C(7)	104.66(19)
C(19)-N(1)	1.276(5)	C(1)-P(1)-C(13)	103.37(18)
N(1)-C(20)	1.446(5)	C(7)-P(1)-C(13)	104.7(2)
Cu(1)-N(2B)	2.063(8)	N(2B)-Cu(1)-P(2)	92.1(2)
Cu(1)-P(2)	2.2174(11)	N(2B)-Cu(1)-P(1)	129.1(2)
P(2)-C(38B)	1.702(15)	N(2B)-Cu(1)-N(1)	86.6(3)
P(2)-C(26B)	1.872(15)	N(2B)-C(44B)-C(43B)	126.3(11)
P(2)-C(32B)	1.933(16)	C(44B)-N(2B)-C(45B)	116.4(10)
C(43B)-C(44B)	1.417(17)	C(38B)-P(2)-C(26B)	112.5(7)
C(44B)-N(2B)	1.311(15)	C(38B)-P(2)-C(32B)	103.5(3)
N(2B)-C(45B)	1.419(14)	C(26B)-P(2)-C(32B)	102.1(6)

Table 2.6. Selected torsion angles (°) for $[Cu(NP)_2][PF_6]$.

C(18)-C(19)-N(1)-C(20)	-179.5(4)
C(19)-N(1)-C(20)-C(21)	135.2(4)
C(13)-C(18)-C(19)-N(1)	14.5(7)
C(43B)-C(44B)-N(2B)-C(45B)	-176.0(12)
C(44B)-N(2B)-C(45B)-C(50B)	137.2(11)
C(38B)-C(43B)-C(44B)-N(2B)	0(2)

2.3.2.3 The Structure of $[Ag(NP)_2][PF_6]$

The structure of the complex is shown in Figure 2.3. The crystal and refinement data are in Table 2.7 with selected bond lengths and angles in Table 2.8 and selected torsion angles in Table 2.9. Hydrogen bonds are given in Table 2.10. Crystals were grown from CH_2Cl_2 with an equal volume of Et_2O. The silver has a distorted trigonal planar geometry with one chelating ligand and a monodentate ligand binding through the phosphorus atom P(1B). The chelate angle P(1A)-Ag(1)-N(20A) 77.25(5)° is much smaller than the P(1B)-Ag(1)-P(1A) 153.77(2)° and P(1B)-Ag(1)-N(20A) 128.08(5)° angles. The angles around the Ag(1) atom equal 359.1° indicating that the coordination is planar. The Ag—P bond lengths Ag(1)-P(1B) 2.3805(6) Å and Ag(1)-P(1A) 2.3945(6) Å are similar despite the difference in the binding of the two ligands. The Ag(1)-N(20A) bond length of 2.4854(19) Å is long compared to a similar complex with a Ag—N distance of 2.333 Å.[21]

The imine bonds have the expected lengths and compare well with similar compounds.[2-10] There is no significant difference between the bond lengths of the imines, C(19A)-N(20A) 1.279(3) Å and C(19B)-N(20B) 1.265(3) Å, despite the difference in coordination. The bonds on either side of the imine are within an acceptable range in all cases with no significant differences between the two ligands. The bond angles about the imine bond are normal.

From Figure 2.3 it is clear that for both ligands the N and P atoms are on the same side of the C(19)—C(18) bond as is required for the ligands to chelate. The torsion angles C(13A)-C(18A)-C(19A)-N(20A) -6.3(4)° and C(13B)-C(18B)-C(19B)-N(20B) -2.6(4)° confirm the relative positions of the P and N atoms. Of note is that this conformation is taken even when the imine is unbound despite the steric hindrance this produces. The imine bonds have an *E* conformation and are planar in the chain with the phenyl groups attached to the nitrogen atoms 30° out of plane on both ligands.

Hydrogen bonds exist within the lattice between the hydrogens of the phenyl rings and the fluorines of the PF_6^-. The hydrogen bond distances range from 2.36 to 2.55 Å with angles ranging from 120.2° to 164.2°.

Figure 2.3. ORTEP diagram of $[Ag(NP)_2][PF_6]$. Thermal ellipsoids are at 50% probability. The PF_6^- ion has been admitted for clarity.

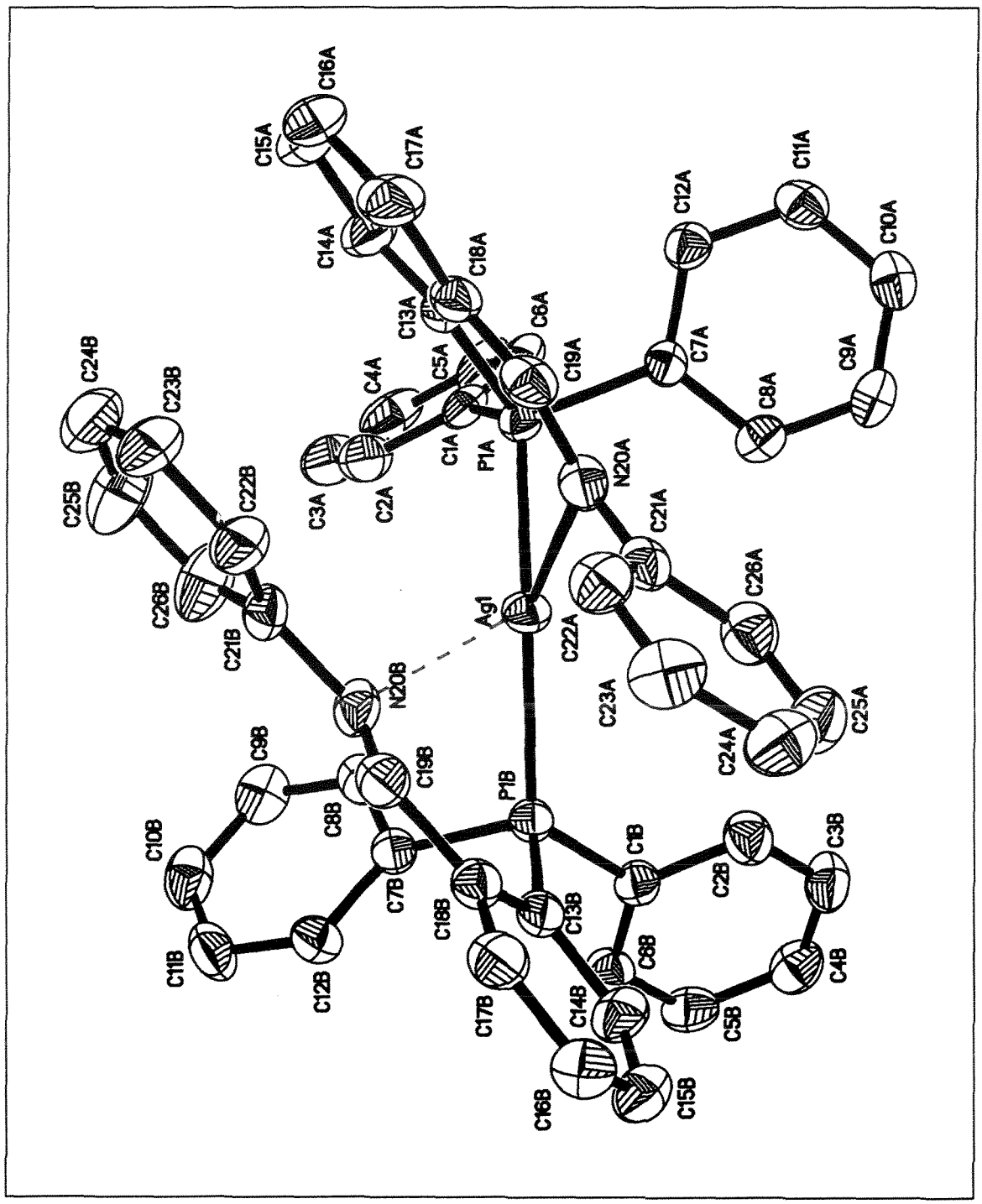

Table 2.7. Crystal data and structure refinement for $[Ag(NP)_2][PF_6]$.

Identification code	ka65	
Empirical formula	$C_{50}H_{40}AgClF_6N_2P_3$	
Formula weight	1019.07	
Temperature	150(2) K	
Wavelength	0.71073 Å	
Crystal system	Monoclinic	
Space group	P2(1)/n	
Unit cell dimensions	a = 14.9300(3) Å	α= 90°
	b = 15.7543(2) Å	β= 106.3730(10)°
	c = 20.3121(3) Å	γ = 90°
Volume	4583.89(13) Å^3	
Z	4	
Density (calculated)	1.477 Mg/m^3	
Absorption coefficient	0.665 mm^{-1}	
F(000)	2068	
Crystal size	0.38 x 0.32 x 0.24 mm^3	
Theta range for data collection	1.51 to 25.36°	
Index ranges	$-17 \le h \le 17$, $0 \le k \le 18$, $0 \le l \le 24$	
Reflections collected	8346	
Independent reflections	8346 [R(int) = 0.0000]	
Completeness to theta = 25.36°	99.6 %	
Absorption correction	None	
Max. and min. transmission	0.8568 and 0.7863	
Refinement method	Full-matrix least-squares on F^2	
Data / restraints / parameters	8346 / 0 / 620	
Goodness-of-fit on F^2	1.063	
Final R indices [I>2sigma(I)]	R1 = 0.0296, wR2 = 0.0653	
R indices (all data)	R1 = 0.0403, wR2 = 0.0708	
Largest diff. peak and hole	1.298 and -0.400 e.Å^{-3}	

Table 2.8. Selected bond lengths (Å) and angles (°) for $[Ag(NP)_2][PF_6]$.

Ag(1)-N(20A)	2.4854(19)	Ag(1)-P(1B)	2.3805(6)
Ag(1)-P(1A)	2.3945(6)	C(18B)-C(19B)	1.469(3)
C(18A)-C(19A)	1.470(4)	C(19B)-N(20B)	1.265(3)
C(19A)-N(20A)	1.279(3)	N(20B)-C(21B)	1.426(3)
N(20A)-C(21A)	1.427(3)	P(1B)-C(7B)	1.821(2)
P(1A)-C(7A)	1.822(2)	P(1B)-C(1B)	1.828(2)
P(1A)-C(1A)	1.828(2)	P(1B)-C(13B)	1.830(3)
P(1A)-C(13A)	1.831(2)	P(1B)-Ag(1)-N(20A)	128.08(5)
P(1A)-Ag(1)-N(20A)	77.25(5)	P(1B)-Ag(1)-P(1A)	153.77(2)
N(20A)-C(19A)-C(18A)	127.1(2)	N(20B)-C(19B)-C(18B)	124.3(2)
C(19A)-N(20A)-C(21A)	119.2(2)	C(19B)-N(20B)-C(21B)	120.0(2)

Table 2.9. Selected torsion angles (°) for $[Ag(NP)_2][PF_6]$.

C(13A)-C(18A)-C(19A)-N(20A)	-6.3(4)
C(18A)-C(19A)-N(20A)-C(21A)	-174.1(2)
C(19A)-N(20A)-C(21A)-C(26A)	-150.0(2)
C(13B)-C(18B)-C(19B)-N(20B)	-2.6(4)
C(18B)-C(19B)-N(20B)-C(21B)	-179.9(2)
C(19B)-N(20B)-C(21B)-C(26B)	-150.8(3)

Table 2.10. Hydrogen bonds for $[Ag(NP)_2][PF_6]$ [Å and °].

D-H...A	d(D-H)	d(H...A)	d(D...A)	<(DHA)
C(3B)-H(3B)...F(1)	0.95	2.54	3.394(3)	149.7
C(10A)-H(10A)...F(9)#2	0.95	2.48	3.072(5)	120.2
C(11A)-H(11A)...F(9)#2	0.95	2.44	3.053(5)	121.7
C(11B)-H(11B)...F(3)#3	0.95	2.46	3.362(3)	158.4
C(16A)-H(16A)...F(1)#4	0.95	2.55	3.473(3)	164.2
C(25B)-H(25B)...F(4)#5	0.95	2.54	3.201(5)	126.8
C(25B)-H(25B)...F(5)#5	0.95	2.36	3.272(6)	160.8

2.3.2.4 The Structure of $[Au(NP)_2][PF_6]$

Figure 2.4 shows one of the two complex ions present in the unit cell. Crystal and structure refinement data is given in Table 2.12. Selected bond lengths and angles are in Table 2.13. Table 2.14 has selected torsion angles. The crystals were grown in CH_2Cl_2 with Et_2O layered on top. The gold atom is in a linear coordination environment with the ligands attached via the phosphorus atoms. The angles P(2B)-Au(B)-P(1B) 172.78(2)° and P(2A)-Au(A)-P(1A) 169.01(2)° show that the linear structure is distorted. The gold phosphorus bond lengths range from 2.3179(7) to 2.3095(7) Å. Table 2.11 gives a the bond lengths and angles for $Au(PPh_3)_2^+$ with varying counter ions for comparison with $[Au(NP)_2][PF_6]$. Good consistency is observed.

Table 2.11. Comparison of bond length (Å) and angles (°).

Anion	Ph_3P—Au—PPh_3		<(PAuP)	Ref
PF_6^-	2.3095	2.3102	172.78	a
	2.3177	2.3179	169.01	
PF_6^-	2.313	2.309	177.41	23
BF_4^-	2.319	2.322	167.36	24
$C(CN)_3^-$	2.316	2.316	180.00	25
NO_2^-	2.312	2.312	171.03	21

a) This work.

The imine bonds are within normal values and have no significant differences from the coordinated imines of $[Cu(NP)_2][PF_6]$ and $[Ag(NP)_2][PF_6]$. The bonds either side of the imine have the expected lengths. The C=N-C angles are all very similar to each other with an average of 120.1°. The angles N=C-C angles have an average of 120.8° which is smaller than for $[Cu(NP)_2][PF_6]$ (126.9°) and $[Ag(NP)_2][PF_6]$ (125.7°).

Despite the fact the imine nitrogen is not coordinated, the torsion angles are similar to the analogous Cu(I) and Ag(I) complexes. The conformation of the ligands has the N and P atoms on the same side of the molecule and the imine bond has a *trans* configuration with the phenyl group attached to the N atom twisted 20° out of plane of the imine bond.

Figure 2.4. ORTEP diagram of $[Au(NP)_2][PF_6]$. Thermal ellipsoids are at 50% probability. The PF_6^- ion has been admitted for clarity.

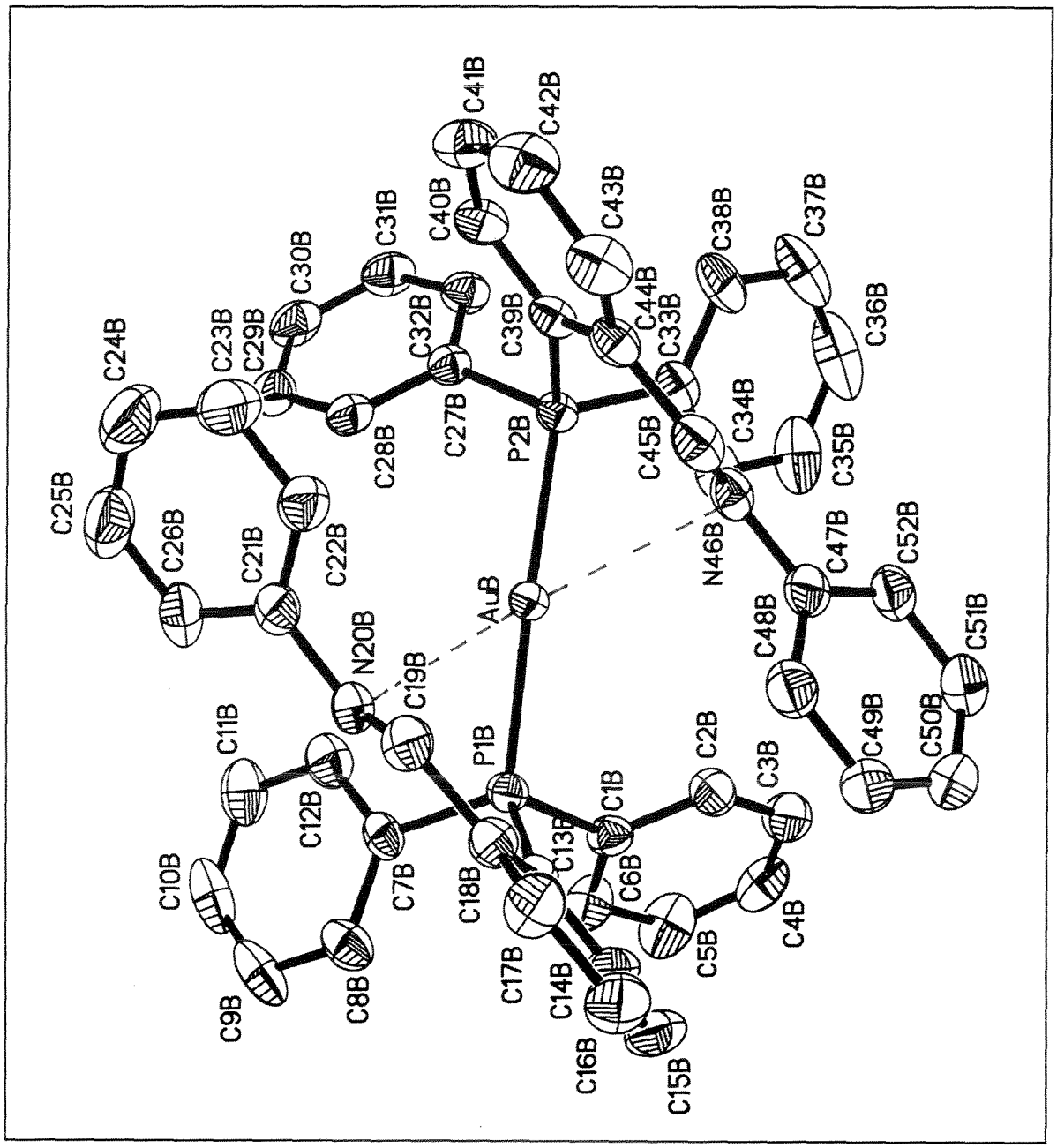

Table 2.12. Crystal data and structure refinement for $[Au(NP)_2][PF_6]$.

Identification code	ka144-squeeze	
Empirical formula	$C_{50}H_{40}AuN_2P_2$	
Formula weight	927.75	
Temperature	150(2) K	
Wavelength	0.71073 Å	
Crystal system	Triclinic	
Space group	P-1	
Unit cell dimensions	a = 14.49030(10) Å	α= 99.9050(10)°
	b = 14.62450(10) Å	β= 90.5480(10)°
	c = 23.9723(3) Å	γ = 99.8900(10)°
Z	4	
Density (calculated)	1.251 Mg/m^3	
Absorption coefficient	3.082 mm^{-1}	
F(000)	1852	
Crystal size	0.30 x 0.30 x 0.24 mm^3	
Theta range for data collection	1.43 to 25.71°	
Index ranges	$-17 \le h \le 17, -17 \le k \le 17, 0 \le l \le 29$	
Reflections collected	18424	
Independent reflections	18424 [R(int) = 0.0000]	
Completeness to theta = 25.71°	98.3 %	
Absorption correction	None	
Max. and min. transmission	0.5250 and 0.4582	
Refinement method	Full-matrix least-squares on F^2	
Data / restraints / parameters	18424 / 0 / 991	
Goodness-of-fit on F^2	1.058	
Final R indices [I>2sigma(I)]	R1 = 0.0227, wR2 = 0.0490	
R indices (all data)	R1 = 0.0306, wR2 = 0.0517	
Largest diff. peak and hole	0.562 and -0.631 $e.Å^{-3}$	

Table 2.13. Selected bond lengths (Å) and angles (°) for $[Au(NP)_2][PF_6]$.

AuA-P(2A)	2.3177(7)	AuB-P(2B)	2.3095(7)
AuA-P(1A)	2.3179(7)	AuB-P(1B)	2.3102(7)
P(1A)-C(7A)	1.822(3)	P(1B)-C(7B)	1.811(3)
P(1A)-C(13A)	1.832(3)	P(1B)-C(1B)	1.827(3)
P(1A)-C(1A)	1.835(3)	P(1B)-C(13B)	1.840(3)
C(18A)-C(19A)	1.463(4)	C(18B)-C(19B)	1.476(4)
C(19A)-N(20A)	1.272(4)	C(19B)-N(20B)	1.276(4)
N(20A)-C(21A)	1.421(4)	N(20B)-C(21B)	1.422(4)
C(44A)-C(45A)	1.463(4)	C(44B)-C(45B)	1.461(4)
C(45A)-N(46A)	1.282(3)	C(45B)-N(46B)	1.280(4)
N(46A)-C(47A)	1.421(4)	N(46B)-C(47B)	1.428(4)
P(2A)-AuA-P(1A)	169.01(2)	P(2B)-AuB-P(1B)	172.78(2)
C(7A)-P(1A)-C(13A)	108.09(12)	C(7B)-P(1B)-C(1B)	104.82(13)
C(7A)-P(1A)-C(1A)	105.49(12)	C(7B)-P(1B)-C(13B)	110.73(13)
C(13A)-P(1A)-C(1A)	104.56(13)	C(1B)-P(1B)-C(13B)	104.46(13)
N(20A)-C(19A)-C(18A)	120.6(3)	N(20B)-C(19B)-C(18B)	120.4(3)
C(19A)-N(20A)-C(21A)	120.4(2)	C(19B)-N(20B)-C(21B)	119.9(3)
N(46A)-C(45A)-C(44A)	120.8(2)	N(46B)-C(45B)-C(44B)	121.5(3)
C(45A)-N(46A)-C(47A)	119.7(2)	C(45B)-N(46B)-C(47B)	120.5(2)

Table 2.14. Selected torsion angles (°) for $[Au(NP)_2][PF_6]$.

C(13A)-C(18A)-C(19A)-N(20A)	19.8(4)	C(13B)-C(18B)-C(19B)-N(20B)	16.7(4)
C(18A)-C(19A)-N(20A)-C(21A)	-175.7(2)	C(18B)-C(19B)-N(20B)-C(21B)	-175.8(3)
C(19A)-N(20A)-C(21A)-C(26A)	-138.2(3)	C(19B)-N(20B)-C(21B)-C(26B)	-143.6(3)
C(39A)-C(44A)-C(45A)-N(46A)	21.9(4)	C(39B)-C(44B)-C(45B)-N(46B)	15.2(4)
C(44A)-C(45A)-N(46A)-C(47A)	-176.2(2)	C(44B)-C(45B)-N(46B)-C(47B)	-178.4(3)
C(45A)-N(46A)-C(47A)-C(52A)	-139.0(3)	C(45B)-N(46B)-C(47B)-C(52B)	-137.5(3)

2.3.2.5 The Structure of [Cu(NP)Br]$_2$

This is the first reported crystal structure of a complex with a chelating phosphorus and nitrogen ligand and a Cu—Cu interaction. It is only the second complex containing a Cu—Cu interaction and P and N donor atoms. The structure of [Cu(NP)Br]$_2$ is given in Figure 2.5 with crystal and refinement data in Table 2.15. Selected bond data are in Tables 2.16 and 2.17. The crystals were obtained by slow recrystallization by Et_2O diffusion into $CHCl_3$ over several days. The complex has a dimeric structure with a Cu—Cu interaction and two bridging Br atoms. The Cu atoms have a distorted tetrahedral structure. The ligands are bidentate through the P and N atoms. The Cu(1)-P(1) bond length is 2.2021(7) Å, which is slightly smaller than Cu—PPh_3 bonds of similar compounds.[18,20] The Cu(1)-P(1) bond length does, however, compare well with those in [Cu(NP)$_2$][PF_6]. The Cu(1)-N(1) 2.213(2) Å bond length is longer than most copper imine bonds.[18,20,26-28] The P(1)-Cu(1)-N(1) 85.28(6)° angle is similar to that in [Cu(NP)$_2$][PF_6].

The Cu(1)-Br(1) 2.3963(4) Å and Cu(1)-Br(1)#1 2.5312(4) Å bond lengths are similar to those of related complexes, however, the difference between the Cu—Br bonds is larger than previously observed.[29-33] The Cu(1)-Br(1)-Cu(1)#1 67.982(13)° bond angle matches those of comparable complexes which range from 59.42° to 72.02°.[29-33] The Br(1)-Cu(1)-Br(1)#1 112.018(13)° bond angle is within the range of a tetrahedral angle and closely matches the literature[29-32]. The small bridging angle about Br and the large Br(1)-Cu(1)-Br(1)#1 allows an interaction between the two coppers giving a Cu(1)—Cu(1)#1 bond length of 2.7571(6). Similar complexes have Cu—Cu bond lengths in the range 2.951-2.606 Å.[29-33] The torsion angle Br(1)#1-Cu(1)-Br(1)-Cu(1)#1 0.0° indicates that the Cu_2Br_2 ring is flat.

The bond lengths of the imine and surrounding bonds are unremarkable. The bond angles about the imine are similar to those in the complexes above with the N(1)-C(19)-C(18) angle being larger than the C(19)-N(1)-C(20) angle. Again the torsion angle C(20)-N(1)-C(19)-C(18) -178.1(2)° shows the imine to be planar in the chain with a *trans* conformation. As is required for chelation the N and P atoms are on the same side of the ligands as shown by the C(13)-C(18)-C(19)-N(1) torsion angle of 14.7(4)°. The phenyl group attached to the N atom is twisted 45° out of plane of the imine bond.

Figure 2.5. The ORTEP diagram of $[Cu(NP)Br]_2$ with thermal ellipsoids at 50% probability.

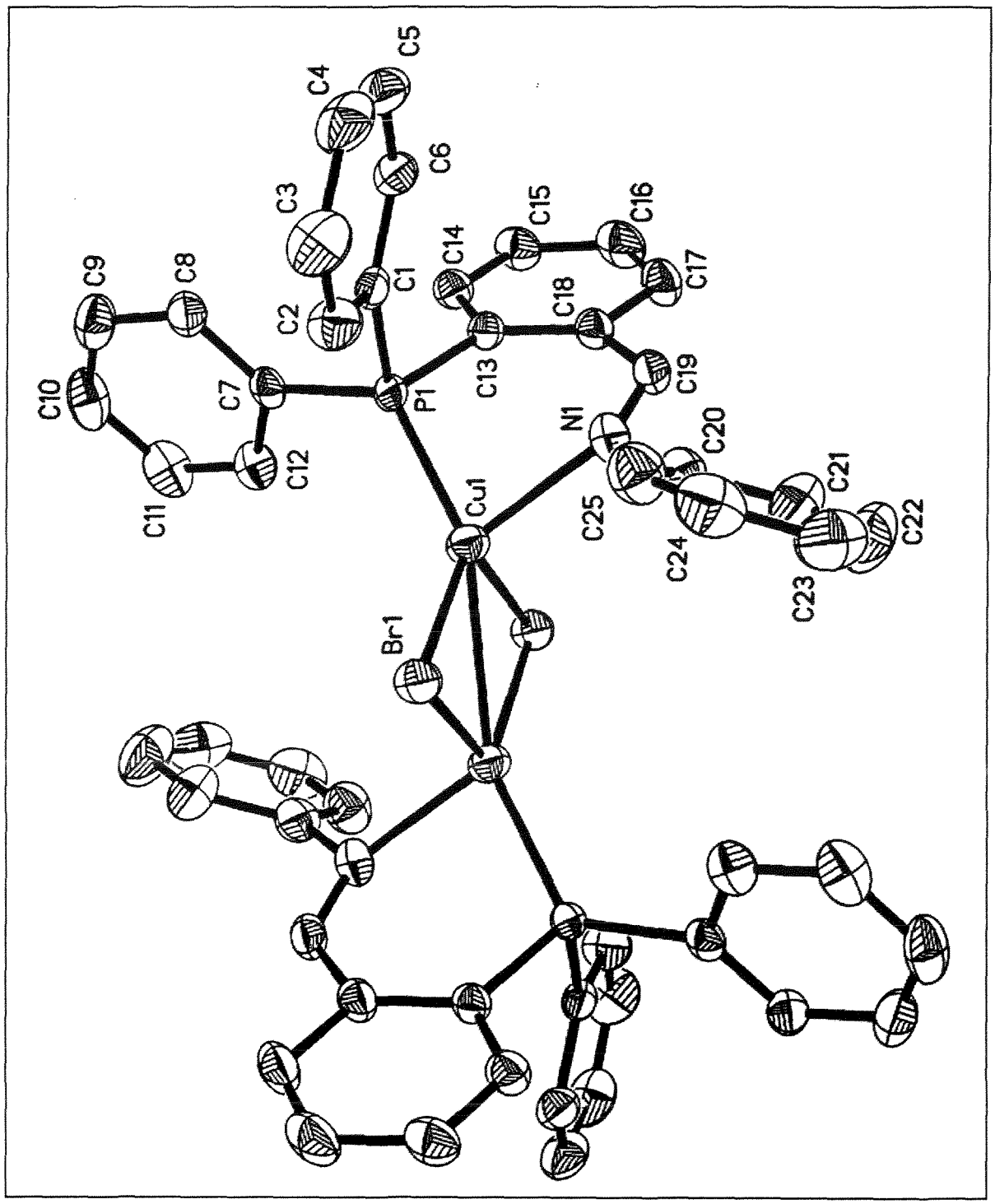

Table 2.15. Crystal data and structure refinement for $[Cu(NP)Br]_2$.

Identification code	ka88	
Empirical formula	$C_{25}H_{20}BrCuNP$	
Formula weight	508.84	
Temperature	150(2) K	
Wavelength	0.71073 Å	
Crystal system	Triclinic	
Space group	P-1	
Unit cell dimensions	a = 8.90000(10) Å	α= 76.92°
	b = 9.84940(10) Å	β= 71.30°
	c = 13.71290(10) Å	γ = 77.9650(10)°
Volume	1096.974(18) Å^3	
Z	2	
Density (calculated)	1.541 Mg/m^3	
Absorption coefficient	2.901 mm^{-1}	
F(000)	512	
Crystal size	0.30 x 0.22 x 0.16 mm^3	
Theta range for data collection	1.59 to 25.69°	
Index ranges	$-10 \le h \le 10$, $-11 \le k \le 12$, $0 \le l \le 16$	
Reflections collected	4137	
Independent reflections	4137 [R(int) = 0.0000]	
Completeness to theta = 25.69°	99.4 %	
Absorption correction	None	
Max. and min. transmission	0.6540 and 0.4765	
Refinement method	Full-matrix least-squares on F^2	
Data / restraints / parameters	4137 / 0 / 262	
Goodness-of-fit on F^2	1.071	
Final R indices [I>2sigma(I)]	R1 = 0.0304, wR2 = 0.0815	
R indices (all data)	R1 = 0.0361, wR2 = 0.0850	
Largest diff. peak and hole	0.850 and -0.779 e.Å^{-3}	

Table 2.16. Selected bond lengths (Å) and angles (°) for $[Cu(NP)Br]_2$.

Cu(1)-P(1)	2.2021(7)	P(1)-Cu(1)-N(1)	85.28(6)
Cu(1)-N(1)	2.213(2)	P(1)-Cu(1)-Br(1)	131.05(2)
Cu(1)-Br(1)	2.3963(4)	N(1)-Cu(1)-Br(1)	113.22(6)
Cu(1)-Br(1)#1	2.5312(4)	P(1)-Cu(1)-Br(1)#1	107.13(2)
Cu(1)-Cu(1)#1	2.7571(6)	N(1)-Cu(1)-Br(1)#1	101.91(6)
Br(1)-Cu(1)#1	2.5312(4)	Br(1)-Cu(1)-Br(1)#1	112.018(13)
P(1)-C(7)	1.826(2)	P(1)-Cu(1)-Cu(1)#1	147.27(3)
P(1)-C(1)	1.828(2)	N(1)-Cu(1)-Cu(1)#1	122.16(6)
P(1)-C(13)	1.838(2)	Br(1)-Cu(1)-Cu(1)#1	58.334(12)
N(1)-C(19)	1.272(4)	Br(1)#1-Cu(1)-Cu(1)#1	53.683(12)
N(1)-C(20)	1.430(3)	Cu(1)-Br(1)-Cu(1)#1	67.982(13)
C(18)-C(19)	1.474(4)	C(19)-N(1)-C(20)	117.7(2)
		N(1)-C(19)-C(18)	126.8(2)

Table 2.17. Selected torsion angles (°) for $[Cu(NP)Br]_2$.

Br(1)#1-Cu(1)-Br(1)-Cu(1)#1	0.0
C(20)-N(1)-C(19)-C(18)	-178.1(2)
C(19)-N(1)-C(20)-C(25)	134.8(3)
C(13)-C(18)-C(19)-N(1)	14.7(4)

2.3.2.6 The Structure of Au(NP)Cl

Figure 2.6 shows the two independent complexes of Au(NP)Cl with a disordered $CHCl_3$ solvent molecule. Tables 2.18, 2.19, 2.20 and 2.21 give crystal data and structure refinement, selected bond lengths and angles, selected torsion angles and hydrogen bonds respectively. Crystals were grown from $CHCl_3$ by addition of n-hexane. The Au atom has a linear coordination with the ligand attached via the P atom and the Cl covalently bound to the Au atom. The angles P(1A)-Au(1A)-Cl(1A) 177.41(4)° and P(1B)-Au(1B)-Cl(1B) 178.22(4)° are very similar to the related compound $Au(PPh_3)Cl$ that has a P-Au-Cl angle of 179.71°.[35] The bond lengths Au(1A)-Cl(1A) 2.2977(11) Å and Au(1B)-Cl(1B) 2.3060(10) Å are within the average Au—Cl bond length range of 2.33±4 Å[34] but are longer than those of $Au(PPh_3)Cl$ which has a Au—Cl bond length of 2.278 Å.[35] Au(NP)Cl has Au(1A)-P(1A) and Au(1B)-P(1B) bond lengths of 2.2411(11) Å and 2.2459(10) Å respectively. Both of these bond lengths are similar to that in $Au(PPh_3)Cl$, with a Au—P bond length of 2.233 Å,[35] but are shorter than those in $[Au(NP)_2][PF_6]$.

Despite being uncoordinated, the imine C=N bond lengths are similar to complexes where the N is coordinated. The bonds either side of the imine are also unremarkable. The angles about the imine bond are the same as those for the previously discussed free ligand and complexes, with the N=C-C angles being larger than the C-N=C angles.

The torsion angles C(18A)-C(19A)-N(20A)-C(21A) 175.8(3)° and C(18B)-C(19B)-N(20B)-C(21B) -175.0(4)° show the imine bond in Au(NP)Cl to have an *E*, or *trans*, arrangement with the two largest groups on opposite sides of the bond. They also show the imine to be planar within the chain. Table 2.20 gives torsion angles that show the phenyl groups on the N atoms to be twisted out of plane with the imine bond by 27° and 22° for each of the unique complexes. The P and N atoms are on the same side of the molecule. This relationship between the P and N atoms is shown by the torsion angles C(13A)-C(18A)-C(19A)-N(20A) 14.6(6)° and C(13B)-C(18B)-C(19B)-N(20B) -13.8(6)°. The linear Cl-Au-P system and imine chain are arranged so the imine chain is staggered by Au(1A)-P(1A)-C(13A)-C(18A) 49.6(4)° and Au(1B)-P(1B)-C(13B)-C(18B) -49.3(4)°. This conformation may provide the lowest energy arrangement.

Intermolecular hydrogen bonds exist (Table 2.21) with the hydrogens making contacts to either a Au or Cl atom. They have a range of 2.52-3.25 Å with the longest being between an imine hydrogen to a Au atom.

Figure 2.6. The ORTEP diagram of Au(NP)Cl with thermal ellipsoids at 50% probability.

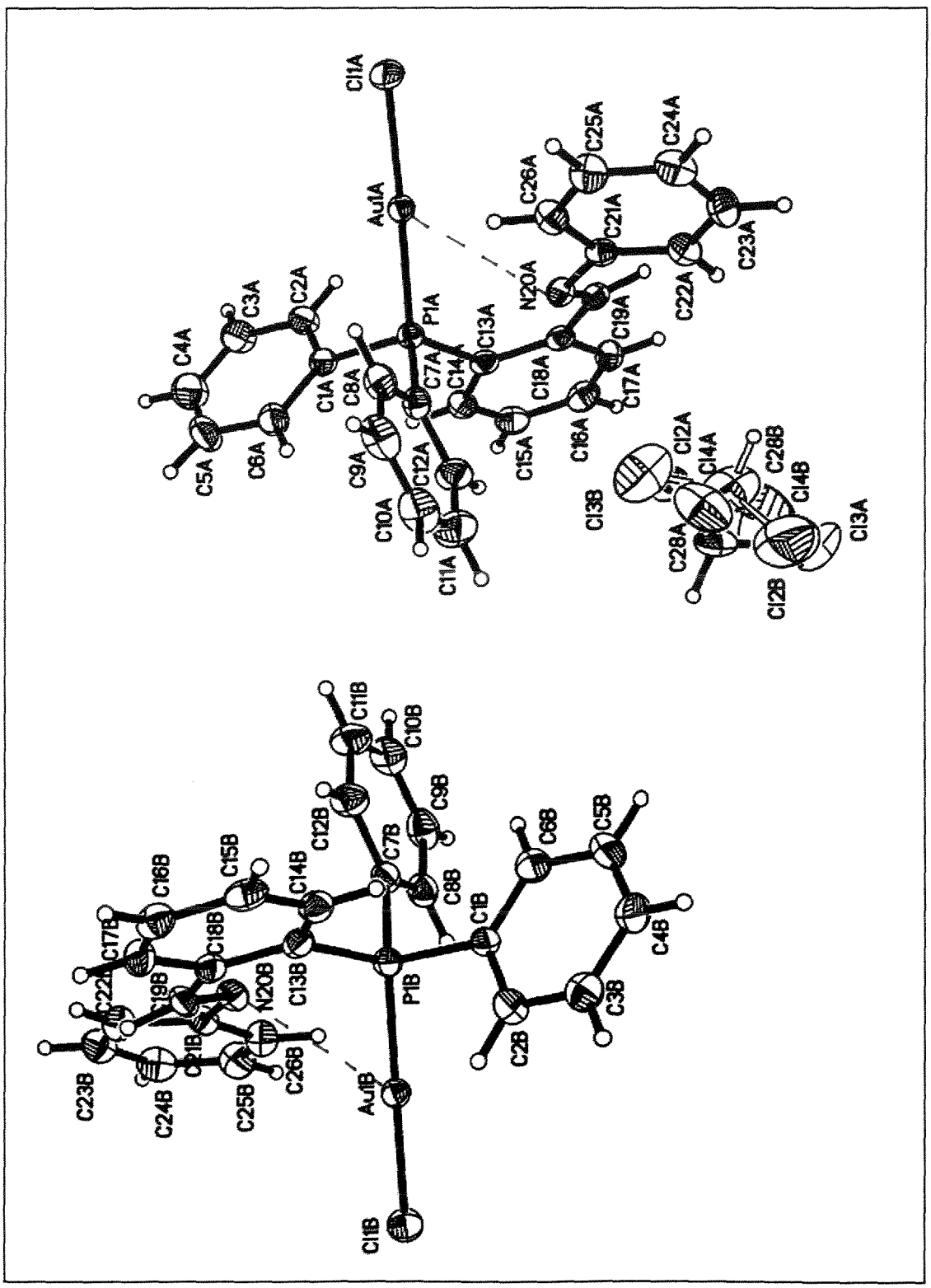

Table 2.18. Crystal data and structure refinement for Au(NP)Cl.

Identification code	ka101	
Empirical formula	$C_{51}H_{41}Au_2C_{15}N_2P_2$	
Formula weight	1314.98	
Temperature	150(2) K	
Wavelength	0.71073 Å	
Crystal system	Triclinic	
Space group	P-1	
Unit cell dimensions	a = 11.0491(2) Å	α= 100.8990(10)°
	b = 12.36540(10) Å	β= 102.0950(10)°
	c = 18.8773(3) Å	γ = 104.8790(10)°
Volume	2355.45(6) Å^3	
Z	2	
Density (calculated)	1.854 Mg/m^3	
Absorption coefficient	6.611 mm^{-1}	
F(000)	1268	
Crystal size	0.34 x 0.18 x 0.16 mm^3	
Theta range for data collection	1.14 to 25.31°	
Index ranges	$-13 \le h \le 12$, $-14 \le k \le 14$, $0 \le l \le 22$	
Reflections collected	8229	
Independent reflections	8229 [R(int) = 0.0000]	
Completeness to theta = 25.31°	95.7 %	
Absorption correction	None	
Max. and min. transmission	0.4177 and 0.2121	
Refinement method	Full-matrix least-squares on F^2	
Data / restraints / parameters	8229 / 6 / 596	
Goodness-of-fit on F^2	1.070	
Final R indices [I>2sigma(I)]	R1 = 0.0236, wR2 = 0.0552	
R indices (all data)	R1 = 0.0311, wR2 = 0.0587	
Largest diff. peak and hole	1.066 and -0.904 e.Å^{-3}	

Table 2.19. Selected bond lengths (Å) and angles (°) for Au(NP)Cl.

Au(1A)-P(1A)	2.2411(11)	Au(1B)-P(1B)	2.2459(10)
Au(1A)-Cl(1A)	2.2977(11)	Au(1B)-Cl(1B)	2.3060(10)
P(1A)-C(7A)	1.820(4)	P(1B)-C(7B)	1.820(4)
P(1A)-C(1A)	1.826(4)	P(1B)-C(1B)	1.831(4)
P(1A)-C(13A)	1.832(4)	P(1B)-C(13B)	1.840(4)
C(18A)-C(19A)	1.473(5)	C(18B)-C(19B)	1.469(5)
C(19A)-N(20A)	1.280(5)	C(19B)-N(20B)	1.278(5)
N(20A)-C(21A)	1.435(5)	N(20B)-C(21B)	1.423(5)
P(1A)-Au(1A)-Cl(1A)	177.41(4)	P(1B)-Au(1B)-Cl(1B)	178.22(4)
N(20A)-C(19A)-C(18A)	121.2(4)	N(20B)-C(19B)-C(18B)	121.7(4)
C(19A)-N(20A)-C(21A)	119.1(4)	C(19B)-N(20B)-C(21B)	120.0(4)

Table 2.20. Selected torsion angles (°) of Au(NP)Cl.

Au(1A)-P(1A)-C(13A)-C(18A)	49.6(4)
C(13A)-C(18A)-C(19A)-N(20A)	14.6(6)
C(18A)-C(19A)-N(20A)-C(21A)	175.8(3)
C(19A)-N(20A)-C(21A)-C(26A)	153.5(4)
Au(1B)-P(1B)-C(13B)-C(18B)	-49.3(4)
C(13B)-C(18B)-C(19B)-N(20B)	-13.8(6)
C(18B)-C(19B)-N(20B)-C(21B)	-175.0(4)
C(19B)-N(20B)-C(21B)-C(26B)	-158.3(4)

Table 2.21. Hydrogen bonds for Au(NP)Cl [Å and °].

D-H...A	d(D-H)	d(H...A)	d(D...A)	<(DHA)
C(25A)-H(25A)...Cl(4B)#1	0.95	2.52	3.31(2)	140.1
C(25B)-H(25B)...Cl(4A)#2	0.95	2.66	3.365(5)	131.5
C(5B)-H(5B)...Cl(2B)#3	0.95	2.68	3.33(2)	126.2
C(28A)-H(28A)...Cl(1B)#4	1.00	2.85	3.661(6)	138.8
C(4B)-H(4B)...Cl(2B)#3	0.95	2.86	3.42(2)	118.4
C(15A)-H(15A)...Cl(1A)#5	0.95	2.88	3.531(4)	127.0
C(16A)-H(16A)...Cl(1A)#5	0.95	2.94	3.561(4)	123.9
C(22B)-H(22B)...Au(1B)#6	0.95	3.03	3.665(4)	125.5
C(22A)-H(22A)...Au(1A)#7	0.95	3.09	3.653(4)	119.2
C(3A)-H(3A)...Au(1B)#8	0.95	3.15	4.086(5)	168.3
C(3B)-H(3B)...Au(1A)#9	0.95	3.17	4.093(5)	164.0
C(19A)-H(19A)...Au(1A)#7	0.95	3.25	4.195(4)	174.2

2.3.2.7 The Structure of Au(NP)Br

Slow diffusion of n-hexane into a $CHCl_3$ solution of the complex yielded pale yellow crystals. The structure of Au(NP)Br is shown in Figure 2.7. The crystal data and structure refinement are given in Table 2.22 and Table 2.23 has selected bond lengths and angles. Table 2.24 has selected torsion angles and Table 2.25 the hydrogen bonds. The bond angle P(3)-Au(1)-Br(1) 177.49(2)° and Figure 2.7 shows the Au to have a distorted linear coordination with the ligand bound via the P atom and the Br covalently bonded to the Au atom. The Au(1)-P(3) bond length of 2.2352(10) Å is shorter than that of $[Au(NP)_2][PF_6]$ but compares well with the similar compounds $Au(PPh_3)Cl$, Au—P 2.233 Å,[35] and $Au(PPh_3)Br$, Au—P 2.237 Å and 2.406 Å.[36,37] The Au(1)-Br(1) distance is 2.4049(9) Å which is in agreement with one structure of $Au(PPh_3)Br$ with a Au—Br bond length of 2.403 Å,[36] while disagreeing with another structure of $Au(PPh_3)Br$ with a Au—Br distance of, 2.250 Å.[37]

The imine bond, C(19)-N(1) 1.274(4) Å, and the bonds either side of the imine bond, C(18)-C(19) 1.454(4) Å and N(1)-C(20) 1.419(4) Å, are unremarkable as are the angles about the imine bond, N(1)-C(19)-C(18) 121.8(3)° and C(19)-N(1)-C(20) 119.7(2)°.

The torsion angles given in Table 2.24 show the ligand to have a *trans* conformation with the N and P atoms on the same side of the molecule. The torsion angles also show that the imine chain is roughly planar with N(1) almost eclipsing C(13) and the phenyl group attached to the N atom twisted by 27°. The linear Br-Au-P and the imine chain are staggered as shown by the Au(1)-P(3)-C(13)-C(18) torsion angle of -49.4(2)°.

The hydrogen bonds range from 2.64 to 2.97 Å and exist between the Cl atoms of the $CHCl_3$, the Br atoms of the complex and aromatic hydrogens.

Figure 2.7. The ORTEP diagram of Au(NP)Br with thermal ellipsoids at 50% probability.

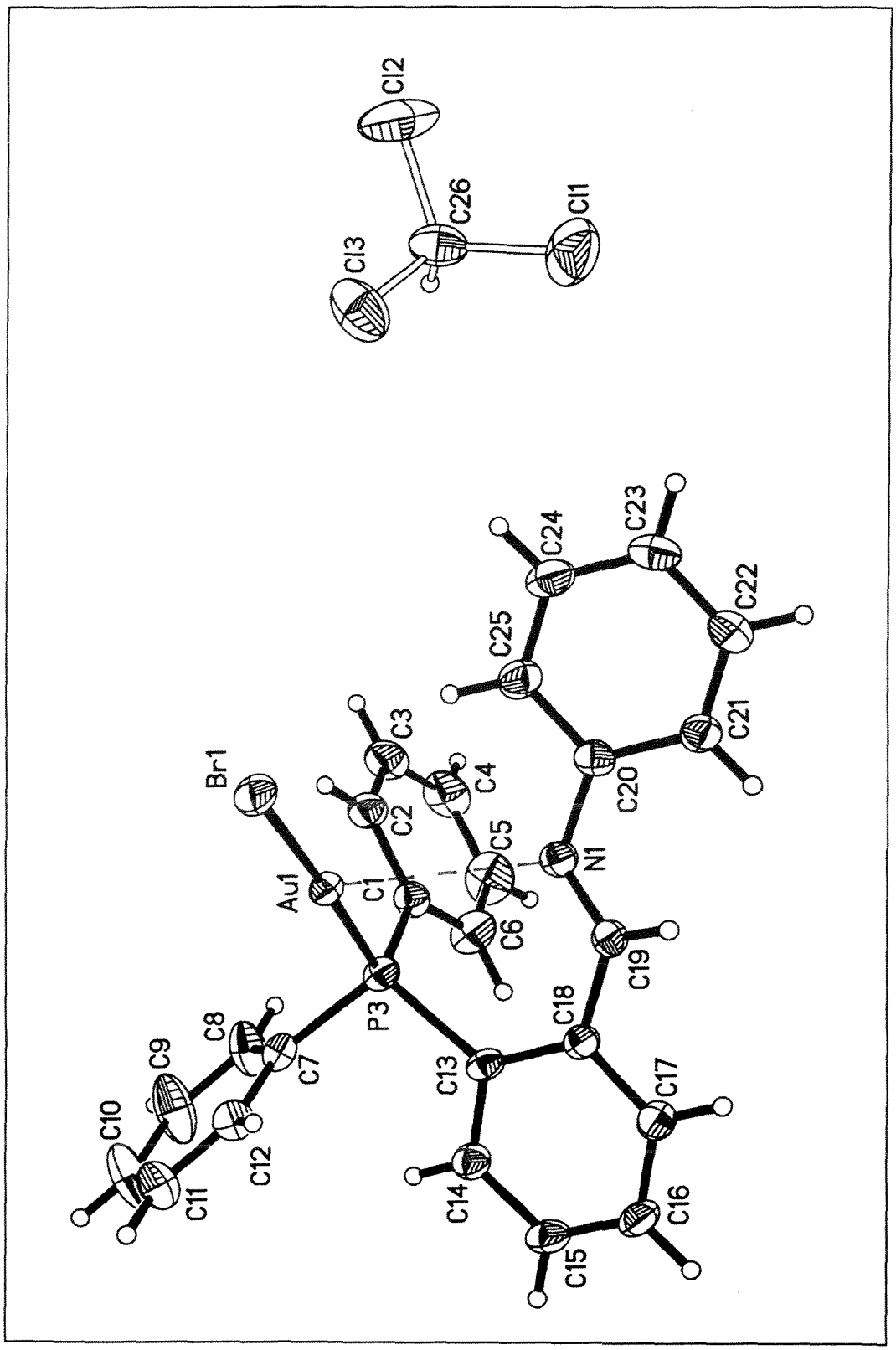

Table 2.22. Crystal data and structure refinement for Au(NP)Br.

Identification code	ka103	
Empirical formula	$C_{51}H_{41}Au_2Br_2C_{13}N_2P_2$	
Formula weight	1403.90	
Temperature	293(2) K	
Wavelength	0.71073 Å	
Crystal system	Triclinic	
Space group	P1	
Unit cell dimensions	a = 9.820(2) Å	α= 75.91(3)°
	b = 11.181(2) Å	β= 71.58(3)°
	c = 12.285(3) Å	γ = 68.49(3)°
Volume	1178.1(4) Å^3	
Z	1	
Density (calculated)	1.979 Mg/m^3	
Absorption coefficient	8.191 mm^{-1}	
F(000)	670	
Crystal size	2 x 3 x 2 mm^3	
Theta range for data collection	1.77 to 25.44°	
Index ranges	$-10 \le h \le 11, -12 \le k \le 13, 0 \le l \le 14$	
Reflections collected	4332	
Independent reflections	4332 [R(int) = 0.0000]	
Completeness to theta = 25.44°	99.3 %	
Absorption correction	None	
Refinement method	Full-matrix least-squares on F^2	
Data / restraints / parameters	4332 / 0 / 298	
Goodness-of-fit on F^2	1.086	
Final R indices [I>2sigma(I)]	R1 = 0.0166, wR2 = 0.0416	
R indices (all data)	R1 = 0.0175, wR2 = 0.0421	
Largest diff. peak and hole	0.471 and -0.729 e.Å^{-3}	

Table 2.23. Selected bond lengths (Å) and angles (°) for Au(NP)Br.

Au(1)-P(3)	2.2352(10)	C(18)-C(19)	1.454(4)
Au(1)-Br(1)	2.4049(9)	C(19)-N(1)	1.274(4)
P(3)-C(1)	1.810(3)	N(1)-C(20)	1.419(4)
P(3)-C(7)	1.821(3)	P(3)-Au(1)-Br(1)	177.49(2)
P(3)-C(13)	1.827(3)	N(1)-C(19)-C(18)	121.8(3)
		C(19)-N(1)-C(20)	119.7(2)

Table 2.24. Selected torsion angles (°) for Au(NP)Br.

Au(1)-P(3)-C(13)-C(18)	-49.4(2)
C(13)-C(18)-C(19)-N(1)	-14.1(4)
C(18)-C(19)-N(1)-C(20)	-175.8(2)
C(19)-N(1)-C(20)-C(25)	-155.4(3)

Table 2.25. Hydrogen bonds for Au(NP)Br [Å and °].

D-H...A	d(D-H)	d(H...A)	d(D...A)	<(DHA)
C(24)-H(24A)...Cl(2)#1	0.93	2.64	3.373(4)	136.5
C(10)-H(10A)...Cl(3)#2	0.93	2.91	3.468(4)	120.2
C(26)-H(26A)...Br(1)#3	0.98	2.94	3.765(7)	142.2
C(15)-H(15A)...Br(1)#4	0.93	2.97	3.662(3)	132.5

2.3.3 *Vibrational Spectroscopy*

2.3.3.1 Far IR Spectra

Selected Far IR spectral results for the Au(NP)X (X = Cl, Br, I) complexes are given in Table 2.26. The ν(Au—X) stretching frequencies are consistent with terminal halides. This is confirmed by comparison with the similar complexes $Au(PPh_3)X$ and $Au(PMe_3)X$ (Table 2.26) .[38] This supports the results of the crystal structures of Au(NP)Cl and Au(NP)Br as presented in Section 2.3.2.

Table 2.26. Selected Far IR spectral results and comparison of Au(NP)X (cm^{-1}).

	ν(Au—X)		
	Cl	Br	I
Au(NP)X[a]	326	215	198
$Au(PPh_3)X$[38]	329	234	189
$Au(PMe_3)X$[38]	312	229	164

a) This work; X = Cl, Br, I.

The Far IR results for the complexes $[Ag(NP)X]_2$ (X = Cl, Br, I) are given in Table 2.27 and suggest dimeric complexes with bridging halides. Upon comparison with the dimeric bridging halide complexes $[Ag(PCy_3)X]_2$[39] and the monomeric terminal halide complexes $Ag(PCy_3)_2X$[40] (Table 2.27) it can be seen that the ν(Ag—X) bands of the $[Ag(NP)X]_2$ complexes may be associated with bridging halides.

Table 2.27. Selected Far IR spectral results and comparison of $[Ag(NP)X]_2$ (cm^{-1}).

	ν(Ag—X)		
	Cl	Br	I
$[Ag(NP)X]_2$[a]	154	113	74
$[Ag(PCy_3)X]_2$[39]	225	189	113
	143	167	83
		135	
		114	
$Ag(PCy_3)_2X$[40]	207	149	121

a) This work, X = Cl, Br, I; Cy = C_6H_{11}.

In contrast no ν(Cu—X) stretching modes could be detected in the Far IR for the complexes $[Cu(NP)X]_2$. From the X-ray structure (Section 2.3.2.5) of $[Cu(NP)Br]_2$ bridging halide ν(Cu—Br) modes would be expected, however, the bands are too weak and are not visible Literature examples for values of bridging ν(Cu—X) stretches are 253-195 cm^{-1} for Cl, 189 and 153 cm^{-1} for Br and 156 cm^{-1} for I.[41-44]

2.3.3.2 Near IR Spectra

Selected Near IR results of the free ligand NP and its complexes are given in Table 2.28. The ν(C=N) stretch of the free ligand is within the standard range of an imine within a conjugated chain.[45,46] Upon coordination of the imine nitrogen to a metal centre the ν(C=N) stretch moves to lower wavenumbers. This trend can be seen for all the complexes of Cu(I) indicating that the imine nitrogen is bound which agrees with the X-ray structure analyses. The complexes of Au(I) move to higher wavenumbers indicating that the imine nitrogen is unbound, a result which is in agreement with the X-ray structure analysis.

The complex $[Ag(NP)_2][PF_6]$ shows splitting of the imine band with one peak remaining close to the free ligand and the other at a lower wavenumber, suggesting a bound and an unbound imine in agreement with the X-ray structure. The ν(C=N) stretch for $[Ag(NP)Cl]_2$ and $[Ag(NP)Br]_2$ suggests that the imines are bound to the Ag(I) centre while $[Ag(NP)I]_2$ appears to have an unbound imine. Unfortunately X-ray structure analysis could not be performed on the halo complexes.

Table 2.28. Selected IR data for the NP ligand and its complexes (cm^{-1}).

	ν(C=N)	ν(PF)
NP[a]	1622	
$[Cu(NP)_2][PF_6]$	1612	845
$[Ag(NP)_2][PF_6]$	1621 1614	841
$[Au(NP)_2][PF_6]$	1624	841
$[Cu(NP)Cl]_2$	1610	
$[Cu(NP)Br]_2$	1618	
$[Cu(NP)I]_2$	1618	
$[Ag(NP)Cl]_2$	1617	
$[Ag(NP)Br]_2$	1617	
$[Ag(NP)I]_2$	1622	
Au(NP)Cl	1624	
Au(NP)Br	1624	
Au(NP)I	1622	

a) Prepared in toluene.

Table 2.29 gives selected near IR results for O_5NP and its complexes. The free ligand O_5NP has a ν(C=N) absorption at lower wavenumbers than that of NP but which is still in the range 1686-1589 cm^{-1} reported for similar compounds.[1,2,47-49] Upon coordination only small changes are observed in the wavenumbers except in the case of the Au(I) complexes that have the expected shift to higher wavenumbers associated with an unbound imine. Both the silver complexes have a 4 cm^{-1} increase in the imine stretch suggesting non-bound imines, while the copper complexes decrease by 2 cm^{-1} which does not give clear evidence of the binding that is implied by the X-ray structure of the corresponding NP complexes. The ether IR bands all fall within the expected range of 1300-1000 cm^{-1} and change little on coordination of the ligand.[45,46,50]

Table 2.29. Selected IR data for the O_5NP ligand and its complexes (cm^{-1}).

	ν(C=N)	ν(C-O-C)	ν(PF)
O_5NP	1614	1260 1235	
$[Cu(O_5NP)_2][PF_6]$	1612	1265	841
$[Ag(O_5NP)_2][PF_6]$	1618	1264 1134	840
$[Au(O_5NP)_2][PF_6]$	1626	1265 1133	842
$[Cu(O_5NP)Cl]_2$	1612	1268 1134	
$[Ag(O_5NP)Cl]_2$	1618	1265 1118	
$Au(O_5NP)Cl$	1626	1269 1137	

In Tables 2.28 and 2.29 the ν(P—F) stretching frequency at about 840 cm^{-1} is consistent with the presence of the PF_6^- anion in the appropriate complexes.

2.3.4 *Nuclear Magnetic Resonance Spectra*

2.3.4.1 The ^1H NMR spectra of the Ligands and Complexes

The most marked difference in the ^1H NMR spectra of the ligands NP and O_5NP (Table 2.30) is the appearance of the $-CH_2-$ ether proton peaks for O_5NP near 4 ppm. They appear in four groups with the protons nearest to the imine having the largest chemical shift as seen for related compounds.[51,52] Proton coupling around the crown ring causes multiple splitting of the signals.

The imine proton signal of the ligands appears as a doublet in the range 8.99-9.27 ppm which is similar to previous reports.[3,4,6,8,22,48,53] The ligand NP has been previously prepared by Chen *et al.*[2] who reported a shift of 10.5 ppm with a similar J_{PH} coupling of 5.1 Hz and by Wehman *et al.*[1] who reported the imine as a doublet at 9.08 ppm. The

other identifiable signal is the proton *ortho* to the phosphorus atom which has a signal at 8.21 ppm (1H, q, J_{PH}=3.87 Hz) for NP and 8.12 ppm (1H, q, J_{PH}=3.47 Hz) for O_5NP.

Table 2.30. Selected ^{31}P and ^{1}H NMR data for the ligands (δ/ppm, Hz).

	^{31}P NMR[a]	^{1}H NMR[b]	
	δ(P)	δ(N=CH)	δ(-CH_2-O-)
NP	-12.12 (s)	9.27 (1H, d, 5.16[c])	
O_5NP	-11.28 (s)	8.99 (1H, d, 5.03[c])	4.08 (2H, t, 4.43[d]) 3.98 (2H, m) 3.89 (4H, m) 3.73 (8H, s)

a) Recorded at 162 MHz, δ/ppm relative to 85% H_3PO_4 with $CDCl_3$ as solvent; b) Recorded at 400 MHz, δ/ppm relative to TMS with $CDCl_3$ as solvent; c) J_{PH}; d) J_{HH}.

In the PF_6^- complexes (Table 2.31) all the imine protons are singlets and show shifts to lower frequencies with the shift size in the order: Cu(I)>Ag(I)>Au(I). As discussed previously, the nitrogen atoms are bound in $[Cu(NP)_2][PF_6]$ and $[Cu(O_5NP)_2][PF_6]$ but are not bound in the corresponding gold salts. Despite only the phosphorus atoms being bound in $[Au(NP)_2][PF_6]$, the imine protons still experience a small shift to lower frequency. This suggests communication may exist between the imine and metal via the phosphorus atom.

Even though the crystal structure of $[Ag(NP)_2][PF_6]$ shows only one of the imine nitrogens is bound, there is only a single imine proton peak in the NMR suggesting an exchange reaction in solution making them appear equivalent.

Table 2.31. Selected ^{31}P and ^{1}H NMR data of the PF_6^- complexes (δ/ppm, Hz).

	^{31}P NMR[a]		^{1}H NMR[b]	
	δ(P)	δ(PF_6^-)	δ(N=CH)	δ(-CH_2-O-)
[Cu(NP)$_2$] [PF_6]	-7.10 (s)	-143.05 (sep, 713[c])	8.26 (2H, s)	
[Ag(NP)$_2$] [PF_6]	12.82 (d, 511.26, 590.53[d])	-142.90 (sep, 713[c])	8.47 (2H, s)	
[Au(NP)$_2$] [PF_6]	45.21 (s)	-142.88 (sep, 713[c])	8.50 (2H, s)	
[Cu(O_5NP)$_2$] [PF_6]	-6.65 (s)	-143.03 (sep, 713[c])	8.23 (2H, s)	3.99 (4H, t, 4.26[e]) 3.83 (4H t, 4.30[e]) 3.38 (20H, d, 6.57[e]) 3.57 (4H, s)
[Ag(O_5NP)$_2$] [PF_6]	13.13 (d, 518.46, 595.01[d])	-142.80 (sep, 714[c])	8.49 (2H, s)	3.83 (12H, m) 3.78 (4H, m) 3.69 (16H, s)
[Au(O_5NP)$_2$] [PF_6]	44.78 (s)	-142.85 (sep, 713[c])	8.56 (2H, s)	3.82 (8H, m) 3.78 (8H, m) 3.70 (16H, m)

a) Recorded at 162 MHz, δ/ppm relative to 85% H_3PO_4 with $CDCl_3$ as solvent; b) Recorded at 400 MHz, δ/ppm relative to TMS with $CDCl_3$ as solvent; c) J_{PF}; d) J(^{107}Ag-^{31}P) and J(^{109}Ag-^{31}P); e) J_{HH}; sep = septuplet.

For the halo complexes (Table 2.32) the imine protons are singlets for the copper and silver and doublets for the gold complexes and all display shifts to lower frequencies with the shift being in the order Cu(I)~Ag(I)<Au(I). As before X-ray structures show the imine nitrogen is bound in the copper and silver but not in the gold complexes.

In both the halo and PF_6^- complexes, the CH_2 protons of the crown ether experience little change in chemical shift upon coordination of the O_5NP ligand, although some changes occur in their relative intensities.

Table 2.32. Selected ^{31}P and ^{1}H NMR data for the halo complexes (δ/ppm, Hz).

	^{31}P NMR[a]	^{1}H NMR[b]	
	δ(P)	δ(N=CH)	δ(-CH_2-O-)
$[Cu(NP)Cl]_2$	-7.32 (s)	8.28 (2H, s)	
$[Cu(NP)Br]_2$	c	8.31 (2H, s)	
Au(NP)Cl	32.19 (s)	8.70 (1H, d, 1.00[d])	
Au(NP)Br	35.30 (s)	8.70 (1H, d, 1.49[d])	
Au(NP)I	39.60 (s)	8.71 (d, 1.55[d])	
$[Cu(O_5NP)Cl]_2$	-6.76 (s)	8.31 (2H, s)	4.02 (4H, t, 4.35[e]) 3.84 (6H, t, 4.37[e]) 3.76 (6H, s) 3.69 (16H, d, 6.62[e])
$[Ag(O_5NP)Cl]_2$	c	8.31 (2H, s)	4.07 (4H, m) 4.03 (4H, t, 4.45[e]) 3.85 (8H, m) 3.72 (16H, d, 5.48[e])
$Au(O_5NP)Cl$	32.80 (s)	8.71 (1H, d, 1.58[d])	4.12 (2H, m) 4.06 (2H, t, 4.42[e]) 3.87 (4H, m) 3.73 (8H, d, 2.42[e])

a) Recorded at 162 MHz, δ/ppm relative to 85% H_3PO_4 with $CDCl_3$ as solvent; b) Recorded at 400 MHz, δ/ppm relative to TMS with $CDCl_3$ as solvent; c) Not soluble; d) J_{PH}; e) J_{HH}.

2.3.4.2 The ^{31}P NMR Spectra of the Ligands and Complexes

Previous work on the NP ligand has reported a ^{31}P signal at –12.8 ppm[1] with similar compounds falling within the range of –15.0 ppm to –9.22 ppm.[3,4,6,8,22,48,53,54] The ligands NP and O_5NP (Table 2.30) compare well with the past work. There has been a shift to lower frequency by the ligands from the starting material 2PCHO (2-(diphenylphosphino)benzaldehyde) at –10.4 ppm.

It is clear from Table 2.31 that there is a large ^{31}P shift upon complexation of the phosphorus atoms of the ligands in the PF_6^- salts. Also as the atomic mass of the metal centre increases the phosphorus signal moves to higher frequency with Au(I) giving the largest shift and Cu(I) the smallest. The presence of the 15-crown-5 moiety has little

effect on the phosphorus signal due to the distance between them. The PF_6^- has consistent placement and coupling.

The trend in the ^{31}P NMR spectra of the halo complexes (Table 2.32) is similar to the PF_6^- salts. The chemical shift of the gold halo complexes follows the sequence I>Br>Cl for the NP ligand. The presence of the 15-crown-5 moiety appears to have little effect on the ^{31}P signal.

Figure 2.8 shows an expansion of a ^{31}P NMR spectrum showing the result of spin-spin Ag—P coupling in the complex $[Ag(NP)_2][PF_6]$. When Ag(I) complexes show enhanced stability, J_{AgP} coupling will be observed. The two natural isotopes of silver, ^{107}Ag and ^{109}Ag, both have a spin of ½ and an abundance of 50% with each isotope having a different coupling constant. Hence for the ^{31}P NMR spectra we see a pair of doublets, one within the other. An assignment can be made, as the ratio of the coupling constants equals the ratio of the gyromagnetic constants (μ).[55]

$$\frac{J(^{107}Ag\text{-}^{31}P)}{J(^{109}Ag\text{-}^{31}P)} = \frac{\mu(^{107}Ag)}{\mu(^{109}Ag)} = 0.865$$

In the ^{31}P NMR spectrum of $[Ag(NP)_2][PF_6]$ (Figure 2.8) a pair of doublets is observed which give the result :

$$\frac{J(^{107}Ag\text{-}^{31}P)}{J(^{109}Ag\text{-}^{31}P)} = \frac{511\ Hz}{591\ Hz} = 0.865$$

The similar complex, $[Ag(O_5NP)_2][PF_6]$, gives a ratio of 0.871.

Figure 2.8. The ^{31}P NMR spectrum of $[Ag(NP)_2][PF_6]$.

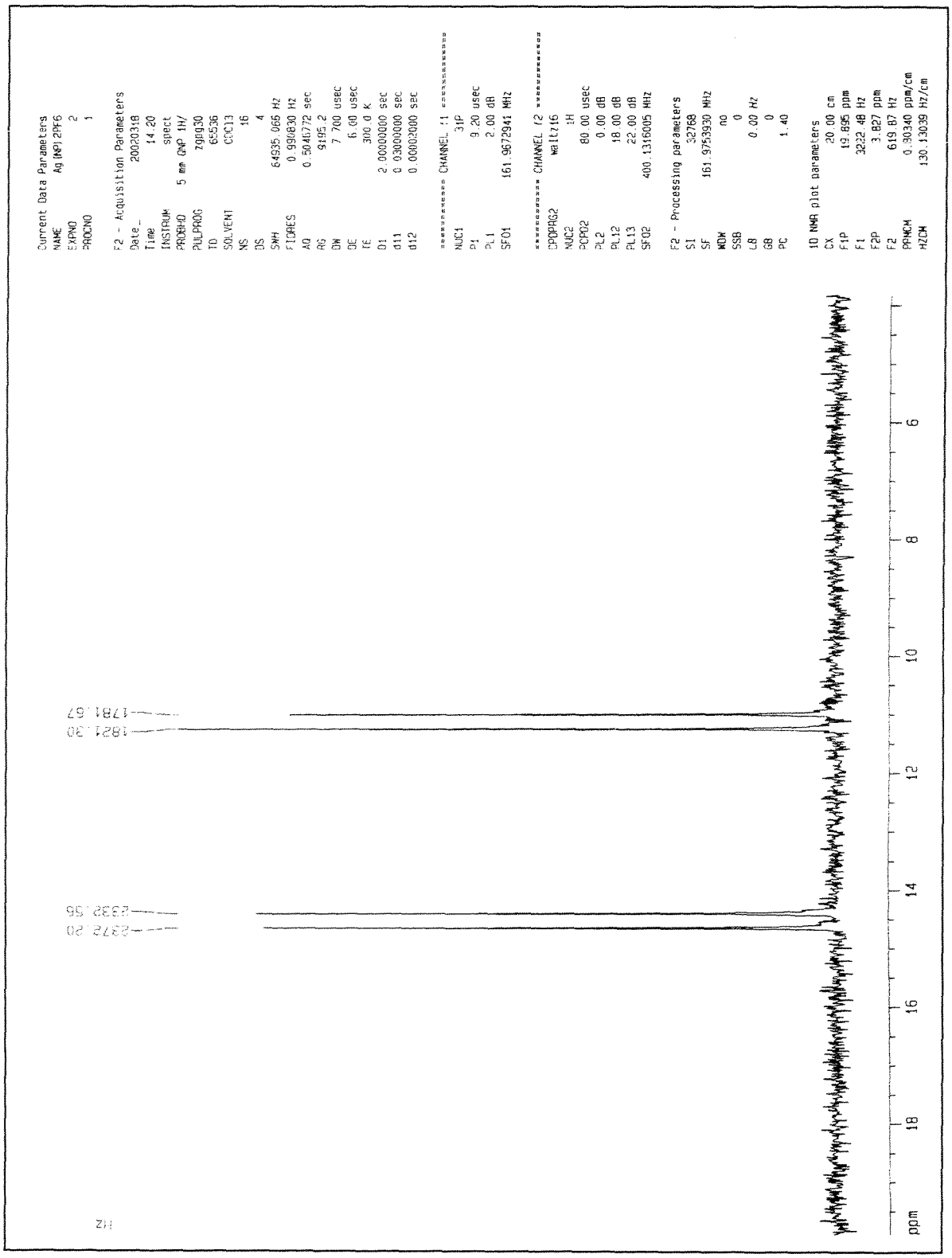

2.3.5 Electrospray Mass Spectroscopy Results

Both the free ligands are observed as the protonated MH^+ ions with NP having a low intensity parent peak while for O_5NP it was the 100% peak (Table 2.33). The PF_6^- salts were observed as the cation $[E(L)_2]^+$, where E is the metal centre (Table 2.34) while the halo complexes all lost a halide giving cations $[Cu_2L_2X]^+$, $[Ag_2L_2X]^+$ and $[Au(L)]^+$ (Table 2.35). In most cases the 100% peak is a fragment of the ligand. Isotope abundance calculations were used to assign the parent peaks and agreed well with the experimental results.

Table 2.33. Selected ESMS data for the ligands (m/z)[a].

	100%	MH^+	$2MH^+$
NP	94.3	366.4 (13%)	
O_5NP	556.3	556.3 (100%)	1111.4 (4%)

a) Relative intensities in parentheses.

Furthermore, the complexes $[E(O_5NP)_2][PF_6]$ (E = Cu, Ag, Au) experience, after the loss of the PF_6^-, the further loss of a ligand to give $[M\text{-}PF_6\text{-}L]^+$. The halide complexes undergo a rearrangement in the gas phase. An unbound ligand is picked up by a $[E(L)]^+$ (E = Cu, Ag, Au) group giving $[E(L)_2]^+$ ions. These have a large intensity and are the most intense peaks in the case of $[Ag(NP)Cl]_2$ and $[Ag(NP)Br]_2$.

Table 2.34. Selected ESMS data of the PF_6^- salts (m/z)[a].

	100%	$[M\text{-}PF_6]^+$	$[M\text{-}PF_6\text{-}L]^+$
$[Cu(NP)_2][PF_6]$	94.3	793.5 (73%)	
$[Ag(NP)_2][PF_6]$	94.3	839.5 (39%)	
$[Au(NP)_2][PF_6]$	927.2	937.2 (100%)	
$[Cu(O_5NP)_2][PF_6]$	60.5	1173.9 (39%)	618.5 (47%)
$[Ag(O_5NP)_2][PF_6]$	130.2	1219.3 (49%)	664.1 (33%)
$[Au(O_5NP)_2][PF_6]$	65.2	1307.3 (33%)	752.1 (3%)

a) Relative intensities in parentheses

A FAB+ mass spectrum of $[Ag(NP)Br]_2$ was taken for comparison with the ESMS results. It confirms the presence of a peak due to $[Ag_2(NP)_2Br]^+$ at 1025 m/z (3%). The FAB+ also shows the peaks for $[Ag(NP)]^+$ at 472 m/z (63%) and $[Ag(NP)_2]^+$ at 841 m/z (100%). The FAB+ shows good agreement with the results from the ESMS spectroscopy.

Table 2.35. Selected ESMS data of the halide complexes (m/z)[a].

	100%	$[M-X]^{+b}$	$[E(L)_2]^{+c}$	$[E(L)]^{+c}$
$[Cu(NP)Cl]_2$	145.1	893.0 (<1%)	793.5 (74%)	428.3 (9%)
$[Cu(NP)Br]_2$	145.1	937.0 (<1%)	793.5 (69%)	428.3 (5%)
$[Cu(NP)I]_2$	145.1	983.0 (1%)	793.5 (33%)	428.3 (1%)
$[Ag(NP)Cl]_2$	839.6	981.0 (1%)	839.6 (100%)	471.0 (10%)
$[Ag(NP)Br]_2$	839.6	1027.0 (2%)	839.6 (100%)	471.0 (5%)
Au(NP)Cl	242.1	562.0 (1%)	927.1 (23%)	n/a
Au(NP)Br	242.1	562.0 (<1%)	927.1 (10%)	n/a
Au(NP)I	242.1	562.1 (<1%)	927.1 (1%)	n/a
$[Cu(O_5NP)Cl]_2$	144.8	1273.3 (<1%)	1173.3 (18%)	618.2 (25%)
$[Ag(O_5NP)Cl]_2$	97.0	1361.2 (<1%)	1219.2 (4%)	662.1 (7%)
$Au(O_5NP)Cl$	206.4	752.2 (34%)	n/a	n/a

a) Relative intensities in parentheses; b) The parent peak, X = Cl, Br, I; c) E = Cu, Ag, Au.

2.4 Summary

The main findings of this chapter are given below.

- The Schiff base reaction provides an efficient and successful method for the synthesis of the iminophosphine ligands *N*-(2-diphenylphosphinobenzylidine)aniline (NP) and *N*-(2-diphenylphosphinobenzylidine)-4'-(benzo-15-crown-5) (O_5NP).
- The crystal structure of the free ligand O_5NP has been determined and shows that the imine has a *trans*, or *E*, conformation.
- The NMR, IR and ESMS spectra confirm the presence of the imine and phosphorus groups in NP and O_5NP and the benzo-15-crown-5 moiety in O_5NP.
- The syntheses of the Cu(I), Ag(I) and Au(I) complexes were successfully completed.
- Crystal structure analyses of $[Cu(NP)_2][PF_6]$, $[Ag(NP)_2][PF_6]$, $[Au(NP)_2][PF_6]$, $[Cu(NP)Br]_2$, Au(NP)Cl and Au(NP)Br have been determined.
- The $[M(L)_2][PF_6]$ (M = Cu, Ag, Au) complexes all contain two ligands for each metal centre and display a clear trend in coordination number with the number of coordinated imines decreasing as the soft nature of the metal centre increases.
- The $[Cu(NP)Br]_2$ complex is one of the 12% of halo bridged di-copper complexes that contain a Cu—Cu interaction.
- The Far IR spectra and crystal structure analyses show the Cu(I) and Ag(I) halo complexes to be dimeric with bridging halides and the Au(I) halo complexes to be monomeric with terminal halides.
- ^{1}H and ^{31}P NMR spectra show that the change in chemical shift of the imine proton and phosphorus upon complexation of the ligand is dependent on the atomic mass of the metal centre.
- A small shift to lower frequencies in the ^{1}H NMR spectra of the imine proton is observed in complexes were the imine is not directly bound to the metal centre.
- ESMS spectra gives the parent ions of the $[M(L)_2][PF_6]$ (M = Cu, Ag, Au) complexes as $[M(L)_2]^+$ and the parent ions of the halo complexes as $[M_2L_2X]^+$, for Cu and Ag and $[ML]^+$ for Au.
- Near IR spectroscopy confirms the presence of the imine, PF_6^- and ether groups in the appropriate complexes.

2.5 References

1. P. Wehman, H. van Donge, A. Hagos, P. Kamer and P. van Leeuwen, *J. Organomet. Chem.*, 535, (1997), 183-193.
2. X. Chen, F. Femia, J. Babich and J. Zubieta, *Inorg. Chim. Acta.*, 315, (2001), 147-152.
3. A. Bacchi, M. Carcelli, M. Costa, A. Leporati, E. Leporati, P. Pelagatti, C. Pelizzi and G. Pelizzi, *J. Organomet. Chem.*, 535, (1997), 107-120.
4. C. Ghilardi, S. Midollini, S. Moneti, A. Orlandini and G. Scapacci, *J. Chem. Soc., Dalton Trans.*, (1992), 3371-3376.
5. E. Ainscough, A. Brodie, P. Buckley, A. Burrell, S. Kennedy and J. Waters, *J. Chem. Soc., Dalton Trans.*, (2000), 2663-2671.
6. P. Bhattacharyya, J. Parr and A. Slawin, *J. Chem. Soc., Dalton Trans.*, (1998), 3609-3614.
7. P. Crochet, J. Gimeno, S. Garcia-Granda and J. Borge, *Organometallics.*, 20, (2001), 4369-4377.
8. R. Rulke, V. Kaasjager, P. Wehman, C. Elsevier, P. van Leeuwen and K. Vrieze, *Organometallics.*, 15, (1996), 3022-3031.
9. W. Wong, J. Gao, W. Wong, W. Cheng and C. Che, *J. Organomet. Chem.*, 471. (1994), 277-282.
10. W. Wong, L. Zhang, Y. Chen, W. Wong, W. Wong, F. Xue and T. Mak, *J. Chem. Soc., Dalton Trans.*, (2000), 1397-1398.
11. P. Atkins, *Physical Chemistry.* 1998. Oxford University Press, Oxford.
12. I. Hanson, *Acta Cryst.*, B34, (1978), 1026-1028.
13. R. Rogers, S. Huggins, R. Henry and A. Bond, *Supramol. Chem.*, 1, (1992), 59-63.
14. S. Talipov, Z. Karimov, B. Ibragimov, A. Tashmukhamedova, N. Saifullina and T. Aripov, *Kristallografiya (Russ.).*, 45, (2000), 492-495.
15. R. Rogers, R. Henry and A. Rollins, *J. Inclusion Phenom., Macrocyclic Chem.*, 13, (1992), 219-232.
16. V. Tkachev, L. Atovmyan, I. Bulgak, V. Zubareva and O. Raevskii, *Zh. Strukt. Khim. (Russ.) (Russ. J. Struct. Chem.).*, 31, (1990), 96-95.
17. Y. Simonov, S. Malinovskii, D. Rudkevich and V. Kal'chenko, *Kristallografiya (Russ.).*, 36, (1991), 887-891.
18. V. Yam, K. Lo and K. Cheung, *Inorg. Chem.*, 34, (1995), 4013-4014.

19. L. Engelhardt, C. Pakawatchai, A. White and P. Healy, *J. Chem. Soc., Dalton Trans.*, (1985), 125-138.
20. V. Yam, Y. Pui, K. Lo and K. Cheung, *J. Chem. Soc., Dalton Trans.*, (1998), 3615-3621.
21. M. Jalil, S. Fujinami, T. Honjo and H. Nishikawa, *Poyhedron.*, 20, (2001), 1071-1078.
22. E. Ainscough, A. Brodie, A. Burrell, X. Fan, M. Halstead, S. Kennedy and J. Waters, *Polyhedron.*, 19, (2000), 2585-2592.
23. R. Staples, C. King, N. Khan, R. Winpenny and J. Fackler, *Acta Cryst.*, C49, (1993), 472-475.
24. J. Wang, *Acta Cryst.*, C52, (1996), 611-613.
25. T. Baukova, D. Kravtsov, L. Kuzmina, N. Dvortsova, M. Porai-Koshits and E. Perevlova, *J. Organomet. Chem.*, 372, (1989), 465-471.
26. M. Garland, J. Marouille and E. Spodine, *Acta Cryst.*, C42, (1986), 299-301.
27. A. Shnulin, Y. Struchkov, K. Mamedov and A. Bezuglaya, *Zh. Strukt. Khim. (Russ.) (Russ. J. Struct. Chem.).*, 18, (1977), 1015-1024.
28. C. Sanders, K. Gillespie, D. Bell and P. Scott, *J. Am. Chem. Soc.*, 122, (2000), 7132-7133.
29. P. Healy, C. Pakawatchai and A. White, *J. Chem. Soc., Dalton Trans.*, (1985), 2531-2539.
30. G. Bowmaker, P. Healy, D. Kepert, J. Kildea, B. Skelton and A. White, *J. Chem. Soc., Dalton Trans.*, (1989), 1639-1644.
31. H. Oshio, T. Watanabe, A. Ohto, T. Ito and H. Masuda, *Inorg. Chem.*, 35, (1996), 472-479.
32. J. Zukerman-Schpector, E. Castellano, A. Mauro and M. Roveri, *Acta Cryst.*, C42 (1986), 302-303.
33. Y. Pennings, W. Driessen and J. Reedijk, *Polyhedron.*, 7, (1988), 2583-2589.
34. J. Kasper and K. Lonsdale, *International tables for x-ray crystallography (Vol. II).* 1962. The Kynoch Press, Biringham.
35. N. Baenziger, W. Bennett and D. Soboroff, *Acta Cryst.*, B32, (1976), 962-963.
36. L. Kuz'mina and N. Dvortsova, *Zh. Neorg. Khim.*, 36, (1991), 2021-2023.
37. L. Engelhardt, C. Pakawatchai, A. White and P. Healy, *J. Chem. Soc., Dalton Trans.*, (1985), 125-133.

38. K. Angermair, G. Bowmaker, E. de Silva, P. Healy, B. Jones and H. Schmidbaur, *J. Chem. Soc., Dalton Trans.*, (1996), 3121-3129.

39. G. Bowmaker, Effendy, P. Harvey, P. Healy, B. Skelton and A. White, *J. Chem. Soc., Dalton Trans.*, (1996), 2459-2465.

40. G. Bowmaker, Effendy, P. Harvey, P. Healy, B. Skelton and A. White, *J. Chem. Soc., Dalton Trans.*, (1996), 2449-2457.

41. E. Ainscough, A. Brodie, A. Burrell, G. Freeman, G. Jameson, G. Bowmaker, J. Hanna and P. Healy, *J. Chem. Soc., Dalton Trans.*, (2001), 144-151.

42. G. Bowmaker, S. Boyd, J. Hanna, R. Hart, P. Healy, B. Skelton and A. White, *J. Chem. Soc., Dalton Trans.*, (2002), 2722-2730.

43. G. Bowmaker, R. Hart, E. De Silva, B. Skelton and A. White, *Aust. J. Chem.*, 50, (1997), 621-626.

44. G. Bowmaker, R. Hart, J. Kildea, E. De Silva, B. Skelton and A. White, *Aust. J. Chem.*, 50, (1997), 605-619.

45. E. Pretsch, P. Bühlmann, C. Affolter, *Structure determination of organic compounds*. 2000. Springer, Berlin.

46. W. Kemp, *Organic spectroscopy*. (3rd Ed.), 1991. MacMillan Education Ltd, London.

47. V. Yam, R. Tang, K. Wong, C. Ko and K. Cheung, *Inorg. Chem.*, 40, (2001), 571-574.

48. G. Crossetti, C. Filgueiras, R. Howie, J. Wardell and C. Ziglio, *Acta Cryst.*, C57, (2001), 1279-1281.

49. P. Beer, C. Crane and M. Drew, *J. Chem. Soc., Dalton Trans.*, (1991), 3235-3242.

50. R. Silverstin and F. Webster, *Spectrometric identification of organic compounds*. (6th Ed.), 1998. John Wiley and Sons Inc, Canada.

51. V. Yam, Y. Pui, K. Cheung and N. Zhu, *New J. Chem.*, 26, (2002), 536-542.

52. V. Yam, K. Wong, V. Lee, K. Lo and K. Cheung, *Organometallics.*, 14, (1995), 4034-4036.

53. L. Crociani, G. Bandoli, A. Dolmella, M. Basato and B. Corain, *Eur. J. Inorg. Chem.*, (1998), 1811-1820.

54. H. Song, Z. Zhang and T. Mak, *Polyhedron.*, 21, (2002), 1043-1050.

55. S. Berger, S. Braun and H. Kalinowski, *NMR spectroscopy of the non-metallic elements*. 1997. John Wiley and Sons Inc, Sussex.

Chapter 3

The Iminophosphine Carbonyl Complexes of Cr(0), Mo(0) and W(0)

3.1 Introduction

In this chapter the syntheses of Cr(0), Mo(0) and W(0) carbonyl complexes of the two iminophosphine ligands *N*-(2-diphenylphosphinobenzylidine)-aniline (NP) and *N*-(2-diphenylphosphinobenzylidine)-4'-(benzo-15-crown-5) (O_5NP) are reported. All complexes were characterised by IR and NMR spectroscopy while X-ray structural analyses of $Mo(CO)_4$(NP) and $Mo(CO)_4$(O_5NP) were performed to determine the coordinating mode of the ligands and to study the effect of the presence of the 15-crown-5 moiety in the $Mo(CO)_4$(O_5NP) complex.

Sanchez *et al.* have reported the characterisation and synthesis of the Mo(0) and W(0) complexes [$M(CO)_4$(*o*-$Ph_2PC_6H_4$-CH=NR)] (R = Me, Et, ^{i}Pr, ^{t}Bu, NH-Me). The X-ray structural analysis of [$Mo(CO)_4$(*o*-$Ph_2PC_6H_4$-CH=NMe)] was reported and the ligand was found to be bidentate through the P and N atoms. The metal centre was octahedral with the P and N atoms in a *cis* conformation.[1]

A preliminary report of the preparation and characterisation of these complexes has been written,[2] and a summary is given here with new interpretations, as well as the previously unreported crystal structure of $Mo(CO)_4$(NP).

3.2 Experimental

3.2.1 Instrumentation

All ^{1}H, ^{31}P and ^{13}C spectra were obtained in 5mm grade 527-PP tubes on a Bruker Avance 400 MHz spectrometer with $CDCl_3$ as solvent (containing TMS as internal standard for ^{1}H and ^{13}C NMR) supplied by Merck. The external standard for ^{31}P was 85% H_3PO_4. ^{1}H NMR spectra were collected at a frequency of 400 MHz, ^{31}C NMR spectra at 100 MHz and ^{31}P NMR spectra at 162 MHz.

Infrared (IR) spectra were obtained on a FT-IR Perkin-Elmer Paragon 1000 spectrometer as either nujol mulls between NaCl disks or as a solution in spectroscopic grade $CHCl_3$ (Ajax Chemicals) as solvent in a NaCl solution cell.

X-ray data sets were collected at the Chemistry Department, Auckland University. The X-ray structure $Mo(CO)_4(O_5NP)$ was solved by the author as a requirement for 123.704 and that of $Mo(CO)_4(NP)$ by Dr. Andreas Derwahl.

Elemental analyses for carbon, hydrogen and nitrogen were performed by the Campbell Microanalytical Laboratory, University of Otago, Dunedin.

Electrospray mass spectra were obtained using a micromass ZMD ESMS quadrupole spectrometer with CH_3CN as solvent and mobile phase.

3.2.2 Materials

All solvents were AR grade and supplied by commercial suppliers. The starting complexes *cis*-$M(CO)_4(Pip)_2$ (M = Mo, W) and $Cr(CO)_4(NBD)$ were prepared from standard methods.[3,4]

3.2.3 The Carbonyl Complexes of Cr(0), Mo(0) and W(0)

The complexes $M(CO)_4(L)$ (M = Mo, W; L = NP, O_5NP) were prepared by refluxing, under N_2, *cis*-$M(CO)_4(Pip)_2$ with L while $Cr(CO)_4(L)$ was prepared by reacting $Cr(CO)_4(NBD)$ with L. The crude reaction solutions were then filtered through kieselguhr. The filtrate was then taken to dryness and the products recrystallised from CH_2Cl_2 with hexane added to induce precipitation. The solid products were isolated and dried *in vacuo*. For details of individual preparations see Table 3.1 and for the elemental analysis see Table 3.2.

Table 3.1. Details of the preparation of the Cr(0), Mo(0) and W(0) carbonyl complexes.

	Starting Complexes	Ligand	Solvent	Reflux time	Yield
$Cr(CO)_4(NP)$	$[Cr(CO)_4(NBD)]$ 0.17 g, 0.65 mmol	NP 0.25 g, 0.70 mmol	Acetone: CH_3CN 1:1 20 ml	2 h	0.188 g 0.36 mmol 53.7%
$Cr(CO)_4(O_5NP)$	$[Cr(CO)_4(NBD)]$ 0.116 g, 0.45 mmol	O_5NP 0.253 g, 0.46 mmol	Acetone: CH_3CN 1:1 20 ml	1.5 h	0.259 g 0.36 mmol 79.7%
$Mo(CO)_4(NP)$	*cis*-$[Mo(CO)_4(Pip)_2]$ 0.25 g, 0.67 mmol	NP 0.27 g, 0.73 mmol	CH_2Cl_2 20 ml	0.5 h	0.310 g 0.54 mmol 80%
$Mo(CO)_4(O_5NP)$	*cis*-$[Mo(CO)_4(Pip)_2]$ 0.28 g, 0.75 mmol	O_5NP 0.42 g, 0.77 mmol	CH_2Cl_2 20 ml	1 h	0.447 g 0.59 mmol 78%
$W(CO)_4(NP)$	*cis*-$[W(CO)_4(Pip)_2]$ 0.255 g, 0.55 mmol	NP 0.20 g, 0.55 mmol	CH_2Cl_2 20 ml	1 h	0.319 g 0.48 mmol 88%
$W(CO)_4(O_5NP)$	*cis*-$[W(CO)_4(Pip)_2]$ 0.243 g, 0.52 mmol	O_5NP 0.287 g, 0.52 mmol	CH_2Cl_2 10 ml	1.5 h	0.317 g 0.37 mmol 72%

NBD = 2,5-norbornadiene; Pip = piperdine

Table 3.2. Elemental analyses for the Cr(0), Mo(0) and W(0) carbonyl complexes (%).

	Found				Calculated		
	C	H	N	Empirical formula	C	H	N
$Cr(CO)_4(NP)$	65.64	3.95	2.65	$C_{29}H_{20}CrNO_4P$	65.78	3.82	2.65
$Cr(CO)_4(O_5NP)$	61.86	4.93	2.10	$C_{37}H_{34}CrNO_9P$	61.74	4.77	1.95
$Mo(CO)_4(NP)$	60.86	3.54	2.51	$C_{29}H_{20}MoNO_4P$	60.74	3.54	2.44
$Mo(CO)_4(O_5NP)$	58.21	4.29	1.83	$C_{37}H_{34}MoNO_9P$	58.20	4.50	1.83
$W(CO)_4(NP)$	52.78	2.92	2.16	$C_{29}H_{20}NO_4PW$	52.66	3.05	2.12
$W(CO)_4(O_5NP)$	51.61	4.24	1.80	$C_{37}H_{34}NO_9PW$	52.19	4.02	1.64

3.3 Results and Discussion

3.3.1 Crystal structures

3.3.1.1 The Structure of $Mo(CO)_4(NP)$

The X-ray structure of $Mo(CO)_4(NP)$ (Figure 3.1) was obtained from dark red crystals grown by slow diffusion of Et_2O into a CH_2Cl_2 solution over several days. The structure refinement and crystal data is in Table 3.3, selected bound lengths and angles in Table 3.4, selected torsion angles in Table 3.5 and hydrogen bonds in Table 3.6. The Mo(0) centre has a distorted octahedral geometry with the NP ligand chelating through the P and N atoms which are *cis* to each other. The small N(20)-Mo(1)-P(1) angle of 76.99(5)° is in line with previously discussed X-ray structural analyses and similar complexes.[1] The OC-Mo-CO angles, with a range of 174.18 to 86.41 , are smaller than expected indicating that the CO groups are bent away from the P and N atoms. The average carbonyl bond distance of 1.151 Å and the average Mo—C bond length of 2.014 Å are similar to other complexes.[1,5] The Mo(1)-N(20) bond length of 2.2784(19) Å is close to that of structural analogues as is the Mo(1)-P(1) bond length of 2.5103(6) Å.[1,5]

The imine bond C(19)-N(20) has a length of 1.285(3) Å which is in agreement with that found in similar compounds. The bonds to either side of the imine C(18)-C(19) and N(20)-C(21) have bond lengths of 1.468(3) Å and 1.454(3) Å which are consistent with the previously described structures (Section 2.3.2). The angles about the imine bond are unremarkable.

The torsion angle C(18)-C(19)-N(20)-C(21) of 169.5(2)° shows the imine to have an *E* conformation with the aryl groups in the *trans* positions. The P and N atoms are both on the same side relative to the C(13)-C(18)-C(19) moiety to enable chelation. The imine nitrogen phenyl ring is 72.2° out of plane with the imine. This twist is larger than that found for other structures in this work and will hinder delocalization through the conjugated imine chain.

A single intermolecular hydrogen bond is present between the imine hydrogen and a carbonyl oxygen (Table 3.6).

Figure 3.1. ORTEP diagram of $Mo(CO)_4(NP)$. Thermal ellipsoids are at 50% probability.

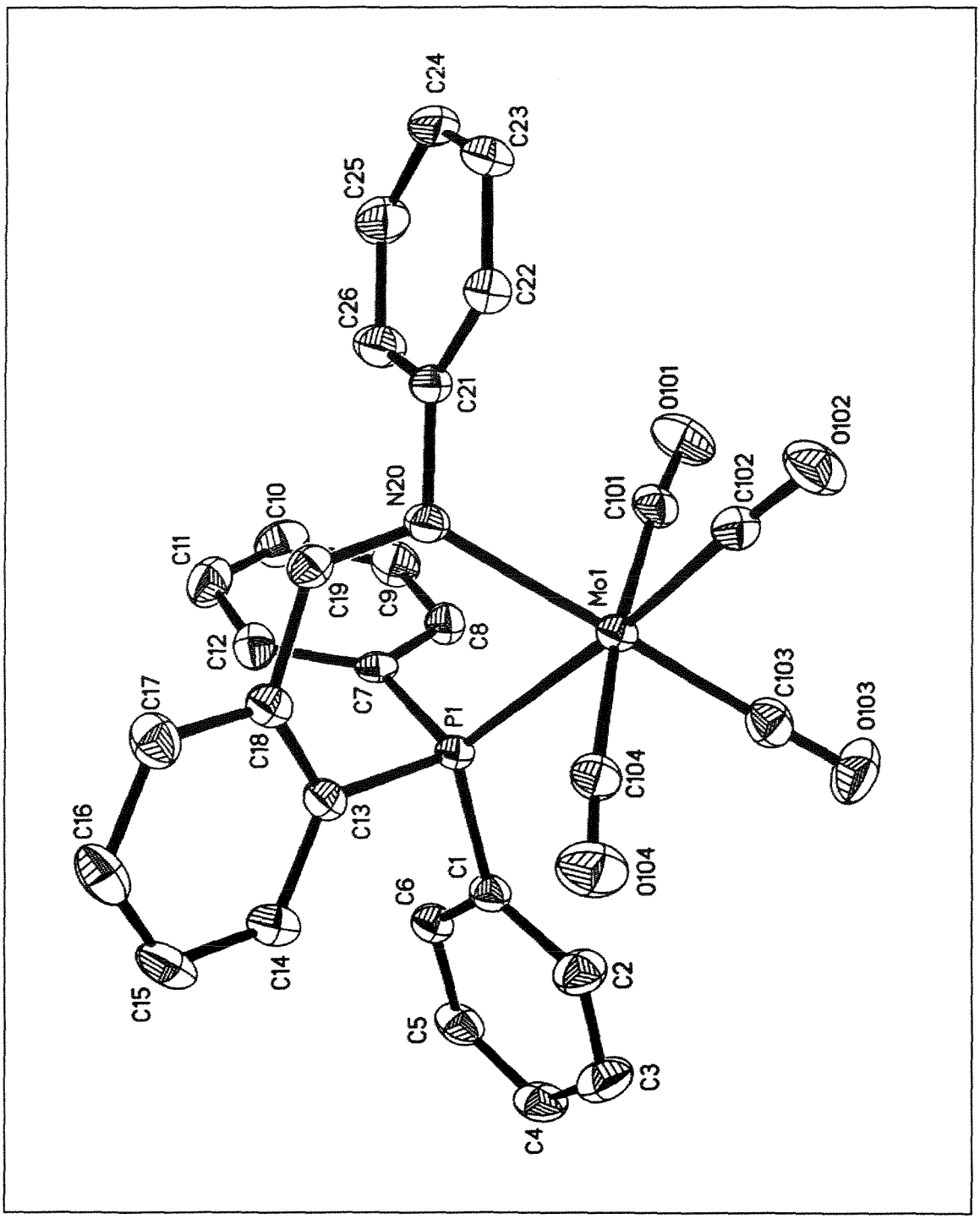

Table 3.3. Crystal data and structure refinement for $Mo(CO)_4(NP)$.

Identification code	ka32	
Empirical formula	$C_{29}H_{20}MoNO_4P$	
Formula weight	573.37	
Temperature	150(2) K	
Wavelength	0.71073 Å	
Crystal system	Monoclinic	
Space group	P2(1)/n	
Unit cell dimensions	a = 12.5353(3) Å	α= 90°
	b = 12.6238(3) Å	β= 94.2850(10)°
	c = 16.5766(4) Å	γ = 90°
Volume	2615.80(11) Å^3	
Z	4	
Density (calculated)	1.456 Mg/m^3	
Absorption coefficient	0.597 mm^{-1}	
F(000)	1160	
Crystal size	0.36 x 0.20 x 0.18 mm^3	
Theta range for data collection	1.97 to 25.02°	
Index ranges	$-14 \le h \le 14$, $0 \le k \le 15$, $0 \le l \le 19$	
Reflections collected	4595	
Independent reflections	4595 [R(int) = 0.0000]	
Completeness to theta = 25.02°	99.7 %	
Absorption correction	None	
Max. and min. transmission	0.9001 and 0.8137	
Refinement method	Full-matrix least-squares on F^2	
Data / restraints / parameters	4595 / 0 / 325	
Goodness-of-fit on F^2	0.983	
Final R indices [I>2sigma(I)]	R1 = 0.0303, wR2 = 0.0752	
R indices (all data)	R1 = 0.0374, wR2 = 0.0782	
Largest diff. peak and hole	0.781 and -0.701 e.Å^{-3}	

Table 3.4. Selected bond lengths (Å) and angles (°) for $Mo(CO)_4(NP)$.

Mo(1)-C(103)	1.975(3)	C(103)-Mo(1)-C(102)	88.50(10)
Mo(1)-C(102)	2.001(3)	C(103)-Mo(1)-C(101)	86.41(10)
Mo(1)-C(101)	2.038(3)	C(102)-Mo(1)-C(101)	88.23(9)
Mo(1)-C(104)	2.042(2)	C(103)-Mo(1)-C(104)	88.63(10)
Mo(1)-N(20)	2.2784(19)	C(102)-Mo(1)-C(104)	88.60(9)
Mo(1)-P(1)	2.5103(6)	C(101)-Mo(1)-C(104)	174.18(10)
P(1)-C(1)	1.827(2)	C(103)-Mo(1)-N(20)	173.10(8)
P(1)-C(7)	1.839(2)	C(102)-Mo(1)-N(20)	96.27(8)
P(1)-C(13)	1.848(2)	C(101)-Mo(1)-N(20)	88.75(8)
C(18)-C(19)	1.468(3)	C(104)-Mo(1)-N(20)	96.45(8)
C(19)-N(20)	1.285(3)	C(103)-Mo(1)-P(1)	98.79(7)
N(20)-C(21)	1.454(3)	C(102)-Mo(1)-P(1)	170.77(7)
N(20)-C(19)-C(18)	126.8(2)	C(101)-Mo(1)-P(1)	97.82(7)
C(19)-N(20)-C(21)	113.53(19)	C(104)-Mo(1)-P(1)	85.94(7)
		N(20)-Mo(1)-P(1)	76.99(5)

Table 3.5. Selected torsion angles (°) for $Mo(CO)_4(NP)$.

C(13)-C(18)-C(19)-N(20)	-34.2(4)
C(18)-C(19)-N(20)-C(21)	169.5(2)
C(19)-N(20)-C(21)-C(22)	107.0(3)
C(19)-N(20)-C(21)-C(26)	-72.7(3)

Table 3.6. Hydrogen bonds for $Mo(CO)_4(NP)$ [Å and °].

D-H...A	d(D-H)	d(H...A)	d(D...A)	<(DHA)
C(19)-H(19)...O(101)#1	0.95	2.46	3.082(3)	122.6

3.3.1.2 The Structure of $Mo(CO)_4(O_5NP)$

Figure 3.2 shows the structure of $Mo(CO)_4(O_5NP)$ and Table 3.7 has the crystal data and structure refinement. Table 3.8 has selected bond lengths and angles; Table 3.9 gives selected torsion angles while Table 3.10 lists the hydrogen bonds. The crystals were grown from a CH_2Cl_2:hexane solution over several days.

The crown ether has the distortion associated with a vacant cavity as seen in previous X-ray structural analyses of benzo-15-crown-5 and its derivatives. The Ph—O bonds are shorter than the CH_2—O bonds (Table 3.8). The Ph—O bonds C(23)-O(27) and C(24)-O(39) have lengths of 1.358(4) Å and 1.383(4) Å which compare well with the literature values of 1.389 to 1.332 Å. The CH_2—O bond lengths of $Mo(CO)_4(O_5NP)$, which have an average of 1.431 Å, also compare well with the literature values of 1.472 to 1.356 Å. The C-O-C angles in $Mo(CO)_4(O_5NP)$ are in the range 118.6(3)°-114.1(3)° compared to 120.79°-106.33° for benzo-15-crown-5 moieties.[6-11]

The Mo centre, as expected, is very close to that reported for $Mo(CO)_4(NP)$. It has a distorted octahedral structure with an average carbonyl bond distance of 1.153 Å and an average Mo—C bond length of 2.06 Å. The chelating angle N(20)-Mo(1)-P(1) 78.00(7)° is small with the carbonyl groups bent away from the ligand and the P and N atoms *cis* to each other. The Mo(1)-N(20) bond length of 2.285(3) Å is similar to that in $Mo(CO)_4(NP)$ and to Mo—N distances of similar compounds.[1,5] This consistency also carries over to the Mo(1)-P(1) bond length of 2.5144(11) Å.

The imine bond length and the angles around it are unremarkable (Table 3.8). The torsion angles C(18)-C(19)-N(20)-C(21) 169.5(2)° and C(13)-C(18)-C(19)-N(20) -34.2(4) show the imine bond to have an *E* conformation and the P and N atoms to be on the same side of the ligand as is necessary for the ligand to be bidentate. When compared with the free ligand, which has the P and N atoms on different sides, it can be seen that there is a change in conformation of the ligand upon complexation. The phenyl ring bound to the imine nitrogen atom is twisted by 72.7° out of plane with the imine chain. This is similar to that observed in $Mo(CO)_4(NP)$ but much larger than previously discussed for the free ligand and its complexes (Section 2.3.2).

There is an intermolecular hydrogen bond between the imine hydrogen and the O(36) oxygen atom of the ether ring. There are also intermolecular and intramolecular hydrogen bonds involving hydrogen and oxygen atoms of the ether ring (Table 3.10).

Overall the addition of the crown ether to the NP ligand has not altered the structure of the metal centre in any significant way.

Figure 3.2. ORTEP diagram of $Mo(CO)_4(O_5NP)$. Thermal ellipsoids are at 50% probability.

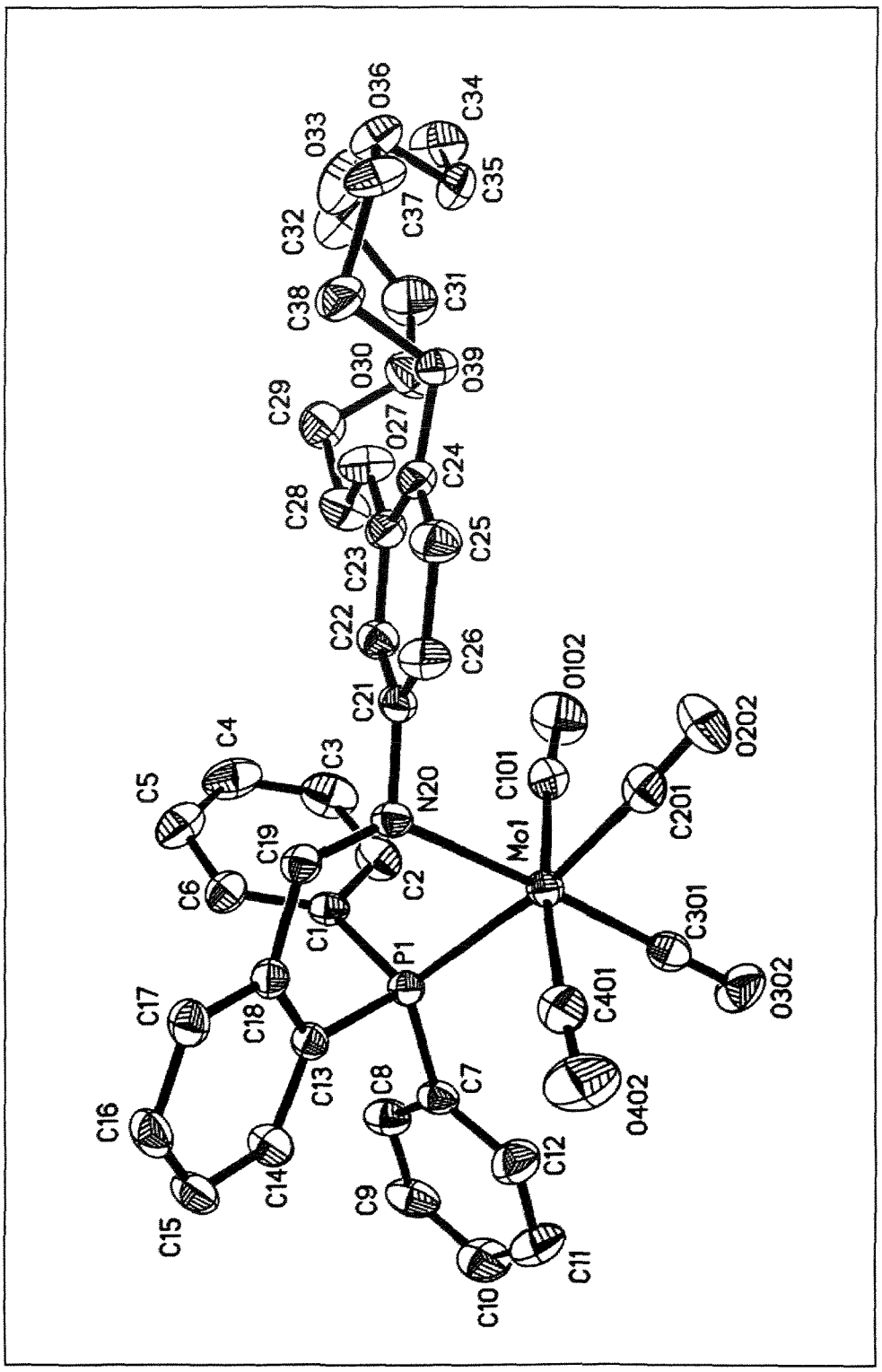

Table 3.7. Crystal data and structure refinement for $Mo(CO)_4(O_5NP)$.

Identification code	kaf	
Empirical formula	$C_{37}H_{34}MoNO_9P$	
Formula weight	763.56	
Temperature	293(2) K	
Wavelength	0.71073 Å	
Crystal system	Triclinic	
Space group	P-1	
Unit cell dimensions	a = 10.478(2) Å	α= 105.86(3)°
	b = 10.763(2) Å	β= 99.74(3)°
	c = 17.068(3) Å	γ = 100.53(3)°
Volume	1771.0(6) Å^3	
Z	2	
Density (calculated)	1.432 Mg/m^3	
Absorption coefficient	0.471 mm^{-1}	
F(000)	784	
Crystal size	2 x 2 x 2 mm^3	
Theta range for data collection	2.03 to 26.38°	
Index ranges	$-12 \le h \le 10$, $-13 \le k \le 13$, $-21 \le l \le 21$	
Reflections collected	22000	
Independent reflections	6951 [R(int) = 0.0294]	
Completeness to theta = 26.38°	95.9 %	
Absorption correction	None	
Refinement method	Full-matrix least-squares on F^2	
Data / restraints / parameters	6951 / 0 / 442	
Goodness-of-fit on F^2	1.037	
Final R indices [I>2sigma(I)]	R1 = 0.0412, wR2 = 0.0967	
R indices (all data)	R1 = 0.0552, wR2 = 0.1042	
Largest diff. peak and hole	1.195 and -0.650 e.Å^{-3}	

Table 3.8. Selected bond lengths (Å) and angles (°) of $Mo(CO)_4(O_5NP)$.

Mo(1)-N(20)	2.285(3)	C(301)-Mo(1)-C(201)	89.65(14)
Mo(1)-P(1)	2.5144(11)	C(301)-Mo(1)-C(101)	87.97(13)
Mo(1)-C(301)	1.975(3)	C(201)-Mo(1)-C(101)	84.20(14)
Mo(1)-C(201)	2.003(4)	C(301)-Mo(1)-C(401)	85.86(13)
Mo(1)-C(101)	2.036(4)	C(201)-Mo(1)-C(401)	91.88(14)
Mo(1)-C(401)	2.050(4)	C(101)-Mo(1)-C(401)	172.71(13)
P(1)-C(13)	1.838(3)	C(301)-Mo(1)-N(20)	177.17(11)
P(1)-C(1)	1.842(3)	C(201)-Mo(1)-N(20)	93.11(11)
P(1)-C(7)	1.842(3)	C(101)-Mo(1)-N(20)	92.89(11)
C(18)-C(19)	1.467(4)	C(401)-Mo(1)-N(20)	93.46(12)
C(19)-N(20)	1.291(4)	C(301)-Mo(1)-P(1)	99.26(10)
N(20)-C(21)	1.456(4)	C(201)-Mo(1)-P(1)	170.80(10)
C(23)-O(27)	1.358(4)	C(101)-Mo(1)-P(1)	93.81(10)
C(24)-O(39)	1.383(4)	C(401)-Mo(1)-P(1)	91.02(10)
O(27)-C(28)	1.438(4)	N(20)-Mo(1)-P(1)	78.00(7)
C(29)-O(30)	1.425(4)	N(20)-C(19)-C(18)	126.2(3)
O(30)-C(31)	1.423(5)	C(19)-N(20)-C(21)	114.0(2)
C(32)-O(33)	1.425(5)	C(23)-O(27)-C(28)	118.6(3)
O(33)-C(34)	1.435(5)	C(31)-O(30)-C(29)	116.7(3)
C(35)-O(36)	1.440(4)	C(32)-O(33)-C(34)	117.8(3)
O(36)-C(37)	1.419(4)	C(37)-O(36)-C(35)	114.1(3)
C(38)-O(39)	1.444(4)	C(24)-O(39)-C(38)	114.8(2)

Table 3.9. Selected torsion angles (°) of $Mo(CO)_4(O_5NP)$.

C(18)-C(19)-N(20)-C(21)	176.9(3)
C(19)-N(20)-C(21)-C(22)	-101.8(3)
C(19)-N(20)-C(21)-C(26)	78.8(4)
C(13)-C(18)-C(19)-N(20)	-26.8(5)

Table 3.10. Hydrogen bonds for $Mo(CO)_4(O_5NP)$ [Å and °].

D-H...A	d(D-H)	d(H...A)	d(D...A)	<(DHA)
C(19)-H(19)...O(36)#1	0.93	2.42	3.153(4)	135.9
C(35)-H(35A)...O(39)	0.97	2.50	3.090(5)	118.9
C(35)-H(35B)...O(30)#2	0.97	2.53	3.447(4)	156.8

3.3.2 Nuclear Magnetic Resonance Spectra

3.3.2.1 ^{1}H and ^{31}P NMR spectra of the Carbonyl Complexes

A change to lower frequencies is experienced by the imine proton upon coordination to the metal center (Table 3.11). For the complexes of O_5NP the shift magnitude is in the order W>Mo>Cr, which mirrors the increase in the size of the atoms. The same trend is not clearly seen for the NP ligand. The CH_2 groups of the crown ether have similar chemical shifts to the free ligand and display the same integral intensity order of 2, 2, 4, and 8. The multiplicity of the $\delta(-CH_2-O-)$ bands suggests coupling around the crown ether.

The ^{31}P NMR chemical shift moves to higher frequencies when coordinated (Table 3.11). The chemical shift decreases in the order Cr>Mo>W for both of the ligands. Coupling to ^{183}W, 14.4% abundance and a nuclear spin of ½, is observed with J_{PW} values of 238 Hz and 296 Hz for the O_5NP and NP complexes.

Table 3.11. Selected ^{1}H and ^{31}P NMR data for the carbonyl complexes (δ/ppm, Hz).

	^{1}H NMR[a]		^{31}P NMR[b]
	δ(CH=N)	δ(-CH_2-O-)	δ(P)
$Cr(CO)_4$(NP)	8.33 (1H, d, 5.17[c])		54.91
$Mo(CO)_4$(NP)	8.19 (1H, d, 2.36[c])		37.13
$W(CO)_4$(NP)	8.20 (1H, d, 2.45[c])		26.30 J_{PW} = 296 Hz
$Cr(CO)_4(O_5NP)$	8.28 (1H, s)	4.06 (2H, s) 3.93 (2H, s) 3.84 (4H, d, 5.88[d]) 3.72 (8H, s)	55.37
$Mo(CO)_4(O_5NP)$	8.15 (1H, d, 2.55[c])	4.06 (2H, m) 3.94 (2H, m) 3.84 (4H, m) 3.72 (8H, d, 3.08[d])	37.39
$W(CO)_4(O_5NP)$	8.12 (1H, d, 7.45[c])	4.05 (2H, m) 3.93 (2H, m) 3.85 (4H, m) 3.72 (8H, d, 3.16[d])	26.70 J_{PW} = 238 Hz

a) Recorded at 400 MHz, δ/ppm relative to TMS with $CDCl_3$ as solvent; b) Recorded at 162 MHz, δ/ppm relative to 85% H_3PO_4 with $CDCl_3$ as solvent; c) J_{HP}; d) J_{HH}.

3.3.2.2 ^{13}C NMR spectra of the complexes

The free ligands NP and O_5NP have ^{13}C NMR δ(CH=N) signals at 159.3 and 157.5 ppm respectively. When this is compared with that of the complexes a clear shift to higher frequency is seen for all the complexes with those of Mo and W being very similar.

The carbonyls can be clearly assigned and these are shown in Table 3.12. Because there are two equivalent CO groups' *cis* to N and P, their signals are higher in intensity allowing for assignment. Previous work[1] has shown that the *trans* to P δ(CO) resonance has coupling constants larger than the *trans* to N δ(CO) resonance allowing assignment of these bands. This results in the highest frequency δ(CO) band for the Mo(0) and W(0) complexes being the *trans* to N and for the Cr(0) complexes the *trans* to P. The $W(CO)_4(NP)$ complex gave ^{13}C-^{183}W coupling of 131.1 Hz

Table 3.12. Selected ^{13}C NMR data for the carbonyl complexes (δ/ppm, Hz)[a].

		δ(CO)		
	δ(CH=N)	*trans* to N[b]	*trans* to P[b]	*cis* to N and P[b]
$Cr(CO)_4(NP)$	171.3 (d, 5.2[c])	224.6 (d, 3.0)[d]	229.8 (d, 12.3)[d]	218.5 (d, 13.1)
$Mo(CO)_4(NP)$	170.1 (d, 3.8[c])	223.1 (d, 7.7)	216.1 (d, 34.5)	208.0 (d, 8.4)
$W(CO)_4(NP)$	170.1 (s)	213.5 (d, 5.3)	209.5 (d, 32.9)	202.6 (d, 6.9, $^1J_{CW}$ = 131.1)
$Cr(CO)_4(O_5NP)$	171.4 (s)	223.5 (d, 2.3)[d]	228.0 (d, 12.6)[d]	216.9 (d, 13.1)
$Mo(CO)_4(O_5NP)$	169.9 (s)	223.1 (d, 8.4)	216.7 (d, 33.6)	208.0 (d, 8.6)
$W(CO)_4(O_5NP)$	170.0 (d, 4.0[c])	213.4 (d, 5.3)	210.3 (d, 32.9)	202.7 (d, 6.8)

a) Recorded at 100 MHz, δ/ppm relative to TMS with $CDCl_3$ as solvent; b) $^2J_{CP}$; c) $^3J_{CP}$: d) Assignments are tentative.

3.3.3 IR spectra

Table 3.13 gives selected nujol mull and $CHCl_3$ solution IR data. All of the carbonyl complexes have four ν(CO) bands which are typical of a *cis*-$[M(CO)_4L_2]$ system. The vibrational modes are shown in Figure 3.3 with their order having been determined[12] as $a_1(1) > a_1(2) > b_1 > b_2$.

Figure 3.3. The ν(CO) modes of a *cis*-$[M(CO)_4L_2]$ system[10].

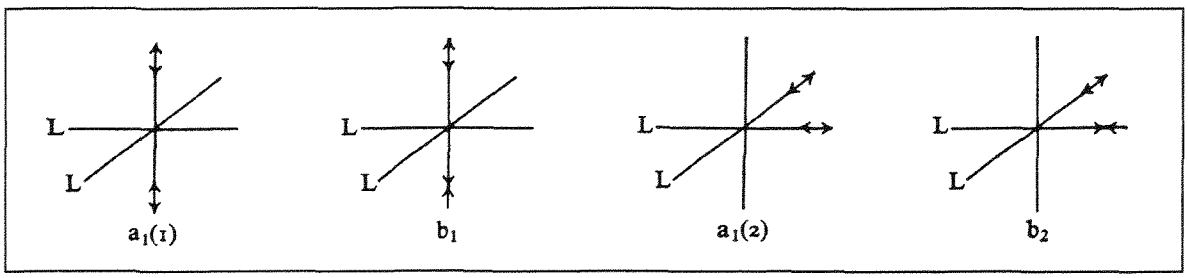

The data (Table 3.13) clearly shows that all the complexes have the expected *cis* configuration and furthermore are in agreement with similar compounds.[1,12] The ν(C=N) stretch moves to lower wavenumbers upon coordination indicating the nitrogen atom is bound to the metal centre.

Table 3.13. Selected IR data of the carbonyl complexes (cm^{-1}).

		ν(CO)[a]			
	ν(C=N)[b]	$a_1(1)$	$a_1(2)$	b_1	b_2
$Cr(CO)_4(NP)$	1588 w	2008 s	1908 s	1892 s	1860 m
$Mo(CO)_4(NP)$	1604 w	2017 s	1914 s	1901 s	1860 m
$W(CO)_4(NP)$	1587 w	2012 s	1904 s	1890 s	1857 m
$Cr(CO)_4(O_5NP)$	1596 m	2007 s	1908 s	1891 s	1859 m
$Mo(CO)_4(O_5NP)$	1598 w	2017 s	1914 s	1898 s	1858 m
$W(CO)_4(O_5NP)$	1592 m	2011 s	1904 s	1887 s	1855 m

[a] In $CHCl_3$. [b] In a nujol mull.

3.3.4 Electrospray Mass Spectroscopy Results

The parent peaks, MH^+, and the isotope calculations confirm the presence of the complexes (Table 3.14). All the parent peaks, which were observed with low intensity, agreed with the isotope calculations. The presence of the $[2M+H]^+$ peaks suggest an association between the individual complexes.

Table 3.14. Selected ESMS data of the carbonyl complexes (m/z).

	MH^+	$[2M+H]^+$
$Cr(CO)_4(NP)$	530 (<1%)	
$Mo(CO)_4(NP)$	574 (1%)	
$W(CO)_4(NP)$	662 (5%)	1323 (<1%)
$Cr(CO)_4(O_5NP)$	720 (<1%)	1441 (<1%)
$Mo(CO)_4(O_5NP)$	766 (4%)	1529 (1%)
$W(CO)_4(O_5NP)$	852 (2%)	1704 (<1%)

3.4 Summary

The main findings of this chapter are given below.

- The Cr(0), Mo(0) and W(0) carbonyl complexes of the NP and O_5NP ligands were successfully synthesized.
- The crystal structures of $Mo(CO)_4$(NP) and $Mo(CO)_4$(O_5NP) have been determined and show the P and N atoms of the ligand to have a *cis* conformation about the octahedral metal.
- IR and ^{13}C NMR spectra show that the P and N atoms have *cis* conformations about the metal centres in all the complexes.
- The ^{1}H NMR spectra of the imine proton move to lower frequencies upon coordination whereas the ^{31}P NMR signal moves to higher frequencies.
- The ^{13}C NMR signals of the carbonyls are metal dependent and decrease in the order Cr>Mo>W.
- The ESMS shows the parent ion, MH^+, for all the complexes.

3.5 References

1. G. Sanchez, J. Serrano, C. Lopez, J. Garcia, J. Pese and G. Lopez, *Inorg. Chim. Acta.*, 306, (2000), 168-173.
2. K. McBeth, *The group VI carbonyl complexes of two iminophosphine ligands. Synthesis, characterization and interaction with alkali cations.* PGDipSci Report, 2001, Massey University.
3. D. Darensbourg and R. Kump, *Inorg. Chem.*, 17, (1978), 2680-2682.
4. H. Werner and R. Prinz, *Chem. Ber.*, 100, (1967), 265-270.
5. E. Ainscough, A. Brodie, P. Buckley, A. Burrell, S. Kennedy and J. Waters, *J. Chem. Soc., Dalton Trans.*, (2000), 2663-2671.
6. I. Hanson, *Acta Cryst.*, B34, (1978), 1026-1028.
7. R. Rogers, S. Huggins, R. Henry and A. Bond, *Supramol. Chem.*, 1, (1992), 59-63.
8. S. Talipov, Z. Karimov, B. Ibragimov, A. Tashmukhamedova, N. Saifullina and T. Aripov, *Kristallografiya (Russ.).*, 45, (2000), 492-495.
9. R. Rogers, R. Henry and A. Rollins, *J. Inclusion Phenom., Macrocyclic Chem.*, 13, (1992), 219-232.
10. V. Tkachev, L. Atovmyan, I. Bulgak, V. Zubareva and O. Raevskii, *Zh. Strukt. Khim. (Russ.) (Russ. J. Struct. Chem.).*, 31, (1990), 96-95.
11. Y. Simonov, S. Malinovskii, D. Rudkevich and V. Kal'chenko, *Kristallografiya (Russ.).*, 36, (1991), 887-891.
12. D. Adams, *Metal–ligand related vibrations*. 1967. Edward Arnold Ltd, London.

Chapter 4

Alkali cation binding by the complexes of O_5NP

4.1 Introduction

In this chapter the cation binding properties of the benzo-15-crown-5 moiety containing complexes of O_5NP are examined. The starting material, 4'-aminobenzo-15-crown-5 (O_5NH_2), and the free ligand, O_5NP, were investigated to assess the effect of the presence of a metal centre. Electrospray mass spectroscopy (ESMS) was used as a qualitative measure of the relative cation binding strengths. X-ray structural analyses of the inclusion complexes $W(CO)_4(O_5NP)Na(PF_6)$ and $[Cu(O_5NP)_2]K[PF_6]_2$ were determined to provide information on the coordination of alkali cations by these complexes.

Tsuda *et al.* investigated the alkali cation binding of 15, 18 and 21 membered benzo- and quino-crown ethers by ESMS. They observed that a plot of relative stability constants versus the ionic radii very closely resembled plots of peak intensities versus ionic radii.[1]

Young *et al.* have used ESMS to determine the stability constants of lariat crown ethers. The method used was verified with known $\log K_s$ values and it was shown that calibration for the relative cationisation efficiencies is necessary.[2,3]

Kempen *et al.* have reported the use of ESMS relative peak intensities to examine the Li^+, Na^+ and K^+ selectivities of a series of dibenzo-16-crown-5 lariat ethers.[4] The heavy metal binding selectivities of caged crowns were also investigated by ESMS.[5]

The graphs in this chapter show the percentage of the maximum peak heights for inclusion complexes where an alkali cation is bound to the sample compound. These were obtained by dividing each peak height by that of the most intense thus making each peak a percentage of the most abundant species. The relative peak heights were then compared with each other.

4.2 Experimental

4.2.1 Instrumentation

X-ray data sets were collected at the Chemistry Departments at Canterbury and Auckland Universities. Professer Geoff Jameson and Dr. Andreas Derwahl solved the X-ray structures.

Electrospray mass spectra were obtained using a micromass ZMD ESMS quadrupole spectrometer with CH_3CN as the solvent and mobile phase.

4.2.2 Materials

All organic solvents were AR grade and all water was deionised and distilled. All alkali metal salts were provided by commercial suppliers. The 4'-aminobenzo-15-crown-5 (O_5NH_2) was supplied by Fluka.

4.2.3 Cation Binding Studies

4.2.3.1 Preparation of the Alkali Cation Solution

The appropriate mass (Table 4.1) of MCl (M = Li, Na, K, Rb, Cs) was added to 25 ml of H_2O to yield an aqueous solution with a concentration of 0.1 mol L^{-1} for each of the alkali chlorides.

Table 4.1. The mass and concentration of MCl.

M	Mass [MCl] (g)	FW [MCl] (g mol^{-1})	moles	Volume (L)	Conc. (mol L^{-1})
Li	0.1060	42.394	0.0025	0.025	0.1000
Na	0.1461	58.442	0.0025	0.025	0.1000
K	0.1870	74.551	0.0025	0.025	0.1000
Rb	0.3023	120.921	0.0025	0.025	0.1000
Cs	0.4208	168.358	0.0025	0.025	0.1000

4.2.3.2 ESMS Sample Preparation

The sample compound (1-2 mg), CH_3CN (0.6 ml), and the alkali chloride solution (0.2 ml) were placed in a 1.5 ml Ependorf tube. The solution was stirred for one minute then left to separate for 4–5 minutes. An aliquot from the top CH_3CN layer (0.4 ml) containing the sample compound with the bound cations was removed and passed through the ESMS device.

Multiple experiments were performed for each of the sample compounds and the results averaged to give relative alkali cation selectivity of the sample compound.

4.3 Results and Discussion

4.3.1 Cation Binding to O_5NH_2 and O_5NP

To investigate the relative cation binding strengths, the peak height of the relevant peak was expressed as a percentage of the most intense of the inclusion peaks. This gives a qualitative measure of the relative binding strengths. Figure 4.2 shows the averaged results of the ESMS cation binding studies of the starting material 4'-aminobenzo-15-crown-5 (O_5NH_2) and the free ligand *N*-(2-diphenylphosphinobenzylidine)-4'-(benzo-15-crown-5) (O_5NP).

The two observed cation binding modes of O_5NH_2 and O_5NP are given in Figure 4.1. The 1:1 complex to cation species arises from the crown enveloping the ion within its cavity or having an ion perched on top of the cavity. The 2:1 complex to cation species occurs when a sandwich complex forms by a cation being bound between two crown ethers.

Figure 4.1. The 1:1 and 2:1 complex to cation species of O_5NH_2 and O_5NP.

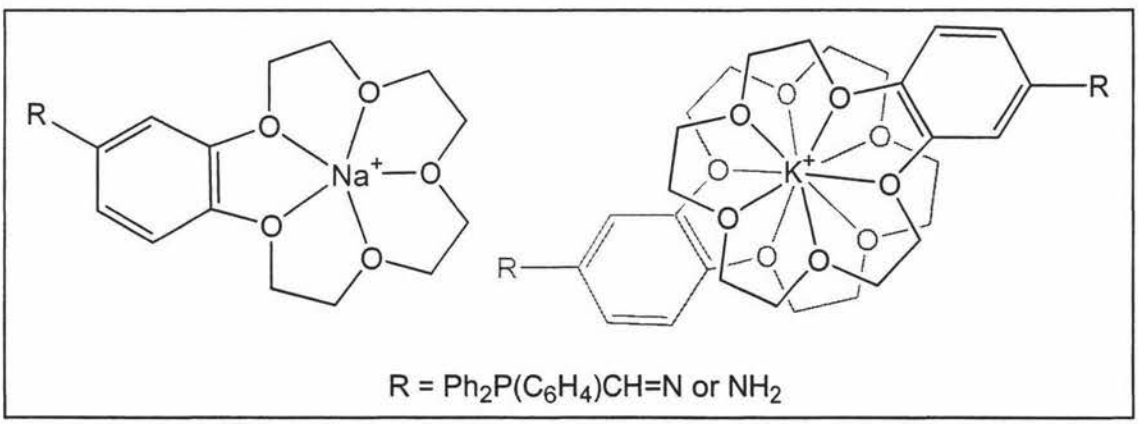

It can be seen that O_5NH_2 shows little selectivity between Na^+ and K^+ in the 1:1 and the 2:1 species. The free ligand O_5NP has improved selectivity especially in the 2:1 ratio. Within the 1:1 species, both O_5NH_2 and O_5NP have a much higher selectivity for both Na^+ and K^+ than any of the other alkali metal ions, which is explained by the close match between the cavity size of a benzo-15-crown-5-ether (2.2-1.7 Å[6]) and the ionic diameter of Na^+ and K^+ (1.94 Å and 2.66 Å[7]). It is surprising, however, that both O_5NH_2 and O_5NP have an apparent preference for K^+ over Na^+, a result which is contradictory

to both previous studies[8,9] and the size of the cation versus the size of the crown's cavity.

Removal of the amine by the formation of an imine bond is a possible cause of the increased selectivity shown by O_5NP. It is unlikely that the low selectivity of O_5NH_2 is due to steric congestion.

The 2:1 species occurs due to the formation of sandwich complexes. The preference of benzo-15-crown-5 to form 2:1 complexes with K^+ is well documented.[1,6,10-13]

Figure 4.2. The relative alkali cation binding strengths of O_5NH_2 and O_5NP.

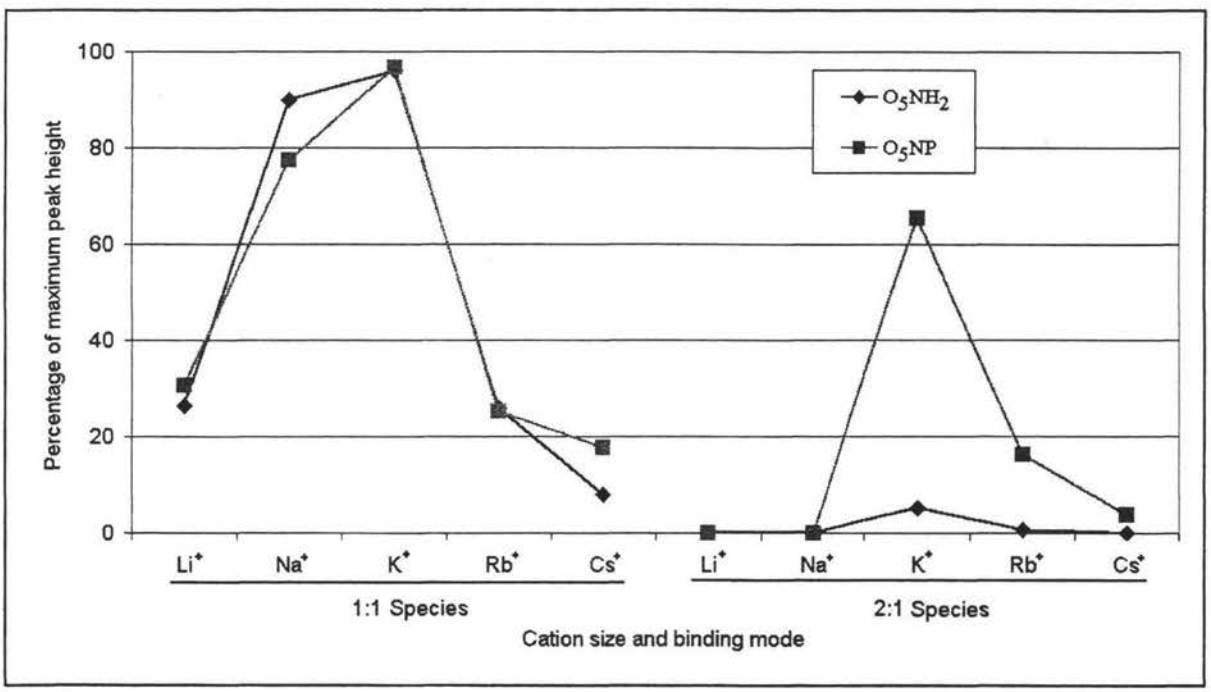

4.3.2 Cation binding to the Cr(0), Mo(0) and W(0) carbonyl complexes

Figure 4.4 shows the averaged results of the cation binding experiments for each of the $M(CO)_4(O_5NP)$ (M = Cr, Mo, W) complexes. The cation selectivity of the complexes is similar to each other with the W complex showing slightly less selectivity for K^+ than those of Cr or Mo. In all the experiments Na^+ had the highest stability for the 1:1 compound to cation species while K^+ had the highest stability with the 2:1 species (Figure 4.3). No other forms of binding were observed.

Figure 4.3. 1:1 and 2:1 cation binding by $M(CO)_4(O_5NP)$.

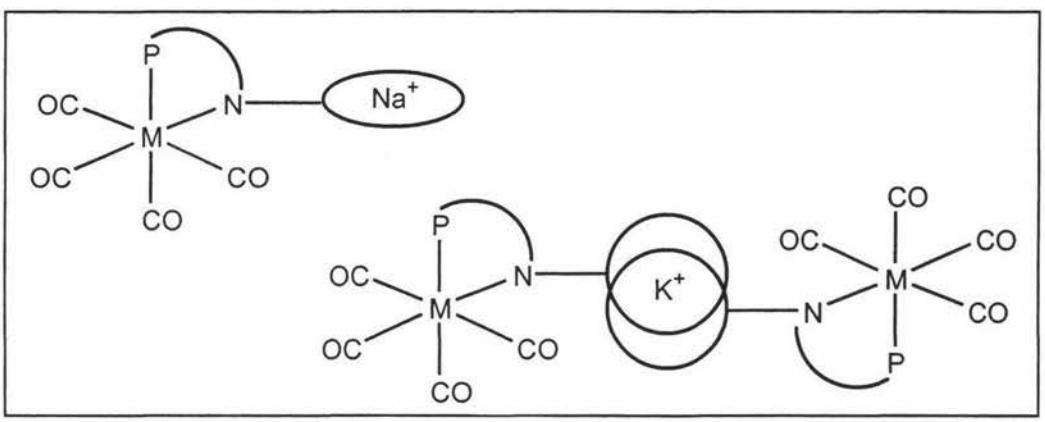

When compared with the results observed for O_5NP it can be seen that complexation of the ligand has affected the selectivity. Selectivity is increased in the 1:1 species and has moved from the small preference for K^+ shown by O_5NP to a larger than expected preference for the Na^+ cation. With the 2:1 species, the selectivity remains the same with the stability of the K^+ inclusion complex having a much higher stability than any other.

These results mirror the mass spectral studies[1] and reported stability constants[8] of the benzo-15-crown-5 moiety. The preference for the Na^+ ion is rationalised by the close match of the benzo-15-crown-5 cavity (2.2-1.7 Å[6]) and the diameter of the alkali cations (Li^+ 1.36, Na^+ 1.94, K^+ 2.66, Rb^+ 2.94, Cs 3.34[7]). The presence of the different transition metal centres does not cause any marked variation in the alkali cation uptake between the complexes.

Figure 4.4. The relative alkali cation binding strengths of $M(CO)_4(O_5NP)$ (M = Cr, Mo, W)

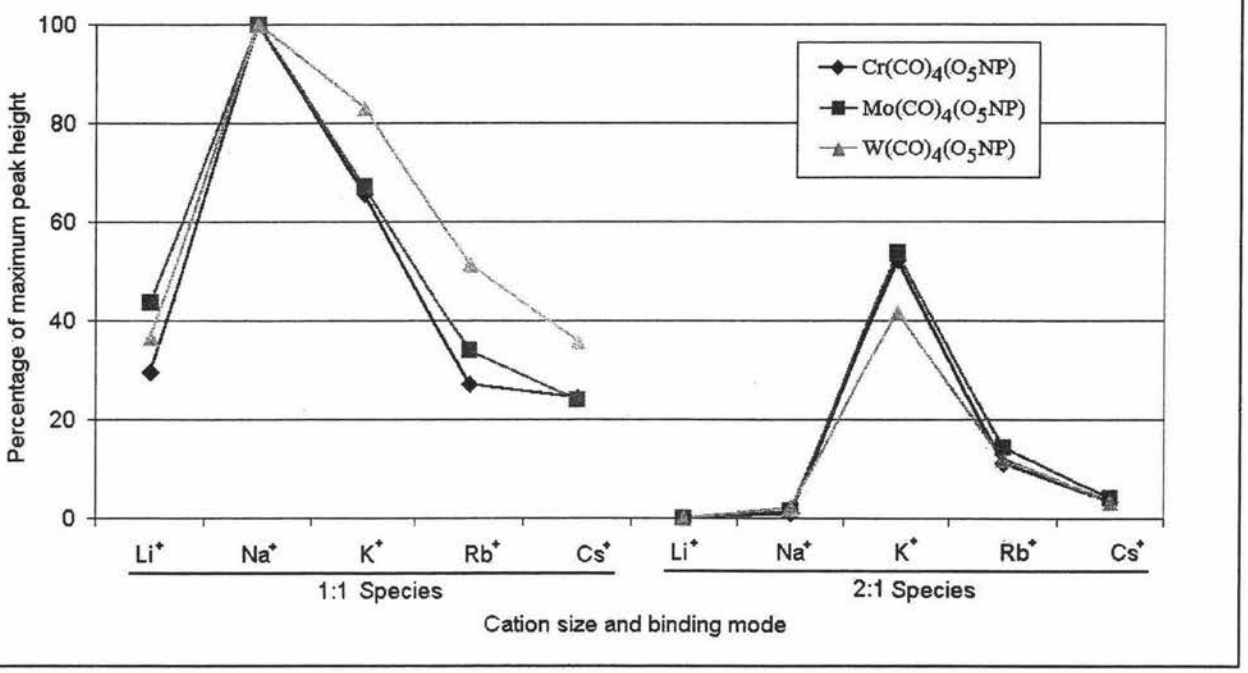

4.3.3 *Cation Binding to the $[M(O_5NP)_2][PF_6]$ complexes (M = Cu, Ag, Au)*

The relative binding strengths of the $[M(O_5NP)_2][PF_6]$ (M = Cu, Ag, Au) complexes is presented in Figure 4.7. Few studies for complexes of this type have been reported. Due to the presence of two ligands in these complexes, there are several possible modes of cation binding. There is the possibility of the complex binding either one cation fully within the cavity of the crown (Figure 4.5a) or of it binding two cations, not necessarily the same, each within a separate crown (Figure 4.5b). A 2:1 complex to cation species could form with a cation sandwiched by two crowns leaving a vacant crown on both of the complexes (Figure 4.5c). Similarly, 2:2 species may occur with two cations being bound between two complexes (Figure 4.5d). Another possibility is a polymeric structure with the cations between crown ethers from different complexes (Figure 4.5e).

Figure 4.5. Some possible cation binding modes of $[M(O_5NP)_2][PF_6]$.

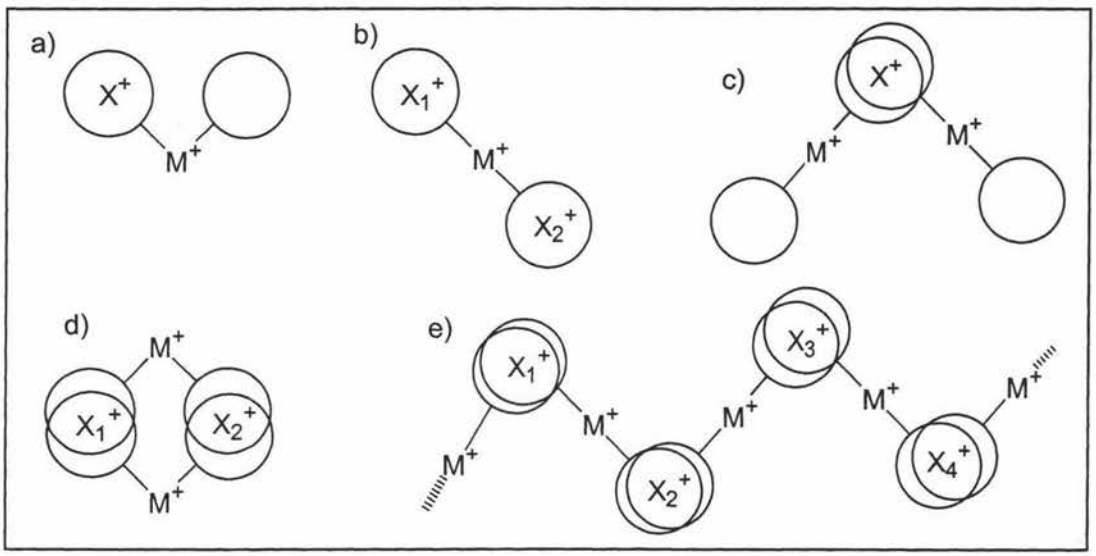

Structures b to e (Figure 4.5) were not observed in the ESMS spectra possibly due to the effects of charge repulsion. The only binding observed was for a 1:1 species where K^+ had the highest binding affinity which suggests that the binding structure had the cation sandwiched between the two benzo-15-crown-5 moieties (Figure 4.6).[14] This however does not remove the possibility of the structure in Figure 4.5a occurring especially with the small Li^+ ion.

Figure 4.6. A probable mode of cation binding by $[M(O_5NP)_2][PF_6]$.

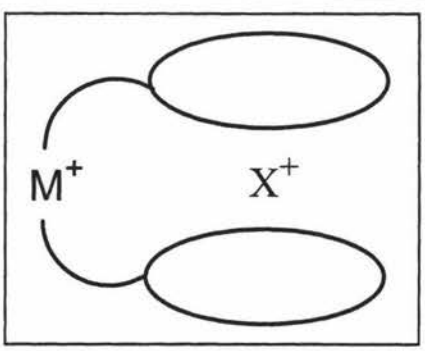

Each of the complexes was selective towards the K^+ ion with $[Ag(O_5NP)_2][PF_6]$ having a much higher relative affinity for K^+ than the other complexes. This selectivity for K^+ can be explained by the cation binding mode given in Figure 4.6 as the affinity for benzo-15-crown-5 to form sandwich complexes with K^+ is well known.[1,6,8-13] The Li^+, Rb^+ and Cs^+ ions have a low selectivity. For Li^+ the ion is too small while Rb^+ and Cs^+

are to large to fit within the ring of the benzo-15-crown-5 or to be sandwiched between the two crowns present in $[M(O_5NP)_2][PF_6]$ (Figure 4.6).

A possible reason for the larger selectivity of $[Ag(O_5NP)_2][PF_6]$ over its Cu and Au analogs may be due to the different coordination modes of the metal centres. If a structural similarly exists between the $[M(NP)_2][PF_6]$ and $[M(O_5NP)_2][PF_6]$ complexes, then the increased K^+ selectivity may be due to the stereochemical requirements of the metal centre. For the Ag complex the ligands show both mono and bidentate modes not seen for the Cu or Au analogues. This geometry may lower the energy required for the distortion of the coordination and so increase the energy gained by binding of K^+.[14]

Figure 4.7. The relative alkali cation binding strengths of $[M(O_5NP)_2][PF_6]$ (M = Cu, Ag, Au).

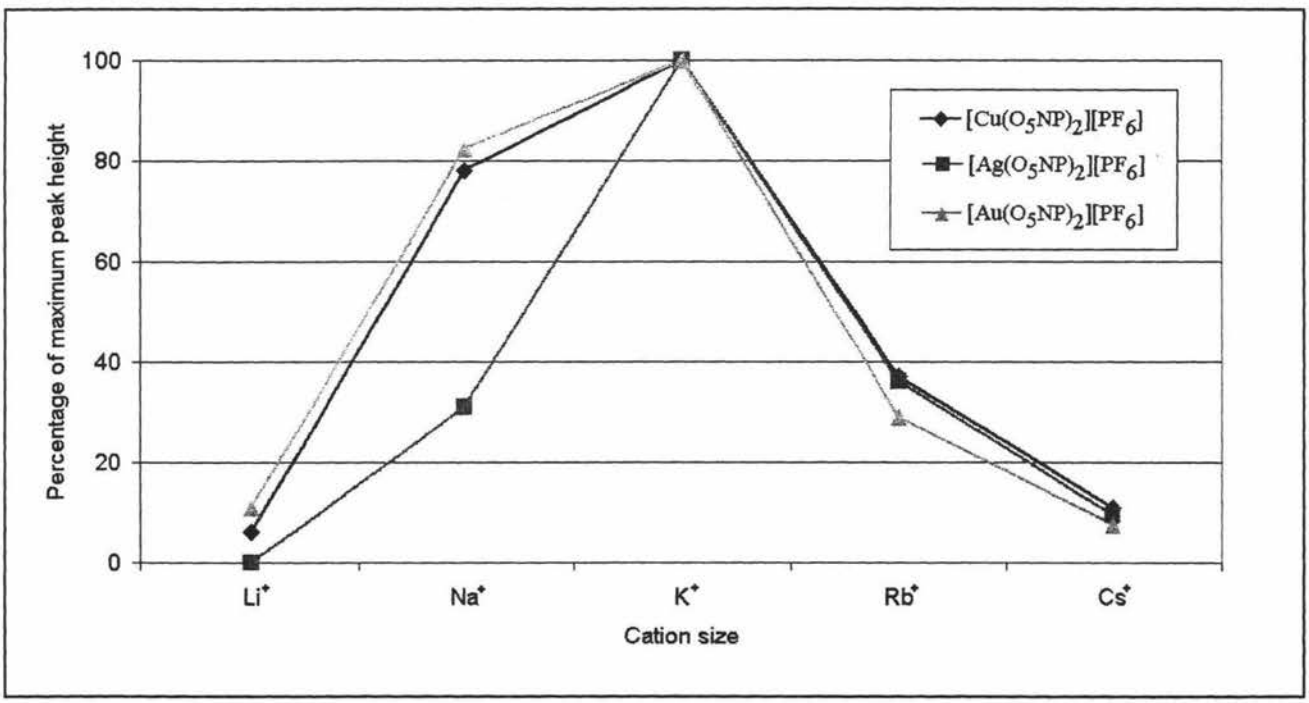

Figure 4.8 shows a typical spectrum of an ESMS experiment of cation binding to $[Au(O_5NP)_2][PF_6]$. It clearly shows the relative selectivity of $[Au(O_5NP)_2][PF_6]$ displayed in Figure 4.7.

Figure 4.8. The ESMS spectra of $[Au(O_5NP)_2M]^{2+}$ (M = Li, Na, K, Rb, Cs)

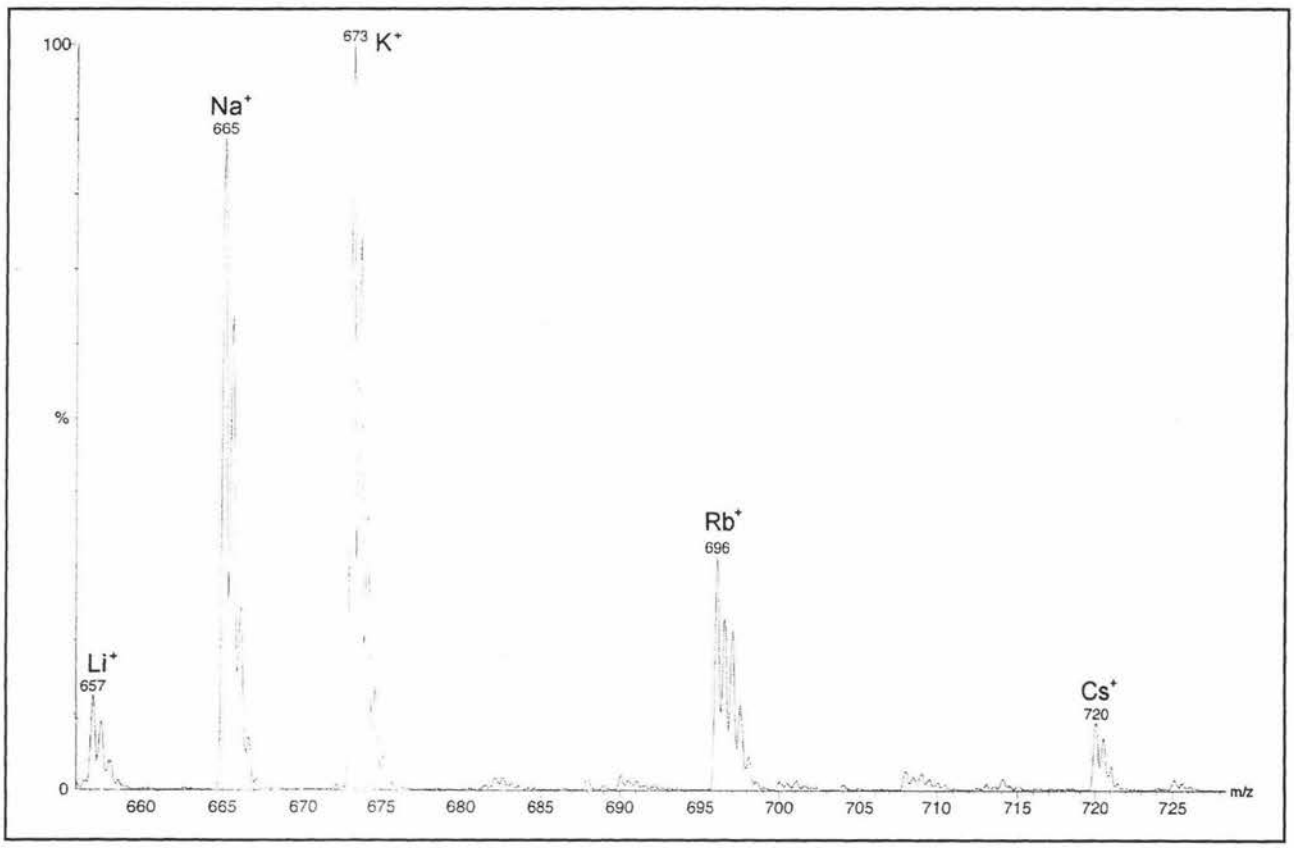

4.3.4 The Cation Binding to the Halide Complexes of Cu(I), Ag(I) and Au(I)

The strong similarities between the O_5NP ligand and its NP counterpart allow the use of the crystal structures of $[Cu(NP)Cl]_2$ and Au(NP)Cl as model structures for the corresponding O_5NP complexes, $[M(O_5NP)Cl]_2$ (M = Cu, Ag) and $Au(O_5NP)Cl$.

The monomer complex $Au(O_5NP)Cl$ probably has a linear coordination with an unbound imine nitrogen. The cation may be bound within the cavity or perched on top of it, giving a 1:1 species, or it may form a 2:1 sandwich complex (Figure 4.9). Peaks corresponding to both of these formations were seen in the ESMS spectra.

Figure 4.9. Possible modes of cation binding by $Au(O_5NP)Cl$.

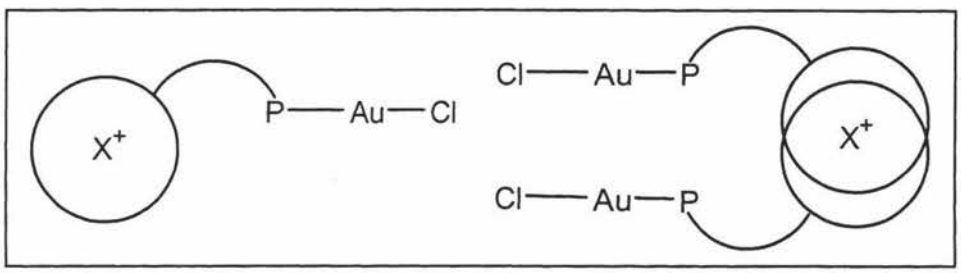

As the $[M(O_5NP)Cl]_2$ (M = Cu, Ag) complexes are possibly dimeric there is the potential for 1:1, 2:1, 1:2 and 2:2 dimer to cation species (Figure 4.10) and polymeric structures similar to the $[M(O_5NP)_2][PF_6]$ complexes (Figure 4.5). It is also conceivable that a 2:3 species can form. However for both the Cu(I) and Ag(I) complexes none of these possibilities occurred as the dimer dissociates to give the monomer $M(O_5NP)Cl$ (M = Cu, Ag). These complexes gave both 1:1 and 2:1 peaks in the mass spectrum suggesting similar species to that formed by $Au(O_5NP)Cl$ (Figure 4.9). The presence of the dimer can not ruled out as the ESMS peaks for the 1:1 dimer to cation species will be identical to those obtained with a 2:1 monomer to cation sandwich species.

Figure 4.10. The 1:1 (a, b), 1:2 (c), 2:1 (d) and 2:2 (e) complex to cation formations possible for cation binding.

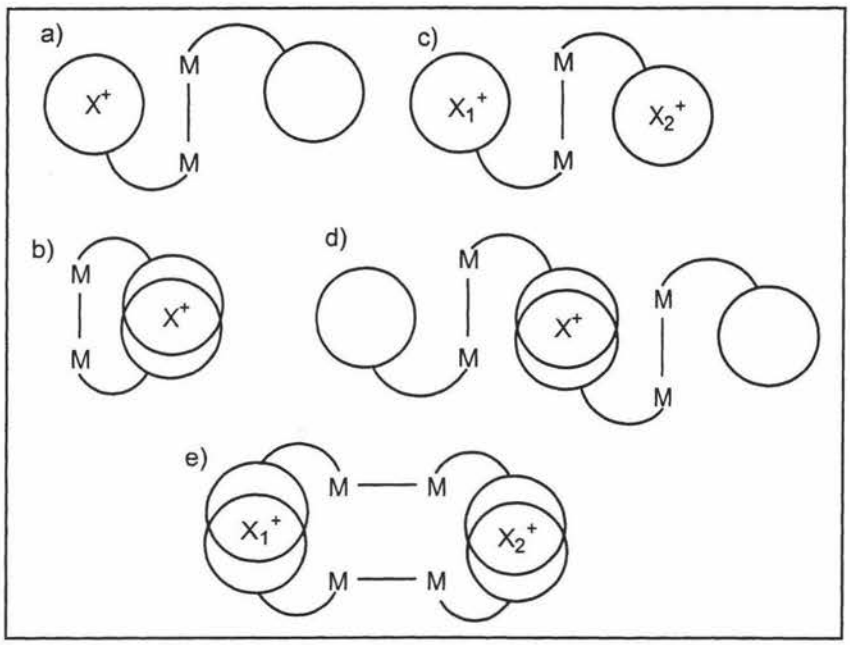

Figure 4.11 shows the averaged results of the ESMS cation binding experiments for $[M(O_5NP)Cl]_2$ (M = Cu, Ag), which were observed as monomeric species, and $Au(O_5NP)Cl$. Each of the complexes displays different selectivities in the 1:1 ratio while in the 2:1 ratio the complexes all have a selectivity for K^+ over the other alkali cations. $Au(O_5NP)Cl$ has a much higher relative preference, in the 2:1 species for K^+, whereas $[Cu(O_5NP)Cl]_2$ or $[Ag(O_5NP)Cl]_2$ showed very little selectivity for the formation of the 2:1 species.

Of the three complexes, only $Au(O_5NP)Cl$ had the expected selectivity for Na^+ in the 1:1 species. $[Ag(O_5NP)Cl]_2$ had a relative peak height of 100% for the K^+ species while the relative peak height of the Na^+ species was 76%. This significant selectivity for K^+ over Na^+ is unusual, but not unique as it has been observed in O_5NP (Figure 4.2). However, a survey of the literature and a comparison of ionic and cavity diameter suggest that Na^+ is preferred by the benzo-15-crown-5 moiety.[8,9]

Figure 4.11. The relative alkali cation binding strengths of $M(O_5NP)Cl$ (M = Cu, Ag, Au).

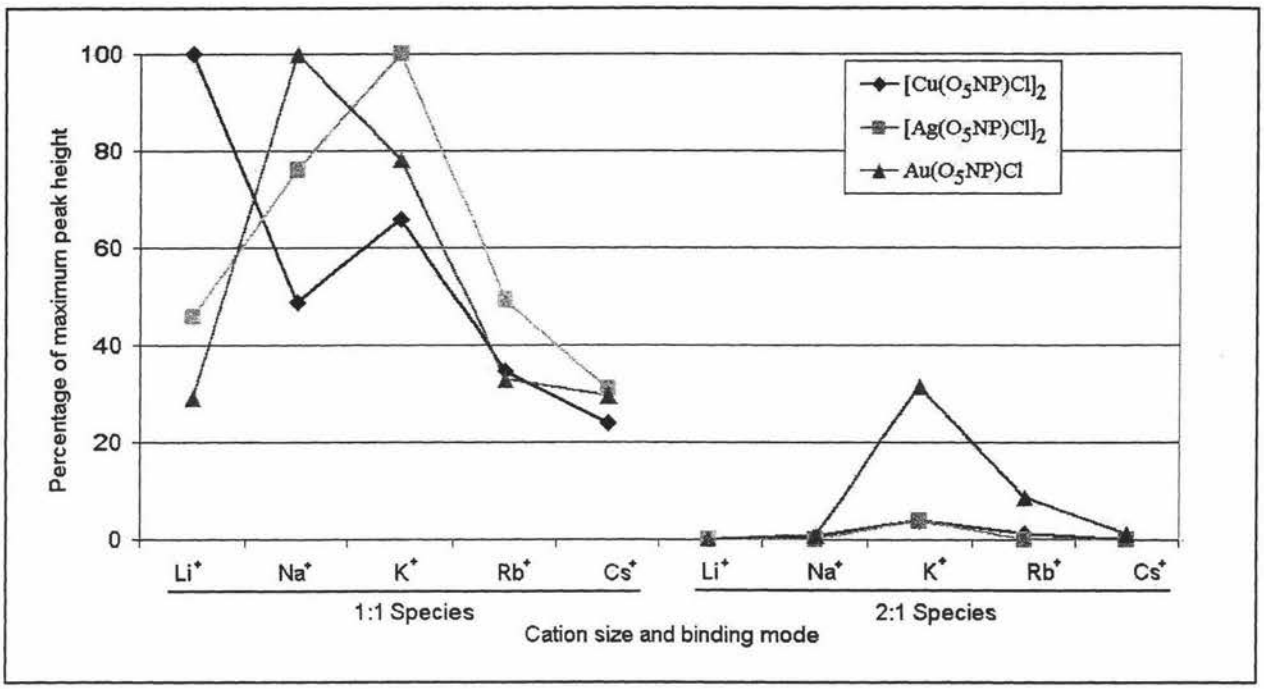

The complex $[Cu(O_5NP)Cl]_2$ is very unusual in that it selects Li^+ over the other cations. Another unusual feature is that it showed higher selectivity for K^+ (66%) over Na^+ (49%). Selectivity for Li^+ has also been reported in other work. Takeda *et al.*[15] has shown that 15-crown-5-ether in propylene carbonate forms the strongest complex with Li^+. It was suggested that this result was due to 15-crown-5 not being able to shield the charge of a cation within its cavity which allows the 15-crown-5:Li^+ complex to have a strong solvation with propylene carbonate. Takeda and Kumazawa[16] have also reported Li^+ to have the most stable formation with benzo-15-crown-5 in CH_3CN. They cited the low solvation strength of Li^+ in CH_3CN causing greater availability of the Li^+ ion to the crown ether as a possible reason for the stability of the species. However these possibilities do not account for the selectivity of $[Cu(O_5NP)Cl]_2$ being different from the other group 11 complexes.

The cause of the unusual selectivity shown by $[Cu(O_5NP)Cl]_2$ and $[Ag(O_5NP)Cl]_2$ is unclear. However the difference in stereochemistry of the group 11 centres and their different sizes are possible factors.

4.3.5 Crystal Structures

4.3.5.1 The structure of $W(CO)_4(O_5NP)Na(PF_6)$

Figures 4.12 and 4.13 show the crystal structure of $W(CO)_4(O_5NP)Na(PF_6)$ with the two orientations held by the PF_6^- in the unit cell. The crystals were produced by stirring $W(CO)_4(O_5NP)$ in CH_2Cl_2 with a slight excess of $NaPF_6$ for two hours. The solution was decanted and pentane added to promote crystal growth over a period of three days. Table 4.2 has the crystal and refinement data and Tables 4.3 and 4.4 have the structural data.

The crystal structure of $W(CO)_4(O_5NP)Na(PF_6)$ (see Figures 4.12 and 4.13) shows a Na^+ ion bound within the crown ether recognition site and tungsten tetracarbonyl in the iminophosphine recognition site of the O_5NP compound. This X-ray structure confirms that the group 6 tetracarbonyl complexes of O_5NP bind alkali cations within the cavity of the benzo-15-crown-5 moiety which is consistent with the results in Section 4.3.2.

The Na—O bond lengths range from 2.395(4) Å to 2.336(4) Å which is in good agreement with the literature range of 2.576 to 2.290 Å.[17-24] From Figures 4.12 and 4.13 it can be seen that the Na(1) atom is displaced from the crown's cavity towards the PF_6^- anion which is either bi or tridentate. The Na—F bonds range from 2.288(8) Å to 2.682(14) Å and are generally shorter than a similar structure with Na—F bond lengths of 2.922 to 2.432 Å.[24]

Comparison of $W(CO)_4(O_5NP)Na(PF_6)$ with $Mo(CO)_4(O_5NP)$ shows a significant difference in both the torsion angles and the angles about the benzo group of the benzo-15-crown-5 moiety. The change in torsion angles range in size from 43.2° to 7° and place adjacent oxygen atoms gauche to each other to accommodate the binding of the Na^+. The bond angles C(24)-O(39)-C(38) (120.1(4)°) and C(25)-O(27)-C(28) (117.2(4)°) have increased by 5.3° and 1.5° respectively, while the bond angles between the benzo group and the oxygens O(39)-C(24)-C(25) (116.4(4)°) and O(27)-C(25)-C(24) (115.3(4)°) have decreased by 2.2° and 4.4° respectively. The bond lengths within the crown are not significantly different from those of $Mo(CO)_4(O_5NP)$. It is of note that no significant changes were observed in the isotropic displacement parameters (U(eq))

of most of the atoms furthest from the benzo group, while most of those closest to the benzo group had increased.

The bond lengths and angles of the imine (Table 4.3) appear unaffected by the presence of the Na^+ when compared to the $Mo(CO)_4(O_5NP)$ complex. The torsion angles about the imine (Table 4.4) show that the imine bond retains its *E* conformation and has the N and P atom on the same side of the C(19)-C(18)-C(13) moiety. However all of the torsion angles have experienced a change from $Mo(CO)_4(O_5NP)$ with the benzo group of the benzo-15-crown-5 being closer to right angles with the imine bond. Whether the changes to the torsion angles are due to the presence of Na^+ or to the replacement of Mo for W remains to be determined.

Relative to the closely related $W(CO)_4(\eta^2\text{-PNN})$ complex[25] (PNN is a P and N bidentate ligand) the W(1)-N(20) and W(1)-P(1) bonds have a shorter (2.245(4) Å) and longer (2.5055(15) Å) bond length respectively. The N(20)-W(1)-P(1) angle of 77.56(10)° is close to the N-W-P angle of 80.74(7)° in $W(CO)_4(\eta^2\text{-PNN})$. The W—C bond lengths range from 2.044(5) to 1.953(5) Å which is in good agreement with those for $W(CO)_4(\eta^2\text{-PNN})$ which range from 2.025(4) Å to 1.955(4) Å.[25] The OC-W-CO angles are very similar to those of $W(CO)_4(\eta^2\text{-PNN})$ and show the carbonyl groups to be bent away from the O_5NP ligand.

Figure 4.12. The ORTEP diagram of $W(CO)_4(O_5NP)Na(PF_6)$ with the PF_6^- bound via two of its F atoms. Thermal ellipsoids at 50% probability.

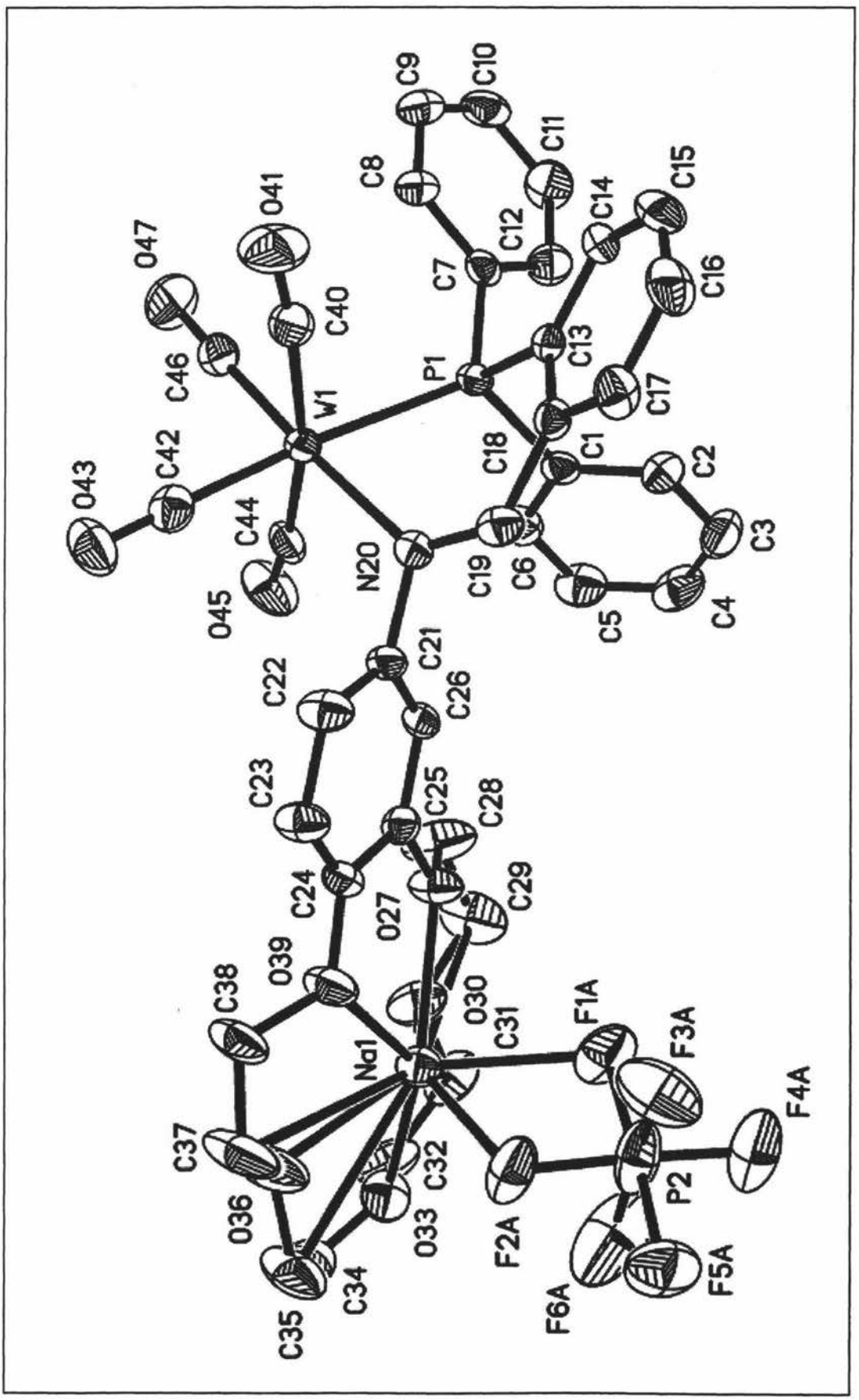

Figure 4.13. The ORTEP diagram of the benzo-15-crown-5 moiety of $W(CO)_4(O_5NP)Na(PF_6)$ with the PF_6^- bound via three of its F atoms. Thermal ellipsoids at 50% probability.

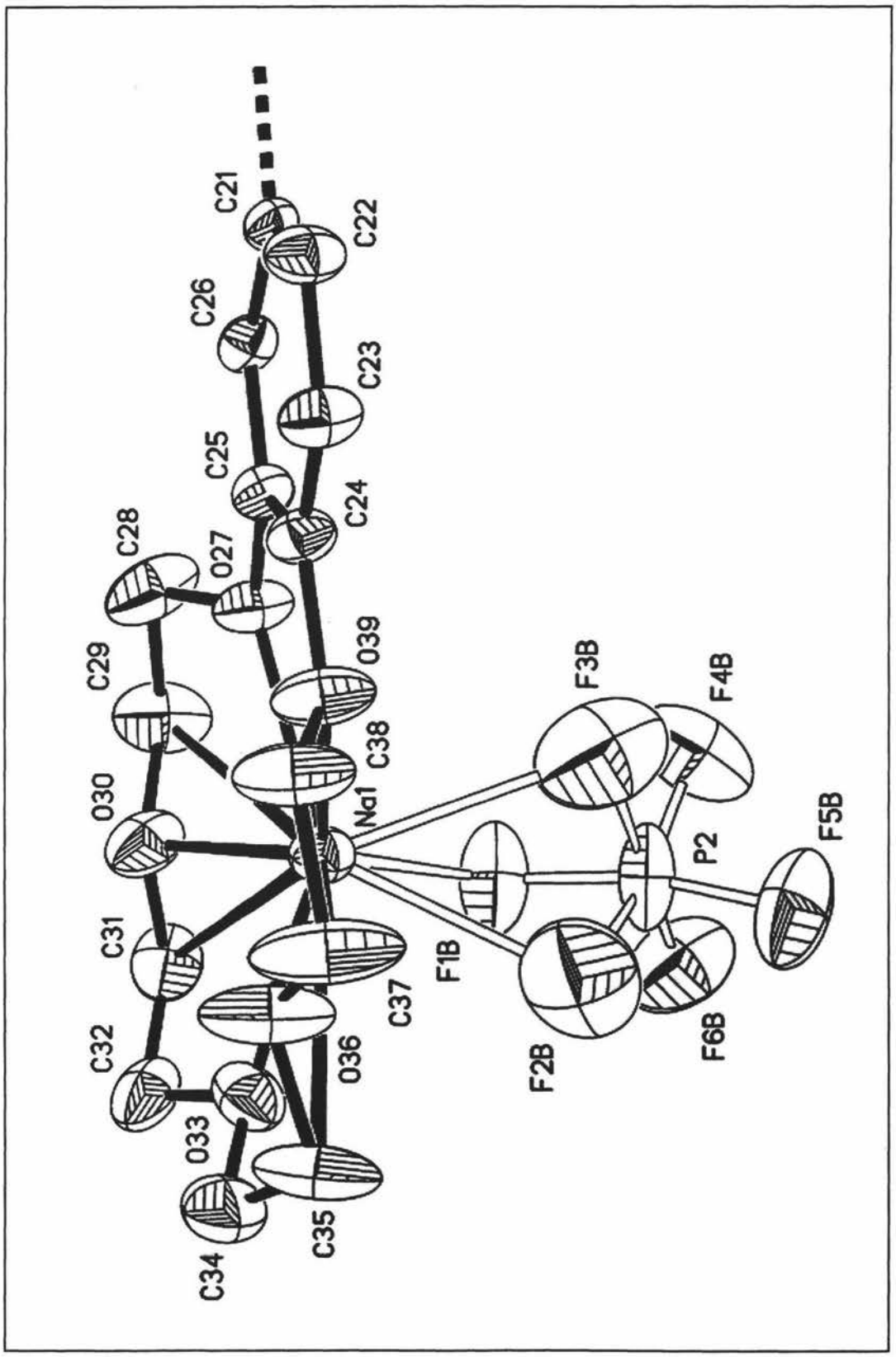

Table 4.2. Crystal data and structure refinement for $W(CO)_4(O_5NP)Na(PF_6)$.

Identification code	ka147	
Empirical formula	$C_{37}H_{34}Cl_2F_6NNaO_9P_2W$	
Formula weight	1090.33	
Temperature	168(2) K	
Wavelength	0.71073 Å	
Crystal system	Triclinic	
Space group	P-1	
Unit cell dimensions	a = 9.253(4) Å	α= 97.588(6)°
	b = 12.237(5) Å	β= 100.326(5)°
	c = 24.212(11) Å	γ = 101.888(5)°
Volume	2598(2) Å^3	
Z	2	
Density (calculated)	1.394 Mg/m^3	
Absorption coefficient	2.460 mm^{-1}	
F(000)	1076	
Crystal size	0.2 x 0.3 x 0.2 mm^3	
Theta range for data collection	2.74 to 26.37°	
Index ranges	$-11 \le h \le 5$, $-15 \le k \le 15$, $-30 \le l \le 30$	
Reflections collected	32884	
Independent reflections	10247 [R(int) = 0.0598]	
Completeness to theta = 26.37°	96.4 %	
Absorption correction	None	
Refinement method	Full-matrix least-squares on F^2	
Data / restraints / parameters	10247 / 112 / 674	
Goodness-of-fit on F^2	0.962	
Final R indices [I>2sigma(I)]	R1 = 0.0392, wR2 = 0.0677	
R indices (all data)	R1 = 0.0687, wR2 = 0.0731	
Extinction coefficient	0.00025(13)	
Largest diff. peak and hole	0.989 and -1.033 e.Å^{-3}	

Table 4.3. Selected bond lengths (Å) and angles (°) for $W(CO)_4(O_5NP)Na(PF_6)$.

W(1)-N(20)	2.245(4)	N(20)-W(1)-P(1)	77.56(10)
W(1)-P(1)	2.5055(15)	C(46)-W(1)-C(42)	91.1(2)
W(1)-C(46)	1.953(5)	C(46)-W(1)-C(44)	85.0(2)
W(1)-C(42)	1.984(5)	C(42)-W(1)-C(44)	88.08(19)
W(1)-C(44)	2.007(5)	C(46)-W(1)-C(40)	84.3(2)
W(1)-C(40)	2.044(5)	C(42)-W(1)-C(40)	87.40(19)
C(18)-C(19)	1.460(6)	C(44)-W(1)-C(40)	168.30(19)
C(19)-N(20)	1.280(5)	C(46)-W(1)-N(20)	175.70(17)
N(20)-C(21)	1.452(5)	C(42)-W(1)-N(20)	93.19(17)
C(24)-O(39)	1.371(5)	C(44)-W(1)-N(20)	94.85(17)
C(25)-O(27)	1.385(5)	C(40)-W(1)-N(20)	96.17(17)
O(27)-C(28)	1.405(6)	C(46)-W(1)-P(1)	98.18(14)
C(29)-O(30)	1.424(6)	C(42)-W(1)-P(1)	170.02(15)
O(30)-C(31)	1.436(6)	C(44)-W(1)-P(1)	96.35(13)
C(32)-O(33)	1.422(6)	C(40)-W(1)-P(1)	89.85(14)
O(33)-C(34)	1.416(6)	N(20)-C(19)-C(18)	127.0(4)
C(35)-O(36)	1.439(6)	C(19)-N(20)-C(21)	114.0(3)
O(36)-C(37)	1.315(7)	O(39)-C(24)-C(25)	116.4(4)
C(38)-O(39)	1.401(5)	O(27)-C(25)-C(24)	115.3(4)
Na(1)-O(30)	2.336(4)	C(25)-O(27)-C(28)	117.2(4)
Na(1)-O(39)	2.372(4)	C(24)-O(39)-C(38)	120.1(4)
Na(1)-O(33)	2.375(4)	O(39)-Na(1)-O(27)	66.50(12)
Na(1)-O(27)	2.389(4)	O(39)-Na(1)-O(36)	68.74(13)
Na(1)-O(36)	2.395(4)	O(33)-Na(1)-O(36)	68.70(13)
Na(1)-F(1A)	2.454(9)	O(30)-Na(1)-O(33)	70.66(14)
Na(1)-F(2A)	2.288(8)	O(30)-Na(1)-O(27)	69.78(12)
Na(1)-F(1B)	2.418(9)	F(2A)-Na(1)-F(1A)	57.4(3)
Na(1)-F(2B)	2.587(14)	F(1A)-Na(1)-P(2)	29.02(17)
Na(1)-F(3B)	2.682(14)	F(2A)-Na(1)-P(2)	29.7(2)
		F(1B)-Na(1)-F(2B)	47.5(3)
		F(1B)-Na(1)-F(3B)	53.0(3)
		F(2B)-Na(1)-F(3B)	45.5(3)

Table 4.4. Selected torsion angles (°) for $W(CO)_4(O_5NP)Na(PF_6)$.	
C(13)-C(18)-C(19)-N(20)	-33.0(7)
C(18)-C(19)-N(20)-C(21)	177.3(4)
C(19)-N(20)-C(21)-C(26)	-94.5(5)
O(39)-C(24)-C(25)-O(27)	-0.1(6)
O(27)-C(28)-C(29)-O(30)	53.0(7)
O(30)-C(31)-C(32)-O(33)	-59.4(6)
O(33)-C(34)-C(35)-O(36)	58.2(6)
O(36)-C(37)-C(38)-O(39)	-44.8(9)

4.3.5.2 The Structure of $[Cu(O_5NP)_2]K[PF_6]_2$

Crystals for X-ray analysis were obtained from a solution of $[Cu(O_5NP)_2][PF_6]$ in CH_2Cl_2 prepared with an excess of KPF_6. The solution was stirred for 1.5 hours and then layered with pentane to promote crystallisation, which occurred after two days.

The structure of $[Cu(O_5NP)_2]K[PF_6]_2$ is given in Figures 4.14 and 4.15. Table 4.5 shows the crystal data and structure refinement, Tables 4.6 and 4.7 show selected structural data and Table 4.8 lists the hydrogen bonds present in the crystal. The structure consists of a Cu(I) center in a distorted tetrahedral geometry. The Cu(I) is bound to the iminophosphine recognition sites of two O_5NP ligands with a K^+ ion sandwiched between the benzo-15-crown-5 moieties. This structure confirms that the $[M(O_5NP)_2][PF_6]$ (M = Cu, Ag, Au) complexes can bind alkali cations in sandwich formations.

The K^+ is bound to all ten oxygen atoms with K—O bond lengths from 3.126(4) to 2.774(3) Å which is within the range 3.656-2.746 Å reported for previous X-ray structures of K^+ sandwiched between two benzo-15-crown-5-ethers.[14,26-39] The O-K-O bond angles between adjacent oxygens range from 62.72(11)° to 49.92(9)°, and 60.90(12)° to 51.61(15)°, for the A and B crowns respectively with an average value of 56.54°. The range of the B crown falls within that for reported for other bridged benzo-15-crown-5-ethers of 61.58-50.58° [14,26,27] while both of the crowns compare well with the 69.62° to 47.74° range for similar compounds that have separate crowns.[28-39] An

unusual feature of the O-K-O angles is that the O(39B)-K(1)-O(27B) bond angle (Figure 4.14) of 52.33(9)° is not the smallest O-K-O angle whereas it is in related structures.[14,26-38]

A comparison of $[Cu(O_5NP)_2]K[PF_6]_2$ with the free ligand O_5NP shows significant differences in the angles between the oxygen atoms and the benzo group. For $[Cu(O_5NP)_2]K[PF_6]_2$ these bond angles range from 115.3(4)° to 113.5(4)° and have all decreased from the free ligand values of 121.0(3)° and 115.8(3)°. Since the C-C-O angles of $[Cu(O_5NP)_2]K[PF_6]_2$ fall within the literature range of 118.72-106.04° [14,26-39] while those of O_5NP do not, it is possible that this is due to the uptake of the K^+ ion.

The C-O-C bond angles of $[Cu(O_5NP)_2]K[PF_6]_2$ range from 120.6(3)° to 94.3(8)° and are in good agreement with the literature.[14,26-39] The C-O-C angles of the oxygen atoms bound to the benzo group are larger than the other C-O-C angles, a trend that has been observed for most similar compounds.[14,26-37] There are significant differences in the benzo-O-C angles between $[Cu(O_5NP)_2]K[PF_6]_2$ (120.6(3)° to 119.1(3)°) the free ligand (120.1(3)° and 115.3(3)°) and the $Mo(CO)_4O_5NP$ complex (118.6(3)° and 114.8(2)°). This may be due to the presence of the K^+ cation.

The torsion angles between the oxygen atoms of the benzo-15-crown-5 range from 68.6(14)° to –65.0(5)° to accommodate the potassium ion. This places the ether groups gauche to each other to minimise steric hindrance.

Bond lengths and angles about the imine are unremarkable and are as expected. The bond lengths Cu(1)-N(20A) 2.066(3) Å and Cu(1)-N(20B) 2.073(3) Å are generally shorter than those of $[Cu(NP)_2][PF_6]$ (2.145(3) Å and 2.063(8) Å) and $[Cu(NP)Br]_2$ (2.213(2) Å) and similar structures[40-44]. However the Cu—P bond lengths of 2.2294(12) Å and 2.2332(11) Å show a significant increase from the above X-ray structures. This could indicate that the K^+ is pulling the crown ethers together and hence forcing the P atoms apart. The N-Cu-P chelated angles (93.06(10)°, 90.27(10)°) show a significant increase from those of $[Cu(NP)_2][PF_6]$ (92.10(2)°, 84.32(10)°) and $[Cu(NP)Br]_2$ (85.28(6)°). The imine bonds have an *E* conformation with the P and N atoms on the same side of the C(19)-C(18)-C(13) bonds. The torsion angles between the benzo groups and the imine carbons differ by 36° to 3.9° from those of $[Cu(NP)_2][PF_6]$ and

$[Cu(NP)Br]_2$. These changes may be due to the rearrangement required for the sandwiching of the potassium cation.

A comparison between the structure of $[Cu(NP)_2][PF_6]$, that lacks a crown moiety, and the structure of $[Cu(O_5NP)_2]K[PF_6]_2$, reported here, suggests the benzo groups of the imines have changed their relative position to each other. The structure of $[Cu(NP)_2][PF_6]$ (Figure 2.2) shows the benzo groups to be pointing away from each other, while in $[Cu(O_5NP)_2]K[PF_6]_2$ (Figures 4.14 and 4.15) they are pointing in the same direction and are close to overlap. This indicates that the binding of K^+ by $[Cu(O_5NP)_2][PF_6]$ in a sandwich formation requires rotation of the ligands about the Cu(I) centre.

There are several hydrogen bonds ranging in lengths of 2.57 to 2.37 Å with all hydrogens bound to F atoms of a PF_6^- group. Both of the ligands have hydrogen bonds between the imine proton and PF_6^- groups. Several exist between hydrogens of the crown ether with the remainder being from hydrogens of aromatic carbons.

Figure 4.14. The ORTEP diagram of $[Cu(O_5NP)_2]K[PF_6]_2$ with thermal ellipsoids at 50% probability.

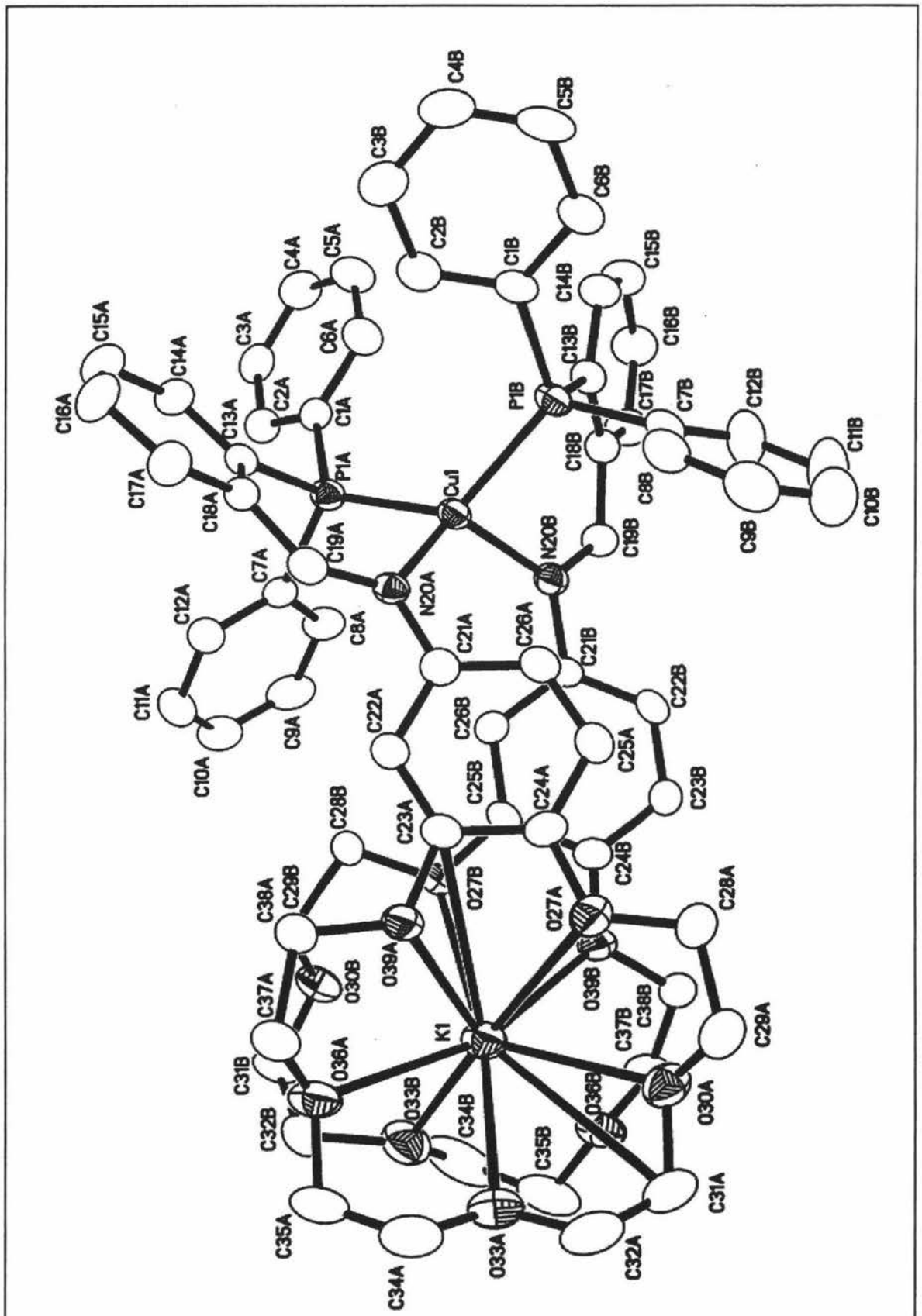

Figure 4.15. The ORTEP diagram of $[Cu(O_5NP)_2]K[PF_6]_2$ displaying the sandwiching of the K^+ cation. Thermal ellipsoids at 50% probability.

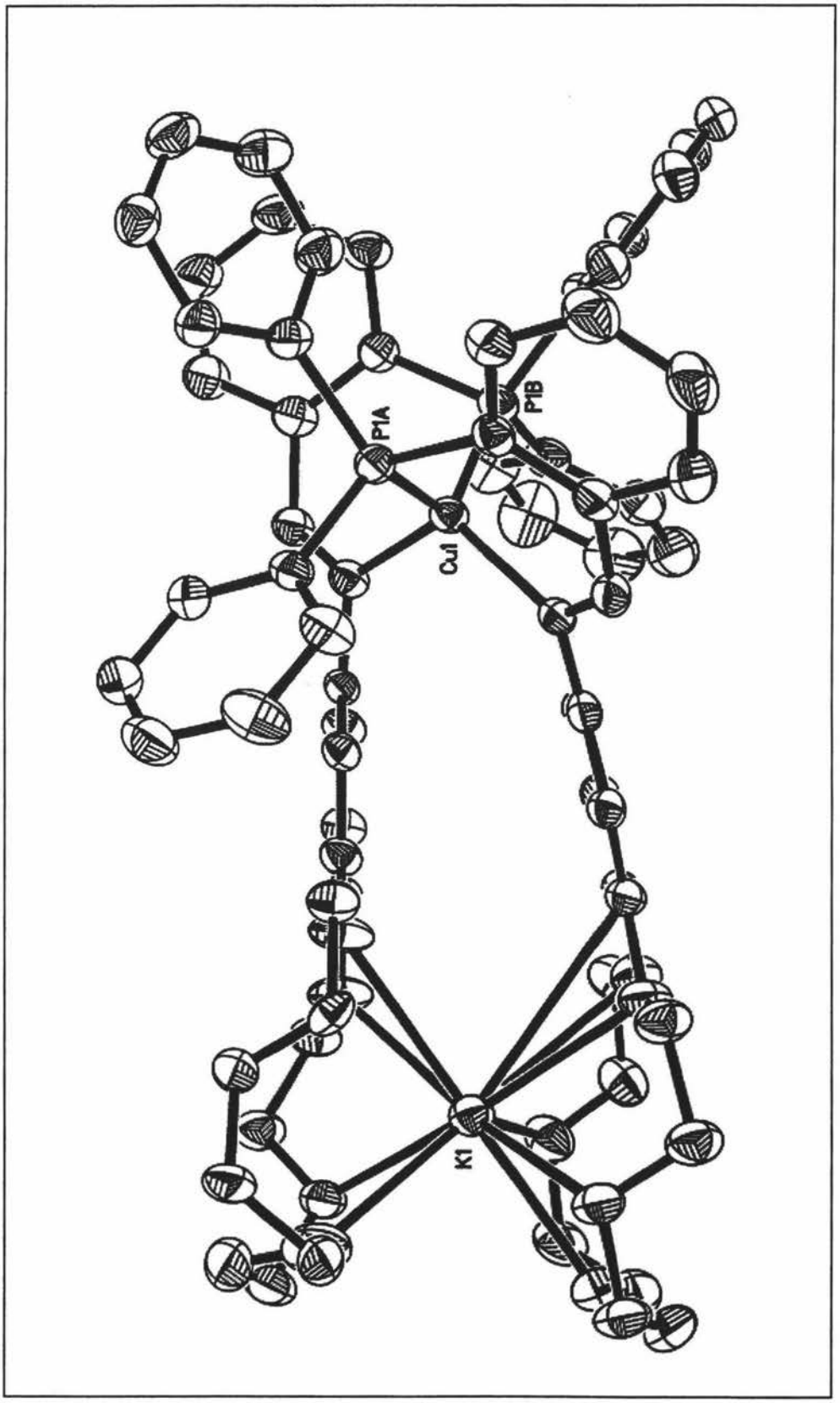

Table 4.5. Crystal data and structure refinement for $[Cu(O_5NP)_2]K[PF_6]_2$.

Identification code	ka148	
Empirical formula	$C_{67}H_{68}Cl_2CuF_{12}KN_2O_{10}P_4$	
Formula weight	1586.65	
Temperature	150(2) K	
Wavelength	0.71073 Å	
Crystal system	Triclinic	
Space group	P-1	
Unit cell dimensions	a = 12.92270(10) Å	α= 96.6210(10)°
	b = 16.62860(10) Å	β= 99.0570(10)°
	c = 17.56620(10) Å	γ = 102.5880(10)°
Volume	3593.97(4) Å^3	
Z	2	
Density (calculated)	1.466 Mg/m^3	
Absorption coefficient	0.613 mm^{-1}	
F(000)	1628	
Crystal size	0.44 x 0.26 x 0.22 mm^3	
Theta range for data collection	1.19 to 25.34°	
Index ranges	$-15 \le h \le 15$, $-19 \le k \le 19$, $0 \le l \le 21$	
Reflections collected	12973	
Independent reflections	12973 [R(int) = 0.0000]	
Completeness to theta = 25.34°	98.7 %	
Absorption correction	None	
Max. and min. transmission	0.8769 and 0.7741	
Refinement method	Full-matrix least-squares on F^2	
Data / restraints / parameters	12973 / 6 / 929	
Goodness-of-fit on F^2	1.053	
Final R indices [I>2sigma(I)]	R1 = 0.0642, wR2 = 0.1806	
R indices (all data)	R1 = 0.0807, wR2 = 0.1951	
Largest diff. peak and hole	1.188 and -1.525 e.Å^{-3}	

Table 4.6. Selected bond lengths (Å) and angles (°) for $[Cu(O_5NP)_2]K[PF_6]_2$.

Cu(1)-N(20A)	2.066(3)	N(20A)-C(19A)-C(18A)	128.5(4)
Cu(1)-N(20B)	2.073(3)	C(19A)-N(20A)-C(21A)	117.5(3)
Cu(1)-P(1A)	2.2294(12)	N(20B)-C(19B)-C(18B)	125.6(4)
Cu(1)-P(1B)	2.2332(11)	C(19B)-N(20B)-C(21B)	116.3(3)
C(18A)-C(19A)	1.479(6)	O(30A)-K(1)-O(27A)	54.61(9)
C(19A)-N(20A)	1.293(5)	O(33A)-K(1)-O(30A)	62.27(11)
N(20A)-C(21A)	1.432(5)	O(33A)-K(1)-O(36A)	61.70(10)
C(18B)-C(19B)	1.486(6)	O(36A)-K(1)-O(39A)	58.22(9)
C(19B)-N(20B)	1.290(5)	O(39A)-K(1)-O(27A)	49.92(9)
N(20B)-C(21B)	1.438(5)	O(27B)-K(1)-O(30C)	51.61(15)
K(1)-O(39B)	2.774(3)	O(33B)-K(1)-O(30C)	55.75(16)
K(1)-O(33A)	2.778(3)	O(33B)-K(1)-O(36B)	60.90(12)
K(1)-O(33B)	2.782(4)	O(39B)-K(1)-O(36B)	58.07(9)
K(1)-O(30A)	2.808(4)	O(39B)-K(1)-O(27B)	52.33(9)
K(1)-O(36A)	2.833(3)	O(39A)-C(23A)-C(24A)	113.5(4)
K(1)-O(39A)	2.854(3)	O(27A)-C(24A)-C(23A)	114.9(4)
K(1)-O(36B)	2.904(3)	O(27B)-C(25B)-C(24B)	114.4(4)
K(1)-O(27B)	3.018(4)	O(39B)-C(24B)-C(25B)	115.3(4)
K(1)-O(30C)	3.125(8)	C(24A)-O(27A)-C(28A)	119.1(4)
K(1)-O(27A)	3.126(4)	C(29A)-O(30A)-C(31A)	113.7(4)
N(20A)-Cu(1)-P(1A)	93.06(10)	C(32A)-O(33A)-C(34A)	113.5(4)
N(20B)-Cu(1)-P(1A)	114.30(10)	C(37A)-O(36A)-C(35A)	113.9(4)
N(20A)-Cu(1)-P(1B)	121.75(10)	C(23A)-O(39A)-C(38A)	119.1(3)
N(20B)-Cu(1)-P(1B)	90.27(10)	C(25B)-O(27B)-C(28B)	117.7(3)
N(20A)-Cu(1)-N(20B)	117.16(13)	C(31C)-O(30C)-C(29C)	114.7(14)
P(1A)-Cu(1)-P(1B)	122.49(4)	C(34B)-O(33B)-C(32C)	94.3(8)
		C(35B)-O(36B)-C(37B)	113.3(4)
		C(24B)-O(39B)-C(38B)	120.6(3)

Table 4.7. Selected torsion angles (°) for $[Cu(O_5NP)_2]K[PF_6]_2$.

C(13A)-C(18A)-C(19A)-N(20A)	22.9(7)
C(18A)-C(19A)-N(20A)-C(21A)	-175.7(4)
C(19A)-N(20A)-C(21A)-C(22A)	39.6(5)
C(13B)-C(18B)-C(19B)-N(20B)	30.0(7)
C(18B)-C(19B)-N(20B)-C(21B)	-174.0(4)
C(19B)-N(20B)-C(21B)-C(26B)	-139.1(4)
O(39A)-C(23A)-C(24A)-O(27A)	0.3(5)
O(27A)-C(28A)-C(29A)-O(30A)	62.3(5)
O(30A)-C(31A)-C(32A)-O(33A)	64.5(6)
O(33A)-C(34A)-C(35A)-O(36A)	-61.5(6)
O(36A)-C(37A)-C(38A)-O(39A)	-65.0(5)
O(39B)-C(24B)-C(25B)-O(27B)	0.8(6)
O(27B)-C(28B)-C(29C)-O(30C)	52.7(17)
O(30C)-C(31C)-C(32C)-O(33B)	68.6(14)
O(33B)-C(34B)-C(35B)-O(36B)	-64.2(6)
O(36B)-C(37B)-C(38B)-O(39B)	-62.5(5)

Table 4.8. Hydrogen bonds for $[Cu(O_5NP)_2]K[PF_6]_2$ [Å and °].

D-H...A	d(D-H)	d(H...A)	d(D...A)	<(DHA)
C(3A)-H(3AA)...F(5)#1	0.95	2.37	3.300(6)	165.6
C(10A)-H(10A)...F(12)#1	0.95	2.46	3.318(7)	149.9
C(19A)-H(19A)...F(1)	0.95	2.41	3.248(5)	147.6
C(22A)-H(22A)...F(1)	0.95	2.43	3.218(5)	140.7
C(29A)-H(29A)...F(10)#2	0.99	2.49	3.276(7)	135.7
C(19B)-H(19B)...F(4)#3	0.95	2.54	3.474(5)	167.6
C(22B)-H(22B)...F(2)#3	0.95	2.47	3.379(5)	161.3
C(32B)-H(32D)...F(6)#4	0.99	2.57	3.419(10)	143.8
C(34B)-H(34D)...F(4)#4	0.99	2.49	3.392(7)	151.8

4.4 Summary

The main findings of this chapter are given below.

- The starting material 4'-aminobenzo-15-crown-5 (O_5NH_2) shows selectivity for both Na^+ and K^+ over the other alkali cations in the 1:1 species while the 2:1 sandwich species has a small selectivity for potassium ions.
- The free ligand *N*-(2-diphenylphosphinobenzylidine)-4'-(benzo-15-crown-5) (O_5NP) selectively binds potassium ions both in the 1:1 and 2:1 species.
- $M(CO)_4(O_5NP)$ (M = Cr, Mo, W) complexes have good selectivity for Na^+ in 1:1 species and K^+ in 2:1 species.
- $[M(O_5NP)_2][PF_6]$ (M = Cu, Ag, Au) complexes bind alkali cations in a 1:1 species via an intramolecular sandwich formation between the benzo-15-crown-5 moieties of the two O_5NP ligands. The complexes are selective towards potassium with $[Ag(O_5NP)_2][PF_6]$ having the strongest selectivity.
- The dimer complex $[Cu(O_5NP)Cl]_2$ breaks down in solution to form the $Cu(O_5NP)Cl$ monomer that selects lithium ions over the other alkali ions. A small selectivity for K^+ is observed in the 2:1 species by this complex.
- The dimer $[Ag(O_5NP)Cl]_2$ forms the monomer in solution and preferentially binds potassium ions over other alkali cations. Little selectivity is seen by the 2:1 species although a small preference for K^+ observed.
- The monomer complex $Au(O_5NP)Cl$ has good selectivity for Na^+ and K^+ in the 1:1 and 2:1 species respectively.
- The prior binding of a transition metal to the O_5NP ligand affects the selectivity of alkali cations by the O_5NP ligand.
- The X-ray structure of $W(CO)_4(O_5NP)Na(PF_6)$ has been determined and confirmed that $W(CO)_4(O_5NP)$ binds Na^+ within the cavity of the benzo-15-crown-5 moiety which experiences significant change to its conformation.
- The X-ray structure of $[Cu(O_5NP)_2]K[PF_6]_2$ has been determined and showed that $[Cu(O_5NP)_2][PF_6]$ binds K^+ in a sandwich formation. this will require rotation of the ligands about the Cu(I) centre to bring the crown ethers together and push the P atoms apart.

4.5 References

1. A. Tsuda, H. Moriwaki and T. Oshima, *J. Chem. Soc., Perkin Trans. 2.*, (1999), 1235-1240.
2. D. Young, H. Hung and L. Liu, *Rapid Commun. Mass Spectrom.*, 11, (1997), 769-773.
3. D. Young, H. Hung and L. Liu, *J. Mass Spec.*, 32, (1997), 432-437.
4. E. Kempen, J. Brodbelt, R. Bartsch, Y. Jang and J. Kim, *Anal. Chem.*, 71, (1999), 5493-5500.
5. S. Blair, J. Brodbelt, A. Marchand, K. Kumar and H. Chong, *Anal. Chem.*, 72, (2000), 2433-2445.
6. C. Pedersen, *J. Am. Chem. Soc.*, 92, (1970), 386-391.
7. C. Pedersen and H. Frensdorff, *Angew. Chem., Int. Ed. Engl.*, 11, (1972), 16-25.
8. R. Izatt, J. Bradshaw, S. Nielsen, J. Lamb and J. Christensen, *Chem. Rev.*, 85, (1985), 271-339.
9. R. Izatt, K. Pawlak and J. Bradshaw, *Chem. Rev.*, 91, (1991), 1721-2085.
10. E. Weber and M. Czugler, *Inorg. Chim. Acta.*, 61, (1982), 33-38.
11. J. Owen, *J. Chem. Soc., Dalton Trans.*, (1980), 1066-1067.
12. P. Beer, M. Drew, R. Knubley and M. Ogden, *J. Chem. Soc., Dalton Trans.*, (1995), 3117-3123.
13. P. Mallinson and M. Truter, *J. Chem. Soc., Perkin Trans. 2.*, (1972), 1818-1823.
14. P. Beer, C. Crane and M. Drew, *J. Chem. Soc., Dalton Trans.*, (1991), 3235-3242.
15. Y. Takeda, H. Yano, M. Ishibashi and H. Isozumi, *Bull. Chem. Soc. Jpn.*, 53, (1980), 72-76.
16. Y. Takeda and T. Kumazawa, *Bull. Chem. Soc. Jpn.*, 61, (1988), 655-658.
17. P. Bernhardt and E. Hayes, *Inorg. Chem.*, 41, (2002), 2892-2902.
18. M. Bush and M. Truter, *J. Chem. Soc., Perkin Trans. 2.*, (1972), 341-344.
19. D. Moody and R. Ryan, *Cryst. Struct. Commun.*, 8, (1979), 933-936.
20. W. Dreissig, Z. Dauter, A. Cygan and J. Biernat, *Inorg. Chim. Acta.*, 96, (1985), 21-27.
21. D. Lemenovskii, I. Nifant'ev, I. Urazowski, E. Perevalova, Y. Slovokhotov and Y. Struchkov, *J. Organomet. Chem.*, 342, (1988), 31-44.
22. W. Herrmann, J. Kuchler, G. Weichselbaumer, E. Herdtweck and P. Kipro, *J. Organomet. Chem.*, 372, (1989), 351-370.

23. P. Beer, H. Sikanyika, C. Blackburn, J. McAleer and M. Drew, *J. Organomet. Chem.*, 356, (1988), C19-C22.
24. B. Koenig, E. Schofield, P. Bubenitschek and P. Jones, *J. Org. Chem.*, 59, (1994), 7142-7143.
25. C. Yang, W. Yeh, G. Lee and S. Peng, *J. Organomet. Chem.*, 598, (2000), 353-358.
26. Z. Li-Tao, L. Bao-Sheng, L. Tian-Bao, H. Hong-Wen and Z. Shao-Hui, *Jiegou Huaxue (Chin.) (J. Struct. Chem.).*, 10, (1991), 167.
27. P. Beer, M. Drew, R. Knubley and M. Ogden, *J. Chem. Soc., Dalton Trans.*, (1995), 3117-3123.
28. P. Mallinson and M. Truter, *J. Chem. Soc., Perkin Trans. 2.*, (1972), 1818-1823.
29. W. Xu, K. Clinger, M. Hackert and N. Poonia, *J. Inclusion Phenom. Macrocyclic Chem.*, 3, (1985), 163-172.
30. W. Sheldrick and N. Poonia, *J. Inclusion Phenom. Macrocyclic Chem.*, 4, (1986), 93-98.
31. Z. Zhixian, Z. Xianxin and H. Jinshun, *Huaxue Xuebao (Chin.) (Acta Chim. Sinica).*, 44, (1986), 870.
32. Z. Zhixian, D. Baoshi, Z. Xianxin, L. Shixiong and H. Jinling, *Jiegou Huaxue (Chin.) (J. Struct. Chem.).*, 6, (1987), 209.
33. A. Mugnoli, Z. Dauter, E. Luboch, A. Cygan and J. Biernat, *J. Inclusion Phenom. Macrocyclic Chem.*, 4, (1986), 407-414.
34. M. Zhi-Hua, Z. Zhong-Hua, H. Zhou, Y. Hong-Wu, Z. Zhi-Xian, Z. Ming-Rui and R. Bo-Yany, *Jiegou Huaxue (Chin.) (J. Struct. Chem.).*, 12, (1993), 266.
35. J. Peters, A. Odom and C. Cummins, *Chem. Commun.*, (1997), 1995-1996.
36. Z. Karimov, S. Talipov, K. Fun, B. Ibragimov, A. Tashmukhamedova and A. Razak, *Zh. Strukt. Khim. (Russ.) (Russ. J. Struct. Chem.).*, 42, (2001), 160-164.
37. J. Pickardt, S. Wiese, L. von Chrzanowski and M. Borowski, *Z. Anorg. Allg. Chem.*, 626, (2000), 2096-2102.
38. J. Pickardt and P. Wischlinski, *Z. Anorg. Allg. Chem.*, 625, (1999), 1527-1531.
39. E. Weber and M. Czugler, *Inorg. Chim. Acta.*, 61, (1982), 33-38.
40. V. Yam, Y. Pui, K. Cheung and N. Zhu, *New J. Chem.*, 26, (2002), 536-542.
41. V. Yam, K. Lo and K. Cheung, *Inorg. Chem.*, 34, (1995), 4013-4014.
42. C. Sanders, K. Gillespie, D. Bell and P. Scott, *J. Am. Chem. Soc.*, 122, (2000), 7132-7133.

43. A. Shnulin, Y. Struchkov, K. Mamedov and A. Bezuglaya, *Zh. Strukt. Khim. (Russ.) (Russ. J. Struct. Chem.).*, 18, (1977), 1015-1024.

44. M. Garland, J. Marouille and E. Spodine, *Acta Cryst.*, C42, (1986), 299-301.

References.

Chapter one.

1. G. Sanchez, J. Vives, J. L. Serrano, J. Perez and G. Lopez, *Inorg. Chim. Acta,* 328, (2002), 74-80.
2. G. Sanchez, J. L. Serrano, M. A. Moral, J. Perez, E. Molins and G. Lopez, *Polyhedron,* 18, (1999), 3057-3064.
3. H. B. Song, Z. Z. Zhang and T. C. W. Mak, *Polyhedron,* 21, (2002), 1043-1050.
4. L. Crociani, G. Bandoli. A. Dolmella, M. Basato and B. Corain, *Eur. J. Inorg. Chem.,* (1998), 1811-1820.
5. P. Wehman, H. M. A. van Donge, A. Hagos, P. C. J. Kamer and P. W. N. M. van Leeuwen, *J. Organomet. Chem.,* 535, (1997), 183-193.
6. Z. Z. Zhang and H. Cheng, *Coord. Chem. Rev.,* 147, (1996), 1-39.
7. P. Papathanasiou, G. Salem, P. Waring and A. C. Willis, *J. Chem. Soc., Dalton Trans.,* (1997), 3435-3443.
8. W. K. Wong, X. P. Chen, W. X. Pan, J. P. Guo and W. Y. Wong, *Eur. J. Inorg. Chem.,* (2002), 231-237.
9. Y. Chen, D. J. Schiffrin, P. Guerriero and P. A. Vigato, *Inorg. Chem.,* 33, (1994), 765-769.
10. E. K. van der Beuken, W. J. J. Smeets, A. L. Spek and B. L. Feringa, *Chem. Commun.,* (1998), 223-224.
11. H. Yoshida, Y. Honda, E. Shirakawa and T. Hiyama, *Chem. Commun.,* (2001), 1880-1881.
12. R. E. Rulke, V. E. Kaasjager, P. Wehman, C. J. Elsevier, P. W. N. M. van Leeuwen and K. Vrieze, *Organometallics,* 15, (1996), 3022-3031.
13. F. Tisato, G. Pilloni, F. Refosco, G. Bandoli, C. Corvaja and B. Corain, *Inorg. Chim. Acta,* 275-276 (1998), 401-409.
14. J. M. Lehn, *Supramolecular chemistry,* 1995, VCH Verlagsgesellschaft, Weinheim.
15. C. J. Pedersen, *J. Am. Chem. Soc.,* 89, (1967), 7017-7036.
16. V. W. W. Yam, Y. L. Pui, W. P. Li, K. K. W. Lo and K. K. Cheung, *J. Chem. Soc., Dalton Trans.,* (1998), 3615-3621.
17. R. M. Izatt, J. S. Bradshaw, S. A. Nielsen, J. D. Lamb and J. J. Christensen, *Chem. Rev.,* 85, (1985), 271-339.
18. G. W. Gokel, *Crown Ethers and Cryptands,* 1991, The Royal Society of Chemistry, Cambridge.
19. R. M. Izatt, K. Pawlak and J. S. Bradshaw, *Chem. Rev.,* 91, (1991), 1721-2085.
20. C. J. Pedersen, *J. Am. Chem. Soc.,* 92, (1970), 386-391.
21. P. R. Mallinson and M. R. Truter, *J. Chem. Soc., Perkin Trans. 2,* (1972), 1818-1823.
22. J. D. Owen, *J. Chem. Soc., Dalton Trans.,* (1980), 1066-1067.
23. E. Weber and M. Czugler, *Inorg. Chim. Acta,* 61, (1982), 33-38.
24. P. D. Beer, M. G. B. Drew, R. J. Knubley and M. I. Ogden, *J. Chem. Soc., Dalton Trans.,* (1995), 3117-3123.
25. A. J. Layton, P. R. Mallinson, D. G. Parsons and M. R. Truter, *J. Chem. Soc., Chem. Comm.,* (1973), 694-695.
26. C. J. Pedersen and H. K. Frensdorff, *Angew. Chem., Int. Ed. Engl.,* 11, (1972), 16-25.
27. Y. Takeda, *Bull. Chem. Soc. Jpn.,* 55, (1982), 2040-2041.
28. V. W. W. Yam, K. M. C. Wong, V. W. M. Lee, K. K. W. Lo and K. K. Cheung, *Organometallics,* 14, (1995), 4034-4036.
29. V. W. W. Yam, K. K. W. Lo and K. K. Cheung, *Inorg. Chem.,* 34, (1995), 4013-4014.
30. V. W. W. Yam, V. Lee, F. Ke and K. Siu, *Inorg. Chem.,* 36, (1997), 2124-2129.
31. V. W. W. Yam, R. P. L. Tang, K. M. C. Wong, C. C. Ko and K. K. Cheung, *Inorg. Chem.,* 40, (2001), 571-574.
32. V. W. W. Yam, R. P. L.Tang, K. M. C. Wong, X. X. Lu, K. K. Cheung and N. Zhu, *Chem. Eur. J.,* 8, (2002), 4066-4076.
33. V. W. W. Yam, R. P. L. Tang, K. M. C. Wong and K. K. Cheung, *Organometallics,* 20, (2001), 4476-4482.
34. V. W. W. Yam, Y. L. Pui, K. K. Cheung and N. Zhu, *New J. Chem.,* 26, (2002), 536-542.
35. V. W. W. Yam, C. H. Lam and K. K. Cheung, *Inorg. Chim. Acta,* 316, (2001), 19-24.
36. V. W. W. Yam, C. K. L. Li and C. L. Chan, *Angew. Chem., Int. Ed. Engl.,* 37, (1998), 2857-2859.
37. A. Tsuda, H. Moriwaki and T. Oshima, *J. Chem. Soc., Perkin Trans. 2,* (1999), 1235-1240.
38. L. A. Barg, R. W. Byrn, M. D. Carr, D. H. Nolan, B. N. Storhoff and J. C. Huffman, *Organometallics,* 17, (1998), 1340-1346.
39. C. Nataro, H. M. Baseski, C. M. Thomas, B. J. Wiza and K. M. Rourke, *Polyhedron,* 20, (2001), 1023-1028.
40. P. V. Bernhardt and E. J. Hayes, *Inorg. Chem.,* 41, (2002), 2892-2902.
41. P. D. Beer, *Endeavour,* 16, (1992), 182-189.
42. P.W. Atkins, *Physical Chemistry,* 1998, Oxford University Press, Oxford.
43. W. Henderson, B. K. Nicholson and L. J. McCaffrey, *Polyhedron,* 17, (1998), 4291-4313.
44. C. Decker, *Electrospray friendly ligands for the mass spectral analysis of transition metal complexes.* DPhil Thesis, 2002, University of Waikato.
45. D. S. Young, H. Y. Hung and L. K. Liu, *J. Mass Spec.,* 32, (1997), 432-437.
46. S. M. Blair, J. S. Brodbelt, A. P. Marchand, K. A. Kumar and H. S. Chong, *Anal. Chem.,* 72, (2000), 2433-2445.
47. S. F. Ralph, P. Iannitti, R. Kanitz and M. M. Sheil, *Eur. Mass Spectrom.,* 2, (1996), 173-179.
48. F. Allain, H. Virelizier, C. Moulin, C. K. Jankowski, J. F. Dozol and J. C. Tabet, *Spectroscopy,* 14, (2000), 127-139.
49. R. A. W. Johnstone, I. A. S. Lewis and M. E. Rose, *Tetrahedron.,* 39, (1983), 1597-1603.
50. D. S. Young, H. Y. Hung and L. K. Liu, *Rapid Commun. Mass Spectrom.,* 11, (1997), 769-773.
51. E. C. Kempen and J. S. Brobdelt, *Anal. Chem.,* 72, (2000), 5411-5416.

Chapter two.

1. P. Wehman, H. M. A. van Donge, A. Hagos, P. C. J. Kamer and P. W. N. M. van Leeuwen, *J. Organomet. Chem.,* 535, (1997), 183-193.
2. X. Chen, F. J. Femia, J. W. Babich and J. Zubieta, *Inorg. Chim. Acta,* 315, (2001), 147-152.
3. A. Bacchi, M. Carcelli, M. Costa, A. Leporati, E. Leporati, P. Pelagatti, C. Pelizzi and G. Pelizzi, *J. Organomet. Chem.,* 535, (1997), 107-120.
4. C. A. Ghilardi, S. Midollini, S. Moneti, A. Orlandini and G. Scapacci, *J. Chem. Soc., Dalton Trans.,* (1992), 3371-3376.
5. E. W. Ainscough, A. M. Brodie, P. D. Buckley, A. K. Burrell, S. M. F. Kennedy and J. M. Waters, *J. Chem. Soc., Dalton Trans.,* (2000), 2663-2671.
6. P. Bhattacharyya, J. Parr and A. M. Z. Slawin, *J. Chem. Soc., Dalton Trans.,* (1998), 3609-3614.
7. P. Crochet, J. Gimeno, S. G. Granda and J. Borge, *Organometallics,* 20, (2001), 4369-4377.
8. R. E. Rulke, V. E. Kaasjager, P. Wehman, C. J. Elsevier, P.W. N. M. van Leeuwen and K. Vrieze, *Organometallics,* 15, (1996), 3022-3031.
9. W. K. Wong, J. X. Gao, W. T. Wong, W. C. Cheng and C. M. Che, *J. Organomet. Chem.,* 471. (1994), 277-282.
10. W. K. Wong, L. L. Zhang, Y. Chen, W. Y. Wong, W. T. Wong, F. Xue and T. C. W. Mak, *J. Chem. Soc., Dalton Trans.,* (2000), 1397-1398.
11. P. W. Atkins, *Physical Chemistry,* 1998, Oxford University Press, Oxford.
12. I. R. Hanson, *Acta Cryst.,* B34, (1978), 1026-1028.
13. R. D. Rogers, S. E. Huggins, R. F. Henry and A. H. Bond, *Supramol. Chem.,* 1, (1992), 59-63.
14. S. A. Talipov, Z. Karimov, B. T. Ibragimov, A. K. Tashmukhamedova, N. Zh. Saifullina and T. F. Aripov, *Kristallografiya (Russ.),* 45, (2000), 492-495.
15. R. D. Rogers, R. F. Henry and A. N. Rollins, *J. Inclusion Phenom., Macrocyclic Chem.,* 13, (1992), 219-232.
16. V. V. Tkachev, L. O. Atovmyan, I. I. Bulgak, V. E. Zubareva and O. A. Raevskii, *Zh. Strukt. Khim. (Russ.) (Russ. J. Struct. Chem.),* 31, (1990), 96-95.
17. Y. A. Simonov, S. T. Malinovskii, D. M. Rudkevich and V. I. Kal'chenko, *Kristallografiya (Russ.),* 36, (1991), 887-891.
18. V. W. W. Yam, K. K. W. Lo and K. K. Cheung, *Inorg. Chem.,* 34, (1995), 4013-4014.

19. L. M. Engelhardt, C. Pakawatchai, A. H. White and P. C. Healy, *J. Chem. Soc., Dalton Trans.*, (1985), 125-138.
20. V. W. W. Yam, Y. L. Pui, K. K. W. Lo and K. K. Cheung, *J. Chem. Soc., Dalton Trans.*, (1998), 3615-3621.
21. M. A. Jalil, S. Fujinami, T. Honjo and H. Nishikawa, *Poyhedron.*, 20, (2001), 1071-1078.
22. E. W. Ainscough, A. M. Brodie, A. K. Burrell, X. Fan, M. J. R. Halstead, S. M. F. Kennedy and J. M. Waters, *Polyhedron,* 19, (2000), 2585-2592.
23. R. J. Staples, C. King, M. N. Khan, R. E. P. Winpenny and J. P. Fackler, *Acta Cryst.*, C49, (1993), 472-475.
24. J. Wang, *Acta Cryst.*, C52, (1996), 611-613.
25. T. V. Baukova, D. N. Kravtsov, L. G. Kuzmina, N. N. Dvortsova, M. A. Porai-Koshits and E. G. Perevlova, *J. Organomet. Chem.*, 372, (1989), 465-471.
26. M. T. Garland, J. Y. Le Marouille and E. Spodine, *Acta Cryst.*, C42, (1986), 299-301.
27. A. N. Shnulin, Y. T. Struchkov, K. S. Mamedov and A. G. Bezuglaya, *Zh. Strukt. Khim. (Russ.) (Russ. J. Struct. Chem.),* 18, (1977), 1015-1024.
28. C. J. Sanders, K. M. Gillespie, D. Bell and P. Scott, *J. Am. Chem. Soc.*, 122, (2000), 7132-7133.
29. P. C. Healy, C. Pakawatchai and A. H. White, *J. Chem. Soc., Dalton Trans.*, (1985), 2531-2539.
30. G. A. Bowmaker, P. C. Healy, D. L. Kepert, J. D. Kildea, B. W. Skelton and A. H. White, *J. Chem. Soc., Dalton Trans.*, (1989), 1639-1644.
31. H. Oshio, T. Watanabe, A. Ohto, T. Ito and H. Masuda, *Inorg. Chem.*, 35, (1996), 472-479.
32. J. Zukerman-Schpector, E. E. Castellano, A. E. Mauro and M. R. Roveri, *Acta Cryst.*, C42, (1986), 302-303.
33. Y. C. M. Pennings, W. L. Driessen and J. Reedijk, *Polyhedron,* 7, (1988), 2583-2589.
34. J. Kasper and K. Lonsdale, *International tables for x-ray crystallography (Vol. II),* 1962, The Kynoch Press, Biringham.
35. N. C. Baenziger, W. E. Bennett and D. M. Soboroff, *Acta Cryst.*, B32, (1976), 962-963.
36. L. G. Kuz'mina and N. V. Dvortsova, *Zh. Neorg. Khim.*, 36, (1991), 2021-2023.
37. L. M. Engelhardt, C. Pakawatchai, A. H. White and P. C. Healy, *J. Chem. Soc., Dalton Trans.*, (1985), 125-133.
38. K. Angermair, G. A. Bowmaker, E. N. de Silva, P. C. Healy, B. E. Jones and H. Schmidbaur, *J. Chem. Soc., Dalton Trans.*, (1996), 3121-3129.
39. G. A. Bowmaker, Effendy, P. J. Harvey, P. C. Healy, B. W. Skelton and A. H. White, *J. Chem. Soc., Dalton Trans.*, (1996), 2459-2465.
40. G. A. Bowmaker, Effendy, P. J. Harvey, P. C. Healy, B. W. Skelton and A. H. White, *J. Chem. Soc., Dalton Trans.*, (1996), 2449-2457.
41. E. W. Ainscough, A. M. Brodie, A. K. Burrell, G. H. Freeman, G. B. Jameson, G. A. Bowmaker, J. V. Hanna and P. Healy, *J. Chem. Soc., Dalton Trans.*, (2001), 144-151.
42. G. A. Bowmaker, S. E. Boyd, J. V. Hanna, R. D. Hart, P. C. Healy, B.W. Skelton and A. H. White, *J. Chem. Soc., Dalton Trans.*, (2002), 2722-2730.
43. G. A. Bowmaker, R. D. Hart, E. N. De Silva, B. W. Skelton and A. H. White, *Aust. J. Chem.*, 50, (1997), 621-626.
44. G. A. Bowmaker, R. D. Hart, J. D. Kildea, E. N. De Silva, B. W. Skelton and A. H. White, *Aust. J. Chem.*, 50, (1997), 605-619.
45. E. Pretsch, P. Bühlmann, C. Affolter, *Structure determination of organic compounds,* 2000, Springer, Berlin.
46. W. Kemp, *Organic spectroscopy.* (3rd Ed.), 1991. MacMillan Education Ltd, London.
47. V. W. W. Yam, R. P. L. Tang, K. M. C. Wong, C. C. Ko and K. K. Cheung, *Inorg. Chem.*, 40, (2001), 571-574.
48. G. L. Crossetti, C. A. L. Filgueiras, R. A. Howie, J. L. Wardell and C. M. Ziglio, *Acta Cryst.*, C57, (2001), 1279-1281.
49. P. D. Beer, C. G. Crane and M. G. B. Drew, *J. Chem. Soc., Dalton Trans.*, (1991), 3235-3242.
50. R. M. Silverstein and F. X. Webster, *Spectrometric identification of organic compounds,* (6th Ed.), 1998, John Wiley and Sons Inc, Canada.
51. V. W. W. Yam, Y. L. P. Pui, K. K. Cheung and N. Zhu, *New J. Chem.*, 26, (2002), 536-542.
52. V. W. W. Yam, K. M. C. Wong, V. W. M. Lee, K. K. W. Lo and K. K. Cheung, *Organometallics,* 14, (1995), 4034-4036.
53. L. Crociani, G. Bandoli, A. Dolmella, M. Basato and B. Corain, *Eur. J. Inorg. Chem.*, (1998), 1811-1820.
54. H. B. Song, Z. Z. Zhang and T. C. W. Mak, *Polyhedron,* 21, (2002), 1043-1050.
55. S. Berger, S. Braun and H. Kalinowski, *NMR spectroscopy of the non-metallic elements,* 1997, John Wiley and Sons Inc, Sussex.

Chapter three

1. G. Sanchez, J. L. Serrano, C. M. Lopez, J. Garcia, J. Pese and G. Lopez, *Inorg. Chim. Acta,* 306, (2000), 168-173.
2. K. A. McBeth, *The group VI carbonyl complexes of two iminophosphine ligands. Synthesis, characterization and interaction with alkali cations.* PGDipSci Report, 2001, Massey University.
3. D. J. Darensbourg and R. L. Kump, *Inorg. Chem.*, 17, (1978), 2680-2682.
4. H. Werner and R. Prinz, *Chem. Ber.*, 100, (1967), 265-270.
5. E. W. Ainscough, A. M. Brodie, P. D. Buckley, A. K. Burrell, S. M. F. Kennedy and J. M. Waters, *J. Chem. Soc., Dalton Trans.*, (2000), 2663-2671.
6. I. R. Hanson, *Acta Cryst.*, B34, (1978), 1026-1028.
7. R. D. Rogers, S. E. Huggins, R. F. Henry and A. H. Bond, *Supramol. Chem.*, 1, (1992), 59-63.
8. S. A. Talipov, Z. Karimov, B. T. Ibragimov, A. K. Tashmukhamedova, N. Zh. Saifullina and T. F. Aripov, *Kristallografiya (Russ.),* 45, (2000), 492-495.
9. R. D. Rogers, R. F. Henry and A. N. Rollins, *J. Inclusion Phenom., Macrocyclic Chem.*, 13, (1992), 219-232.
10. V. V. Tkachev, L. O. Atovmyan, I. I. Bulgak, V. E. Zubareva and O. A. Raevskii, *Zh. Strukt. Khim. (Russ.) (Russ. J. Struct. Chem.),* 31, (1990), 96-95.
11. Y. A. Simonov, S. T. Malinovskii, D. M. Rudkevich and V. I. Kal'chenko, *Kristallografiya (Russ.),* 36, (1991), 887-891.
12. D. Adams, *Metal–ligand related vibrations,* 1967, Edward Arnold Ltd, London.

Chapter four.

1. A. Tsuda, H. Moriwaki and T. Oshima, *J. Chem. Soc., Perkin Trans. 2,* (1999), 1235-1240.
2. D. S. Young, H. Y. Hung and L. K. Liu, *Rapid Commun. Mass Spectrom.*, 11, (1997), 769-773.
3. D. S. Young, H. Y. Hung and L. K. Liu, *J. Mass Spec.*, 32, (1997), 432-437.
4. E. C. Kempen, J. S. Brodbelt, R. A. Bartsch, Y. Jang and J. S. Kim, *Anal. Chem.*, 71, (1999), 5493-5500.
5. S. M. Blair, J. S. Brodbelt, A. P. Marchand, K. A. Kumar and H. S. Chong, *Anal. Chem.*, 72, (2000), 2433-2445.
6. C. J. Pedersen, *J. Am. Chem. Soc.*, 92, (1970), 386-391.
7. C. J. Pedersen and H. K. Frensdorff, *Angew. Chem., Int. Ed. Engl.*, 11, (1972), 16-25.
8. R. M. Izatt, J. S. Bradshaw, S. A. Nielsen, J. D. Lamb and J. J. Christensen, *Chem. Rev.*, 85, (1985), 271-339.
9. R. M. Izatt, K. Pawlak and J. S. Bradshaw, *Chem. Rev.*, 91, (1991), 1721-2085.
10. E. Weber and M. Czugler, *Inorg. Chim. Acta,* 61, (1982), 33-38.
11. J. D. Owen, *J. Chem. Soc., Dalton Trans.*, (1980), 1066-1067.
12. P. D. Beer, M. G. B. Drew, R. J. Knubley and M. I. Ogden, *J. Chem. Soc., Dalton Trans.*, (1995), 3117-3123.
13. P. R. Mallinson and M. R. Truter, *J. Chem. Soc., Perkin Trans. 2,* (1972), 1818-1823.
14. P. D. Beer, C. G. Crane and M. G. B. Drew, *J. Chem. Soc., Dalton Trans.*, (1991), 3235-3242.
15. Y. Takeda, H. Yano, M. Ishibashi and H. Isozumi, *Bull. Chem. Soc. Jpn.*, 53, (1980), 72-76.
16. Y. Takeda and T. Kumazawa, *Bull. Chem. Soc. Jpn.*, 61, (1988), 655-658.
17. P. V. Bernhardt and E. J. Hayes, *Inorg. Chem.*, 41, (2002), 2892-2902.
18. M. A. Bush and M. R. Truter, *J. Chem. Soc., Perkin Trans. 2,* (1972), 341-344.

19. D. C. Moody and R. R. Ryan, *Cryst. Struct. Commun.*, 8, (1979), 933-936.
20. W. Dreissig, Z. Dauter, A. Cygan and J. F. Biernat, *Inorg. Chim. Acta*, 96, (1985), 21-27.
21. D. A. Lemenovskii, I. E. Nifant'ev, I. F. Urazowski, E. G. Perevalova, Y. L. Slovokhotov and Y. T. Struchkov, *J. Organomet. Chem.*, 342, (1988), 31-44.
22. W. A. Herrmann, J. G. Kuchler, G. Weichselbaumer, E. Herdtweck and P. Kipro, *J. Organomet. Chem.*, 372, (1989), 351-370.
23. P. D. Beer, H. Sikanyika, C. Blackburn, J. F. McAleer and M. G. B. Drew, *J. Organomet. Chem.*, 356, (1988), C19-C22.
24. B. Koenig, E. Schofield, P. Bubenitschek and P. G. Jones, *J. Org. Chem.*, 59, (1994), 7142-7143.
25. C. C. Yang, W. Y. Yeh, G. H. Lee and S. S. Peng, *J. Organomet. Chem.*, 598, (2000), 353-358.
26. Z. Li-Tao, L. Bao-Sheng, L. Tian-Bao, H. Hong-Wen and Z. Shao-Hui, *Jiegou Huaxue (Chin.) (J. Struct. Chem.)*, 10, (1991), 167.
27. P. D. Beer, M. G. B. Drew, R. J. Knubley and M. I. Ogden, *J. Chem. Soc., Dalton Trans.*, (1995), 3117-3123.
28. P. R. Mallinson and M. R. Truter, *J. Chem. Soc., Perkin Trans. 2*, (1972), 1818-1823.
29. W. Xu, K. Clinger, M. L. Hackert and N. S. Poonia, *J. Inclusion Phenom., Macrocyclic Chem.*, 3, (1985), 163-172.
30. W. S. Sheldrick and N. S. Poonia, *J. Inclusion Phenom. Macrocyclic Chem.*, 4, (1986), 93-98.
31. Z. Zhixian, Z. Xianxin and H. Jinshun, *Huaxue Xuebao (Chin.) (Acta Chim. Sinica)*, 44, (1986), 870.
32. Z. Zhixian, D. Baoshi, Z. Xianxin, L. Shixiong and H. Jinling, *Jiegou Huaxue (Chin.) (J. Struct. Chem.)*, 6, (1987), 209.
33. A. Mugnoli, Z. Dauter, E. Luboch, A. Cygan and J. F. Biernat, *J. Inclusion Phenom. Macrocyclic Chem.*, 4, (1986), 407-414.
34. M. Zhi-Hua, Z. Zhong-Hua, H. Zhou, Y. Hong-Wu, Z. Zhi-Xian, Z. Ming-Rui and R. Bo-Yany, *Jiegou Huaxue (Chin.) (J. Struct. Chem.)*, 12, (1993), 266.
35. J. C. Peters, A. L. Odom and C. C. Cummins, *Chem. Commun.*, (1997), 1995-1996.
36. Z. Karimov, S. A. Talipov, K. K. Fun, B. T. Ibragimov, A. K. Tashmukhamedova and A. Razak, *Zh. Strukt. Khim. (Russ.) (Russ. J. Struct. Chem.)*, 42, (2001), 160-164.
37. J. Pickardt, S. Wiese, L. von Chrzanowski and M. Borowski, *Z. Anorg. Allg. Chem.*, 626, (2000), 2096-2102.
38. J. Pickardt and P. Wischlinski, *Z. Anorg. Allg. Chem.*, 625, (1999), 1527-1531.
39. E. Weber and M. Czugler, *Inorg. Chim. Acta*, 61, (1982), 33-38.
40. V. W. W. Yam, Y. L. Pui, K. K. Cheung and N. Zhu, *New J. Chem.*, 26, (2002), 536-542.
41. V. W. W. Yam, K. K. W. Lo and K. K. Cheung, *Inorg. Chem.*, 34, (1995), 4013-4014.
42. C. J. Sanders, K. M. Gillespie, D. Bell and P. Scott, *J. Am. Chem. Soc.*, 122, (2000), 7132-7133.
43. A. N. Shnulin, Y. T. Struchkov, K. S. Mamedov and A. G. Bezuglaya, *Zh. Strukt. Khim. (Russ.) (Russ. J. Struct. Chem.)*, 18, (1977), 1015-1024.
44. M. T. Garland, J. Y. Marouille and E. Spodine, *Acta Cryst.*, C42, (1986), 299-301.

Errata:

1st examiner

1. page xiv, line 15, "ml" should read "mL".

2. page 3, line 5, "Thus allowing" should read "This allows".

6. page 14, last line, "columbic" should read "Coulombic".

7. page 38, start of the first paragraph should read, "Crystals were obtained from slow recrystallization of the complex from CH_2Cl_2 layered with Et_2O. Structure refinement and crystal data are in Table 2.4, selected bond lengths and angles in Table 2.5 and selected torsion angles in Table 2.6. The copper has a tetrahedral coordination with both NP ligands being bidentate via the phosphorus and nitrogen atoms (Figure 2.2)."

8. page 46, Table 2.11, I agree that Table 2.11 refers to PPh_3 ligands but I view the NP ligand as a substituted PPh_3.

9. page 50, last paragraph, 1st sentence should read "The bond lengths of the imine and surrounding bonds are normal".

10. page 56, Table 2.18, 2nd line should read "Empirical formula $C_{51}H_{41}Au_2Cl_5N_2P_2$". (The structural analysis of Au(NP)Cl gives a ratio of 2 complexes to 1 $CHCl_3$ which is in agreement with the elemental analysis).
page 61, Table 2.22, 2nd line should read "Empirical formula $C_{51}H_{41}Au_2Br_2Cl_3N_2P_2$" (The structural analysis of Au(NP)Br gives a ratio of 2 complexes to 1 $CHCl_3$ which is in agreement with the elemental analysis).

11. page 72, 3rd sentence should read "In a few cases the 100% peak is likely to be a solvent/cation aggregate". (A cone voltage of 30V was used for all ESMS spectra).

2nd examiner.

Page 8. Table 1.2 should be labelled "logK values of benzo-15-crown-5 alkali complexes".

Structure of O_5NP.
Page 37. Table 2.2, The bond length C(12)-O(4) 1.699(16) should be replaced with C(12)-O(4A) 1.338(9), the bond angle C(13)-O(4A)-C(12) should be reported as 108.4° (13).
Page 35. Figure 2.1, the atom labelled O(4) should be relabelled O(4A).
Page 33. last sentence should be absent.

Structure of $[Cu(NP)_2][PF_6]$.
Page 38, The structure was squeezed to remove disordered solvent and PF_6^-. The size of the void volume was 489 $Å^3$ and the number of electrons in the void was 237. The microanalytical data, page 26, indicates that for each complex there is $1PF_6^-$ and $¾CH_2Cl_2$ As there are 4 complexes within the unit cell this suggests a void volume of 37×18 $Å^3 = 666$ $Å^3$ with 396 electrons within this void. Hence the electron count provided by squeeze does NOT match that expected from the microanalytical data. The anisotropic displacement ellipsoids are best achieved after rigorous effort.

Structure of $[Ag(NP)_2][PF_6]$.
Page42. There is a significant contact between Ag(1) and N(20B) which has a length of Ag(1)-N(20B) 2.67 Å. This changes the coordination of the Ag metal centre to a distorted tetrahedral. The Ag(1) atom is –0.1129 Å out of the N(20A), P(1B), P(1A) plane suggesting that the N(20B)-Ag(1) interaction is weak.
Page 45. Table 2.8 should include: Ag(1)-N(20B) 2.67 Å, N(20B)-Ag(1)-P(1A) 124.40°, N(20B)-Ag(1)-N(20A) 83.81° and N(20B)-Ag(1)-P(1B) 71.34°.
Page 45. Table 2.10, Symmetry transformations used to generate equivalent atoms: #1 -x+2, -y+2, -z+2; #2 x+1/2, -y+3/2, z+1/2; #3 x-1/2, -y+3/2, z-1/2; #4 x-1, y, z; #5 x, y+1, z.

Structure of $[Au(NP)_2][PF_6]$.
Page46. The Au-N distances range from 2.983-3.065 Å and indicate that the imine nitrogens have significant interaction with the Au centres. This gives the complex a distorted tetrahedral geometry with a coordination of 2 strong 2 weak.
This structure has been squeezed to remove disordered solvent and PF_6^-. The size of the void volume was 1151 $Å^3$ and the number of electrons in the void was 541. The microanalytical data, page 30, indicates that for each complex there is $1PF_6^-$ and no solvent As there are 4 complexes within the unit cell this suggests a void volume of 28×18 $Å^3 = 504$ $Å^3$ with 276 electrons within this void. Hence the electron count provided by squeeze does NOT match that expected from the microanalytical data. This is likely to be due to the lack of solvent in the microanalytical data.

Page 49.Table 2.13 should include: N(20A)-Au(A) 3.042 Å, N(46A)-Au(A) 3.041 Å, N(20B)-Au(B) 2.983 Å, N(46B)-Au(B) 3.065 Å, N(20A)-Au(A)-P(1A) 61.78°, N(20A)-Au(A)-P(2A) 125.57°, N(20A)-Au(A)-N(46A) 111.41°, N(46A)-Au(A)-P(1A) 124.11°, N(46A)-Au(A)-P(2A) 63.01°, N(20B)-Au(B)-P(1B) 63.00°, N(20B)-Au(B)-P(2B) 123.1°, N(20B)-Au(B)-N(46B) 113.30°, N(46B)-Au(B)-P(1B) 124.11°, N(46B)-Au(B)-P(2B) 61.9°.

Structure of Au(NP)Cl.
Page 54. The Au-N distances of 3.087 and 3.140 Å are suggestive of a long but significant interaction resulting in a distorted trigonal planar geometry for the metal centre.
Page 57. Table 2.19 should include: Au(1A)-N(20A) 3.140 Å, Au(1B)-N(20B) 3.087 Å, N(20A)-Au(1A)-P(1A) 62.4°, N(20A)-Au(1A)-Cl(1A) 119.90°, N(20B)-Au(1B)-P(1B) 63.8°, N(20B)-Au(1B)-Cl(1B) 117.28°.
Page 58. Table2.21, Symmetry transformations used to generate equivalent atoms: #1 x-1,y,z; #2 x+1,y+1,z; #3 -x+1,-y,-z+1; #4 -x+2,-y+1,-z+1; #5 x+1,y,z; #6 -x+2,-y+2,-z+1; #7 -x+1,-y,-z+2; #8 x,y,z+1; #9 x,y,z-1.

Structure of Au(NP)Br.
Page 59. The Au(1)-N(1) 3.110 Å distance suggests a weak interaction resulting in a distorted trigonal planar geometry for the Au centre.
Page 61. Table 2.22, line 7 should read "Space group P-1".
Page 62. Table 2.23 should report: Au(1)-N(1) 3.110 Å, N(1)-Au(1)-P(3) 63.0°, N(1)-Au(1)-Br(1) 119.28°.
Page 62. Table 2.25, Symmetry transformations used to generate equivalent atoms: #1 -x+1,-y,-z+1; #2 -x+2,-y+1,-z; #3 x-1,y,z; #4 x,y+1,z.

Structure of $Mo(CO)_4(NP)$.
Page 85. Table 3.6, Symmetry transformations used to generate equivalent atoms: #1 -x+3/2,y-1/2,-z+1/2.

Structure of $Mo(CO)_4(O_5NP)$.
Page 90. Table3.10, Symmetry transformations used to generate equivalent atoms: #1 -x+1,-y+1,-z+2; #2 -x+2,-y+1,-z+2.

Structure of $[Cu(O_5NP)_2]K[PF_6]_2$.
Page 124. Table 4.8, Symmetry transformations used to generate equivalent atoms: #1 -x+1,-y,-z+1; #2 x-1,y,z-1; #3 x-1,y,z; #4 -x+1,-y,-z.